NASA Contractor Report 3832

An Experimental Investigation of Gas Jets in Confined Swirling Air Flow

Ronald M. C. So, Saad A. Ahmed, and Hukam C. Mongia

GRANT NAG3-260
SEPTEMBER 1984

NASA

NASA Contractor Report 3832

An Experimental Investigation of Gas Jets in Confined Swirling Air Flow

Ronald M. C. So, Saad A. Ahmed,
and Hukam C. Mongia
Arizona State University
Tempe, Arizona

Prepared for
Lewis Research Center
under Grant NAG3-260

National Aeronautics
and Space Administration

**Scientific and Technical
Information Branch**

1984

Table of Contents

Table of Contents (Cont'd)

Table of Contents (Cont'd)

NOTATION

English Letters

D	diameter of tube or jet
$\dot{M}$	momentum flux at any tube cross-section or of jet
p	static pressure
r	radial coordinate
R	radius of tube
Re	Reynolds number based on tube or jet diameter
S	swirl number
u	instantaneous or fluctuating axial velocity
u'	RMS u velocity
U	mean axial flow
U	average U velocity at an x location
U_{av}	average upstream velocity along x-direction
W	mean circumferential velocity
w	instantaneous or fluctuating circumferential velocity
w'	RMS w velocity
x	axial coordinate

Greek letters

θ	vane angle
ν	kinematic viscosity of fluid
ρ	density of fluid
Ω	angular velocity

Subscripts

a	air or ambient condition
h	helium
j	jet

Subscripts (Cont'd)

o	centerline
T	tube
u	upstream
w	wall
∞	surrounding condition

ABSTRACT

The understanding of the fluid dynamics of jets in confined swirling flows is of basic importance to designers of turbine combustors and solid fuel ramjets used to power missiles fired from cannons. Although there have been numerous investigations on the characteristics of confined jets and co-axial jets, little is known of the behavior of jets in a confined swirling flow, especially jets of a lighter fluid issuing into a heavier fluid. The present investigation addresses this latter question directly and reports on the fluid dynamics of gas jets of different densities in confined swirling flows.

A swirler of the vane design is used to impart swirl to the flow inside a plexiglass tube, 125 mm in diameter. The jet, with a diameter of 8.73 mm, is situated in the center of the swirler so that the tube axis is aligned with the jet axis. Both the swirler and the jet Reynolds number can be changed if required. The experiment is carried out with gases of different densities and the jet velocities are selected to give the same jet momentum flux for each gas. Mean velocity and turbulence measurements are made with a one-color, one-component laser velocimeter operating in the forward scatter mode.

Results for air and helium/air jets show that jets in confined flow with large area ratio are highly dissipative. As a result, both air and helium/air jet centerline velocity decays rapidly. However, the similarity between air and helium/air jets ends here. For air jets, the jet-like behavior in the tube center disappears at about 20 diameters downstream of the jet exit. This phenomenon is independent of the initial jet velocity. The turbulence field at this point also decays to that of the background swirling flow. On the other hand, a jet-like behavior in the tube center is noticed even at 40 diameters for helium/air jets. The subsequent flow and turbulence field

depend highly on the initial jet velocity. Since the jets are fully turbulent, therefore, independent of jet Reynolds number, and the jet momentum fluxes for both air and helium/air are the same, the cause of this difference in behavior is attributed to the combined action of swirl and density difference.

This observation can have significant impact on the design of turbine combustors and solid fuel ramjets subject to spin.

1. INTRODUCTION

1.1 Motivation

Annular gas turbine combustors are designed to give complete combustion between fuel and oxidant in the shortest possible distance and uniform velocity and temperature distributions at the exit end of the combustor. To achieve these objectives, the liquid fuel is atomized and thoroughly mixed with air before injecting into the combustor. Secondary air jets are used to deliver more air for mixing and reaction. Both the fuel-air and the secondary air jets can be swirling or non-swirling. Also, the swirling can be in the same direction or counter to each other. It is believed that through the creation of a recirculation region in the flow field and the anchoring of the flame in this region, complete combustion can be achieved efficiently. Further downstream, dilution air jets are installed in the combustor to burn off unburnt fuel, to lower the gas temperature and above all to thoroughly mix the gas and give a uniform distribution of velocity and temperature at the combustor exit. This last requirement is of utmost importance because a non-uniformity of 50°F in the temperature distribution will decrease the life of the first stage turbine blades significantly. It is also found that the dilution air jets are crucial to the attainment of uniform temperature distribution in a relatively short combustor. Without them, the flow and temperature fields at the combustor exit are just not uniform.

The reason for this is not clear. It could be due to insufficient length for mixing. It could also be due to the confinement of the lighter combustion products, which are at a higher temperature, by heavier swirling air, which is relatively cool. A similar mixing problem exists in solid fuel ramjet used to power missile fired from cannons. There, the problem reflects itself as a

significant decrease in ramjet combustion efficiency when the missile is subject to spin.

In solid fuel ramjet combustion, the flame is detached from the fuel surface and a layer of fuel vapor mixed with combustion products exists between the flame and the surface. Once the ramjet is rotated, as in the case of a cannon-fired missile, the lighter oxidant air and gas products could be prevented from mixing with the heavier fuel vapors by the action of radial pressure gradient. This, in turn, could lead to a decrease in combustion efficiency.

From these two examples, it is evident that the phenomenon resulting from the mixing of a lighter swirling or non-swirling gas with a swirling heavier external gas is of great interest to combustor designers. Unfortunately, little is known of this turbulent mixing phenomenon, even in the case of homogeneous mixing. Therefore, some basic understanding of this behavior is needed before the observations noted in gas turbine combustors and solid fuel ramjets subject to spin can be remedied and improved combustor designs put forward.

1.2 Brief Discussion of Related Work

The fluid dynamics of the flow described in the previous two examples are very complicated. It involves turbulent mixing of different density gases, chemical reactions, their interaction with the flow field and heat transfer. A complete understanding of this phenomenon is not possible at present because even the idealized flow of non-isothermal, non-reacting turbulent mixing of different density gas streams in a swirling environment is a little understood problem. The difficulty in trying to understand this idealized problem is

further compounded by the lack of knowledge in the corresponding isothermal flow behavior. On the other hand, a substantial amount of knowledge has been accumulated in the basic elements that make up the isothermal flow. Some of the important elements are: confined swirling flows, coaxial jets with and without swirl and inhomogeneous mixing in a free or confined environment. Therefore, it will be helpful to the present investigation to briefly review some recent past work in these three areas.

Isothermal confined swirling flows have been studied by numerous investigators. Among the more recent work that is relevant to the present study can be mentioned the investigations of Yajnik and Subbaiah (1973), Weske and Sturov (1974), Cheng (1978) and Tan (1980). In the investigation of Yajnik and Subbaiah (1973), the effects of variable initial swirl on turbulent pipe flow were examined. The initial swirl produced by guide vanes was small and amounted to a swirl number range of $0 \leq S \leq .155$. Consequently, flow reversal did not take place and similarity conditions were found to exist at about 50 diameters downstream of the entrance. The turbulence field was not studied; however, skin friction at the pipe wall was found to obey the logarithmic law but with the additive coefficient dependent on swirl. Weske and Sturov (1974) examined the decay of swirl and turbulence field in a pipe flow. In their investigation, the swirl was produced by rotating a section of the pipe. The swirl number investigated was substantially larger than those studied by Yajnik and Subbaiah (1973) and ranged from 0 to 3. Consequently, flow similarity was not found. The turbulence field was found to decay quickly. However, its decay was a strong function of the swirl number, S.

Turbulent mixing of two gas streams of the same density with and without swirl was investigated by Cheng (1978) in a coaxial annulus. The two streams can be swirled in the same or opposite directions and the swirl number

investigated was limited to ~ 1. This investigation was quite different from those of Yajnik and Subbaiah (1973) and Weske and Sturov (1984). Instead of studying the swirl effects on confined turbulent flows, it examined the effects of swirl on axisymmetric mixing layers. No detailed study of the flow field was presented. The main emphasis was on flow visualization of the mixing interface. Results showed that except for the case with no swirl in the inner stream and swirl in the outer stream, the mixing interface for all swirling combinations were unstable. Also, the flow structure was observed to be three dimensional and slightly flattened in the azimuthal direction. A similar study with different density gas streams was carried out by Tan (1980). Flow visualization revealed that the interaction of the density field with the resulting radical pressure gradient set up by swirl might have influenced the evolution of the flow structures. However, since relatively few runs were carried out for the co-flowing streams with density difference, definite conclusions about the effects of density difference on swirling flows could not be reached. This is unfortunate, otherwise, some insight could be gleaned from this experiment to help formulate the present investigation.

Turbulent mass and momentum transfer in coaxial jets with and without swirl have been investigated by numerous researchers. Among the recent work on homogeneous fluids can be mentioned the studies of Habib and Whitelaw (1979, 1980), Vu and Gouldin (1980) and Johnson and Bennett (1981). The mixing of different density streams was examined by Alpinieri (1964). The geometry of the test facility was quite similar in the investigations of Habib and Whitelaw (1979, 1980) and Johnson and Bennett (1981). Flow from the axisymmetric coaxial jets was issued into a large circular tube. The area ratio of the tube to the outer jet was ~ 8 in Habib and Whitelaw's experiment and ~ 4.3 in Johnson and Bennett's experiment. On the other hand, the

studies of Alpinieri (1964) and Vu and Gouldin (1980) were carried out in a circular tube with a coaxial jet located at the entrance to the tube. The area ratio of the jets was ~ 16 for Alpinieri's experiment and ~ 18 for Vu and Gouldin's experiment. None of these geometries was typical of actual combustor geometry. Therefore, the results of these experiments should be interpreted with caution when they were applied to explain combustor flows.

The investigations of Habib and Whitelaw (1979, 1980) were carried out for two velocity ratios and swirl numbers of 0 and .23. Although centerline recirculation was not observed at S = .23, the results did indicate that such recirculation would exist as S was increased. On the other hand, recirculation due to flow confinement disappeared even at S = .23 and a velocity ratio of 3. Without swirl, this recirculation would increase with increasing velocity ratio. Stronger turbulence was observed along with this increase in recirculation zone. Mass transfer in the form of a passive scalar was studied by Johnson and Bennett (1981). Their measurements were reported at one velocity ratio of ~ 3.2, and with the exception of the confinement ratio, the other conditions were quite similar to those of Habib and Whitelaw. A major result of their investigation was the discovery of a large region of counter-gradient turbulent axial mass transport. This phenomenor occurred in the region where the annular jet fluid was accelerating the inner jet fluid. Besides, they also found that the axial mass transport correlation coefficients were greater than the corresponding momentum transport coefficients. This is an indication that the assumption of unity Lewis number may not be very appropriate in the calculation of turbulent flow with mass transfer.

Mass transfer in different density streams was investigated by Alpinieri (1964). The study was carried out with H_2 and CO_2 jets issuing into an annular air jet. Therefore, inner jet fluid lighter and heavier than outer

annular jet fluid was investigated. The study was not exactly isothermal, because the inner jet temperature was 6 - 36°F higher than the annular jet temperature. Consequently, the mixing phenomenon would also be affected by thermal as well as gravitational buoyancy effects. The velocity ratio investigated ranged from .8 to ~ 2. Only mean profiles of velocity and concentration were measured. Therefore, the results did not reveal the existence of any region of counter-gradient turbulent mass transport as that found by Johnson and Bennett (1981). However, their results also showed that mass diffused more readily than momentum.

Isothermal mixing between two streams of the same density swirling in the same or opposite directions was investigated by Vu and Gouldin (1980). Although they also studied the case where only one stream was swirling, their results were reported for a non-swirling external stream. Therefore, useful information relevant to the present investigation cannot be gleaned from their results. The swirl number range investigated by Vu and Gouldin was $-.51 \leq S \leq .71$. Results showed that outer swirl had strong effects on the formation of a recirculation zone and mixing in the shear interface. As the outer swirl number was decreased from counter-swirl to co-swirl conditions, the size of the recirculation zone diminished, so were the reversed flow velocities. Also, stronger turbulence was found in the interface under counter-swirl conditions than co-swirl conditions. These findings were discussed in relation to reacting flows in actual combustors. However, in light of the studies by Alpinieri (1964), Tan (1980), and Johnson and Bennett (1981), caution should be exercised when these results are applied to explain actual combustor flows where density difference effects are prevalent.

Turbulent free shear mixing with density variation produced by different density streams or by different temperature streams have been studied by

numerous investigators. A brief and fairly up-to-date discussion of this phenomenon is provided by Schetz (1980). Both planar mixing (e.g. Brown and Roshko 1974; Batt 1977) and axisymmetric mixing (e.g. Zukkay et al 1964; Becker et al 1967; Chriss 1968; Abramovich et al 1969; Reynolds 1976; Sforza and Mons 1978; Birch et al 1978) of different density and/or temperature gas streams have been extensively studied. Among the major findings were the effects of ρ_j/ρ_∞ and U_j/U_∞ on the potential core. Zakkay et al (1964) and Chriss (1968) found that the two parameters appear together in the form $\rho_j U_j/\rho_\infty U_\infty$. However, the study of Abramovich et al (1969), covering a range $.27 \leq \rho_\infty/\rho_j \leq 8.2$ including heated jets, showed that the velocity and density parameters were influential separately. Centerline decay of mean velocity and concentration was influenced strongly by ρ_j/ρ_∞. For given U_j/U_∞, the decay of mean concentration was more rapid as the value of ρ_j/ρ_∞ decreased (Chriss 1968). In spite of this, both the centerline velocity and concentration were found to follow a power law decay, even though widely different values were reported for the exponents (Schetz 1980).

Mass transfer rates in planar and axisymmetric mixing of different density streams were reported by Reynolds (1976), Brown and Roshko (1974) and Batt (1977). The turbulent Schmidt number reported for planar mixing was ~ .5 as compared to a value of .7 for the axisymmetric case. This difference between planar and axisymmetric mixing has not been explained adequately by the investigators. In addition, Reynolds (1976) found that the turbulent Schmidt number, instead of being constant, actually increased from about .7 in the jet core to about 1.2 away from the core. Such variation in trend was also indicated by Brown and Roshko (1974) for the planar mixing case.

The effects of ρ_j/ρ_∞ on the entrainment rate in round jets have been examined in detail by Ricou and Spalding (1961) and Sforza and Mons (1978).

They found that the entrainment rate normalized by the jet mass flow rate was a simple function of the parameter $(\rho_\infty/\rho_j)^{1/2}\ (x/D_j)$.

Detailed measurements of concentration fluctuation have been attempted by numerous investigators. Among those who used hot-wire techniques can be mentioned D'Souza (1968), Way and Libby (1970, 1971), Stanford and Libby (1974) and Brown and Roshko (1974). Optical techniques were used by Becker et al (1967), Batt (1977) and Birch et al (1978). Again, studies were carried out on both planar and axisymmetric free shear layers. The concentration probability density function was found to vary from a delta function in one side of the mixing layer to a near Gaussian distribution in the center and then to another delta function on the other side of the mixing layer. This was not found to be the case for axisymmetric jets (Birch et al 1978). Here, consistent deviation from Gaussian statistics along the jet centerline was measured.

Finally, a recent work on confined jet by Janjua et al (1983) should also be mentioned. The circular air jet was directed into an axisymmetric chamber whose diameter was twice that of the jet. With this geometry, the confined jet flow should be considered similar to flows over a backward facing step and should be compared with similar flows analyzed by Eaton and Johnston (1980). Nevertheless, the authors found that the turbulence field decayed quickly from a jet-dominated field into one that was fairly uniform across the chamber in about 5 jet diameters. Whether such behavior can be expected when the chamber diameter is many times larger than the jet diameter is a question that needs to be answered.

This brief review, even though it may not be very complete, indicates that the mixing phenomenon in turbine and ramjet combustors as discussed in Sec. 1.1 is a little investigated phenomenon. Although many related phenomena

with one or several of the parameters important to non-isothermal and isothermal variable density mixing have been singled out for investigation, there are still many unanswered questions that need to be addressed. The present investigation is formulated to answer some of these questions. With its completion, it is hoped that a better understanding of the flow phenomenon can be achieved.

1.3 Present Objectives

From the brief discussion in Sec. 1.2, it can be seen that non-isothermal mixing of a light fluid jet with confined swirling flow of a heavier fluid has not been investigated in detail. Since this is the phenomenon, as pointed out in Sec. 1.1, that has the most impact on the design of gas turbine and ramjet combustors, the basic objective of the present investigation should, therefore, be directed to the study of this phenomenon. In actual combustors, mixing is very much affected by the heat release due to reaction. However, since not much is known about the more basic problem of isothermal mixing in the presence of confined swirl, a first attempt to understand this complicated phenomenon is to study the less complex problem of isothermal mixing with swirl. In order that the present results can be readily applied to explain combustor characteristics, the flow in the initial mixing region, or the near field of the immersed jet, is examined in detail first. For most combustors, the length-to-diameter ratio varies from 4 to 8. The initial mixing region usually does not occupy more than one half the combustor length. Therefore, the region of interest is limited to the first 2-4 diameters of the combustor.

With this in mind, the present investigation is set up to examine the fluid dynamics in the first 2-4 diameters of cylindrical combustors. The flow

characteristics that result are due to the mixing of a light fluid jet with the surrounding swirling flow of a heavy fluid. Temperatures of the two streams are maintained equal so that isothermal mixing results, and the parameters of importance in the problem are the density ratio, the swirl characteristic, the Reynolds numbers, combustor geometry, jet-to-flow velocity ratio, jet-to-flow momentum flux ratio, and pressure drop behavior.

Since the primary objective of the present investigation is to study the effects of density ratio and swirl on mixing, the experiment is designed to isolate these two parameters for investigation. The Reynolds number effects can be eliminated by examining fully turbulent flows. Also, combustor geometry can be fixed by restricting the investigation to one particular combustor, namely axisymmetric combustor for ease of investigation. It is hoped to eliminate the dependence on pressure drop behavior by investigating flows with small jet mass flow rate addition to the combustor. Since for a given swirl but different density ratio, either the jet-to-flow velocity ratio or the jet-to-flow momentum flux ratio can be kept constant, but not the two simultaneously, the present experiment is also designed to include these two parameters for investigation. In view of the large number of runs to be carried out, this first effort is focused on a particular swirl flow given rise by a swirler from an actual combustor. Several density ratios are chosen. These range from $\rho_j/\rho_a = \sim .2$ to 1. This can be achieved by choosing the jet fluid to be air and helium/air mixture and the surrounding fluid to be air. Several velocity and momentum ratios are investigated for each density ratio. Therefore, the experiments taken together would provide a good estimate of the effects of density ratio and swirl on isothermal mixing in an axisymmetric combustor.

Section 2 of this report describes the test facility, the diagnostic

technique and the data reduction procedure. This is followed by a discussion of the test matrix to be carried out. The results obtained are presented and analyzed in detail in Sec. 4. Conclusions drawn are outlined in Sec. 5. Finally, further work is discussed in Sec. 6.

2. EXPERIMENTAL SET-UP

2.1 The Test Facility

A schematic of the test facility used in this experiment is shown in Figures 1 and 2. Briefly, it consists of a swirler mounted inside a plexiglas tube of circular cross section. The plexiglass tube has an I.D. of 125 mm and an O.D. of 140 mm. It is bored to give a uniform and smoothly polished inner surface. The outer surface is also polished to give minimum distortion to laser light paths passing through the tube wall. Total length of plexiglass tubing used is 4.5 m. For ease of fabrication, the tube is segmented into 1.5 m sections and these are joined together using flanges. O-rings are installed between flanges to prevent leakage. The first section downstream of the contraction is .61 m long. It houses a honeycomb section 15 cm long which serves to straighten out the flow and to dampen any large scale disturbances. The swirler, shown in Figures 3 and 4, is mounted at the downstream end of this section (Figure 5). A steel tube, with an I.D. of 6.35 mm, is mounted at about 15 cm upstream of the swirler and is used to supply air or helium to the nozzle in the swirler (Figure 3). The swirler, nozzle and the tube are all adjusted to give good axial alignment. Immediately downstream of this section is the test section which is ~ .76 m long (Figure 5). Two test sections are made, one with wall pressure taps distributed along the length of the tube, the other without for use in LDA measurements. The return air duct is a PVC tube with an I.D. of ~ 32.5 cm. This is connected to the plexiglass tube via a diffuser and a 125 mm I.D. aluminum tube. A blower powered by a 25 hp motor is used to suck air through the test section. In order to reduce the noise in the whole set-up, two settling chambers are mounted one at each end of the blower. Since the motor is a constant speed motor, the rate of mass

flow through the test facility is controlled by a gate valve located upstream of the contraction section. The temperature of the incoming air is controlled by two evaporative coolers mounted on the roof at the inlet to the test facility. Since the compressed air supply for the air jet experiment is already at room temperature, thermal effects can be easily eliminated. On the other hand, if bottled-gas is used to supply helium for the helium jet experiment, a heat exchanger is required to bring the helium temperature up to room temperature level in order to avoid thermal effects in a variable density flow. This is achieved by passing the helium gas through a copper coil immersed in hot water (Figure 6) before delivering to the jet nozzle in the center of the swirler. The water temperature can be varied by controlling the power supplied to the heating element. This arrangement is found to be very satisfactory and the air/helium temperatures can be set to within 1°F of each other. Therefore, the mixing phenomenon studied is one of isothermal mixing with density difference between the two streams.

The swirler (Figures 3 and 4) is provided for the present experiment by Garrett Turbine Engine Company. It is made of stainless steel. The vanes are flat plates set at an angle of 66° and are not extended all the way to the center nozzle. Instead, a plate of ~ 53 mm diameter is placed between the vanes and the center nozzle. The center nozzle is designed to give a fully turbulent low subsonic jet for both air and helium. If the jet Reynolds number is calculated based on a jet diameter of 6.35 mm for helium, the highest Re_j obtained is still $< 10^4$. Therefore, the jet is essentially transitional and would not be independent of Re. In order to ensure a fully turbulent jet, even for helium, the jet nozzle is designed with a backward facing step as shown in Figure 3. According to Eaton and Johnston (1980), the flow downstream of the reattachment point in a backward facing step is

essentially turbulent even though the upstream flow may be laminar. Also, the reattachment length is ~ 8–10 step height. In view of this, the nozzle is designed to give an abrupt expansion of 6.35 mm to 8.73 mm diameter. The length of the nozzle after the expansion is 12.7 mm, which is ~ 11 step height. With this modification, it is found that the jets are fully turbulent for all test conditions investigated in the present experiment.

The swirl number, S, can be conveniently used to characterize swirling flow. It is defined in terms of angular and axial momentum fluxes associated with the mean flow, thus

$$S = \frac{\int_0^R UWr^2 dr}{R\int_0^R U^2 r dr} \quad . \tag{1}$$

If $\bar{U}$ is the average velocity and Ω is the angular velocity, then

$$\pi R^2 \bar{U}^2 = 2\pi \int_0^R U^2 r dr \quad , \tag{2}$$

$$\pi \Omega R^4 \bar{U} = 2\pi \int_0^R UWr^2 dr \quad . \tag{3}$$

Therefore, S can be simplified to

$$S = \frac{\Omega R}{\bar{U}} = \frac{\bar{W}}{\bar{U}} \quad . \tag{4}$$

For swirling motion produced by vanes with constant angle, S is given by

$$S \cong \frac{\bar{W}}{\bar{U}} = \tan \Theta \quad . \tag{5}$$

Since $\Theta = 66°$ for the present vane design, $S \cong 2.25$. The present swirler

therefore gives a high swirl number flow in the tube.

2.2 Diagnostic Instrument

Velocity measurements are taken with a DISA Model 55L laser-Doppler anemometer (LDA) employing the forward scatter mode as shown in Figure 7. This system is utilized since it can measure one velocity component at a point in the flow field regardless of the physical and thermodynamic properties of the fluid and without disturbing the flow. A 15 mw helium-neon laser (wave length λ = 632.8 nm) provides the coherent light source. This beam is split and one of the beams is shifted 40 MHz utilizing a Bragg cell to enable detection of high degrees of turbulence and to accept reversed flow in the axial direction. The resulting pair of beams is then passed through a beam expander and a 31 cm focal length lens. Beam separation can be varied arbitrarily and the largest value (75.6 mm) is chosen to minimize the sampling volume length as much as possible and to improve signal-to-noise ratio. The resulting beam intersection angle is 13.9° in air and yields an ellipsoidal sampling volume of dimensions 0.99 mm length and 0.12 mm width. When a particle passes through the intersection of the two beams, causing the fringe pattern to move, the intensity of light received by the photomultiplier is modulated. Since the particles are very small, they move with the same speed as the fluid particles and yield a Doppler frequency proportional to their velocities. Electronic processing is performed utilizing a 55L90A frequency counter to measure the value of the Doppler frequency, f_D, and to determine the velocity component normal to the fringes. The relation between these quantities is

$$V = \lambda f_D / 2 \sin\left(\frac{\theta}{2}\right) \quad , \tag{6}$$

where f_D is the Doppler frequency, θ is the beam intersection angle (θ = 13.9°), V is the velocity in the plane of the beams and perpendicular to the bisector of the included angle θ.

The set-up is also equipped with a DISA 55N10 frequency shifter which allows reversed flow measurements and enables the user to measure highly disturbed flows and fluctuating flows with zero mean velocity. It also enables the user to determine the direction of the flow and to eliminate to a high degree directional signal bias. Furthermore, frequency shift allows optimum matching of the Doppler signal to the range of the signal processor. Therefore, frequency shift is used in the present set-up. The frequency shifter produces a 40 MHz signal which is used to drive a Bragg cell, placed in the optical path of one of the laser beams, and in this way the beam is frequency shifted by $f_B = \pm$ 40 MHZ. Therefore, the signal detected by the photomultiplier is $f_D \pm f_B$ which is fed to a mixer as shown in Fig. 7. The output of the mixer is $f_D \pm f_o$, where f_o may be selected in the range 10 kHz to 9 MHz as required by the velocity range.

The DISA 55L90A signal processor amplifies and filters the signal fed by the frequency shifter as shown in Figure 7. In principle, the LDA counter works as a timing device or a stop watch (500 MHz clock) which can be programmed to measure the time between certain events. The counter can be set to measure the time for 8 zero crossings of the filtered signal, validate the output and allow analog or digital data read-out as shown in Figure 7. The processor also measures 5 zero crossing and compares with the 8 cycles result to ensure the signal is a valid one-particle signal. Since the LDA counter systems are designed for use in situations where low seeding particle concentration occurs and also where seeding concentration is difficult to control, the counter system is a perfect choice for the present set-up. The counter is

equipped with a validation unit and a data-rate module, which facilitates monitoring of the Doppler signal when setting up and making the preliminary adjustments. This allows the voltage of the photomultiplier and the amplification to be set so that the best signal quality is obtained.

For the present set-up, all measurements are made in the horizontal plane passing through the tube axis and the vertical plane perpendicular to the tube axis (Figure 8). The former gives u, the axial velocity, while the latter gives w, the circumferential velocity. Radial velocity is not measured because of the difficulties associated with translating the sample volume in the vertical direction using available equipment. The traversing mechanism used is a DISA 57H00 traversing table with a DC motor drive. A digital control system fully integrated with the computer is used to keep track of position even when it is used in the manual mode. This allows the user to switch the mechanism from manual to automatic mode without a new initialization procedure. The standard traversing range is 600 mm and the spacial resolution is ~ 1/64 mm.

Artificial seeding is used to improve the LDA signal quality and frequency resolution. This is provided by a DISA 55L18 seeding generator which is comprised of a carefully developed liquid atomizer and separator. The liquid used is a mixture of water and glycerine (50:50%). Compressed air is used to atomize the liquid and to carry the atomized droplets to the main flow. The droplet size is centered about 1 μm, and its concentration can be regulated by changing the air inlet pressure to the atomizer. In general, seeding particles are introduced into the flow system in the same plane of measurement which gives better signal quality.

2.3 Data Acquisition and Reduction

A minicomputer data handling system is used in the present experiment. The master control over the system is provided through the user's terminal. This allows all measurement to be performed under program control from a console device. A specially developed computer program sets up all necessary information and controls data collection and transfer at each measuring point. Three blocks of 1024 samples are collected together with Doppler frequency and time between samples. The choice is made of three blocks of data only because the results do not vary significantly when the number of data blocks is increased to four or more. Reduced data can be displayed instantaneously or stored on a floppy disk for later processing. The system consists of the following:

(1) A standard DISA 57G20 buffer interface which provides communication between the PDP-11/03 computer and the DISA 55L90A counter processor. It is essentially a handshake between the counter and the computer to enable the user to set the counter under program control. This buffer is also needed because the input rate to the computer is much smaller than the data rate generated by the counter.

(2) A DEC PDP 11/03-L minicomputer with a dual disk drive and a 64 Kb CPU. The computer incorporates two floppy disks, a console terminal (Digital VT100) and a graphic printer (Digital DEC Writer IV). A picture of the various instruments and control terminal is shown in Figure 9.

A computer program using standard methods of analyses to calculate the statistics, spectra and correlations of LDA signals is developed for use in the PDP 11/03 computer in conjunction with other programs for data acquisition. In developing the program, special consideration is given to the

biasing effect associated with the use of a frequency counter to process data in highly turbulent or disturbed flows. This effect arises because the number of data points sampled by the counter may be correlated with the physical flow parameters, in particular, with the magnitude of the velocity passing through the measuring volume (see for example George 1976; Erdman and Gellert 1976; Hosel and Rodi 1977; George 1978; Buchhave and George 1978; Melinand and Charnay 1978; Buchhave et al 1979). These references also discuss other corrections related to random sampling times. For the present, it is enough to note that all velocities are corrected utilizing resident time bias as follows:

$$U = \frac{\sum_1^N u_j \, a_j}{\sum_1^N a_j} \quad , \tag{7}$$

$$u'^2 = \frac{\sum_1^N (u_j - U)^2 \, a_j}{\sum_1^N a_j} \quad , \tag{8}$$

where N is the total number of data points and a_j is the weighting factor. For resident time measurement, a_j is the total burst time. In the present study, only the mean and variance of the LDA signals are calculated and reported.

2.4 Qualification of Test Facility

Before actual experimentation is begun, the test facility is checked for the followings. These are flow upstream of the swirler, jet flow, flow immediately downstream of the swirler, various methods of seeding the flow, symmetry check of the flow and pressure drop in the test section. A brief

description of each of these preliminary experiments is given below.

2.4.1 Upstream Flow

This experiment is carried out to characterize the flow upstream of the swirler and to ascertain that the incoming flow is indeed axisymmetric and turbulent. To do this, the flow at $x/D_T = -1.1$, where x is measured from the plane of the swirler, is measured. Seeding of the flow is provided by seeding holes upstream of the honeycomb (Figure 5). The stainless steel tubing is disconnected from the swirler so that the actual flow in the tube is studied. Measurements are made of the flow on the horizontal plane across the whole tube. It is found that the flow is indeed very axisymmetric in this plane. The distributions of U(r) and u'(r) across half the tube is shown in Figure 10. Uniform flow is achieved in the central 65% of the tube, and the turbulent intensity, u'/U, in this region is fairly uniform and equal to ~ 5.5%. The average velocity across the tube is 6.8 m/s. Therefore, the tube Reynolds number, Re_T, is 5.49×10^4. The Reynolds number is high enough for the flow to be turbulent and is about the same for all Re_j tested (Table 8), so it is set as the upstream flow condition for all subsequent experiments.

2.4.2 Jet and Swirling Flows

The objective of the present investigation is to examine isothermal inhomogeneous turbulent mixing in a swirling environment. In order to eliminate Reynolds number dependence, the flow created should be fully turbulent. A fully turbulent upstream flow has been created. This together with a fully turbulent jet flow will give the flow behavior required. Even though the jet Reynolds numbers are small for the range of conditions tested

(Table 8), the jets are made fully turbulent by the special design incorporated into the jet nozzle (Figure 3). Two different methods are used to determine the velocity of the jet at its exit plane. One is to use a rotor-meter to measure the volume flow delivered to the jet nozzle. Assuming the velocity at the jet exit to be uniform, the jet velocity U_j can be determined. Another method is to position a pitot-static probe at the jet exit. Thus, the centerline U_j can be measured. A series of U_j measurements are made using these two techniques. The results show that the measured U_j's agree to within $\pm$ 3% of each other. While these measurements are performed, the pressure gauge settings for the various U_j conditions are also noted. This then provides a curve of gauge pressure setting versus U_j for setting the jet condition. Subsequent experiments are carried out with the jet condition set according to this curve.

The flow angle immediately downstream of the swirler is checked to see if it is given by (5). Two sets of measurements are made; one with $U_j = 0$ and another with an air jet and U_j = 25.4 m/s. The measurements are made at $x/D_j = 1$, since it is not possible to get any closer with the present set-up. Measured U, W from r = 47.5 mm to 59.5 mm are plotted as shown in Figure 11. It can be seen that the flow angle behind the swirler is fairly constant in this region and is in good agreement with (5). For r < 47.5 mm, the flow angle begins to decrease, which reflects the effect of the center plate in the swirler. Therefore, the initial swirling flow set up near the tube wall is essentially that created by the swirler.

2.4.3 Effects of Seeding

In anticipation of the fact that seeding the helium jet is going to

destroy the integrity of the jet, several experiments are carried out to investigate the effects of seeding on the measured behavior of the flow in the test section. Altogether three experiments are performed. One is to seed the flow using the seeding holes located upstream of the honeycomb (Figure 5). Another is to seed the flow using a circular copper tube with small holes drilled along the axis of the tube. The tube is introduced diametrically across the plexiglass tube upstream of the swirler and in the plane of measurement. A third experiment is carried out with seeding also introduced to the jet as shown in Figure 5. The flow properties at x/D_j = 1.5 and 40 are measured to determine the effects of seeding. All experiments are performed with an air jet set at U_j = 66.8 m/s in the presence of an external swirling flow. It is found that the LDA signals obtained with the flow seeded via seeding holes located upstream of the honeycomb are not of as high a quality as those obtained by seeding the flow through the introduction of the copper tube in the plane of measurement. Typically, the data rate is much lower and hence frequency resolution is not as good. Consequently, the first method of seeding is discarded in favor of the second.

If the jet is not seeded, then the question remains as to whether the same result would be measured in the jet region. No difference in the measurements are detected at x/D_j = 40 (see Figures 37-40). The measurements at x/D_j = 1.5, where the jet is very prominent, are shown in Figure 12. It can be seen that, to within experimental errors, the measured U and u' obtained using the second and third seeding method are essentially the same. Also, the data rate for both cases is approximately equal and follows closely the curve shown in Figure 13. In view of this, it is decided to just seed the flow by introducing the copper tube in the plane of measurement.

This method of seeding works satisfactorily for air jets into air.

However, it fails to give reasonably accurate and repeatable measurements for helium jets with air, swirling and non-swirling. The reason is not enough seeding can diffuse into the mixing region in the jet near field for accurate measurements to be carried out. Far downstream, the flow is very well mixed and seeding the external flow alone is sufficient. Since the main interest of the present study is in the jet near field, the helium jet experiments have to be carried out by seeding both the jet and the surrounding air. This compromises the integrity of the helium jet and gives rise to a jet of helium/air mixture, since the seeding particles are carried by a stream of air. The mixture density of the jet is maintained low by using a minimum amount of seeding required to give reliable measurements in the jet near field. Assuming the air and the helium are homogeneously mixed inside the jet nozzle, the mixture density can be determined from a composition measurement. Although pure helium jets cannot be investigated, this arrangement allows for the examination of a light fluid jet issuing into a confinement of air.

2.4.4 Symmetry Check

In the process of investigating the effects of seeding, the quality of the LDA signals and the counter data rate are also examined. The data rate can be adjusted by varying the validation rate in the counter. A typical plot of the data rate across the test section at $x/D_j = 1$ and for an air jet set at $U_j = 25.4$ m/s is shown in Figure 13. Seeding for this measurement is via upstream flow only. Very high data rate (~ 25 kHz) is obtained near the wall. However, this decreases to about 2 kHz near the centerline. With sacrifice made in the validation rate, which is around 20% for the data shown in Figure 13, the data rate near the tube center can be adjusted to < 3 kHz. Thus, very

high quality signals are obtained. Seeding the jet in addition to upstream seeding does not improve the data rate significantly, even in the jet region. Consequently, all subsequent measurements are made with a data rate distribution approximately as shown in Figure 13.

Having decided on the method of seeding and the data rate distribution, the flow in the test section is checked for symmetry. Two experiments using air jets are run; one with U_j = 58.6 m/s, the other with U_j = 77.0 m/s. In the first experiment, measurements of U(r) and u'(r) at x/D_j = 4.3 are obtained. Flow characteristics at x/D_j = 7.5, 15.4, 20.9 are measured for the second experiment. These results are shown in Figures 14-16. In general, the flow is quite symmetric about the tube axis. Symmetry is also observed in the turbulence field. Therefore, the test facility gives the flow conditions rquired by the experiment.

2.4.5 Repeatability and Correctness of Measurements

An indication that the measurements in the test section are quite repeatable is provided by the results shown in Figure 12. Further evidence is obtained by repeating some measurements of the reported experiments in Sec. 2.4.4. Although these results are not shown here, they, in general, show that the measured u is quite repeatable. This means that the flow established under fixed conditions is very stationary. Also, additional evidence of repeatability can be found from among the reported results in this report. A comparison of the measurements obtained at x/D_j = 1 and 40 for both the air and helium/air jet experiments are given in Figures 37-40 and 55-57. The results show that not only are the measurements of mean quantities repeatable, so are the measurements of the turbulent stresses.

As for the correctness of the measurements, a continuity check, as discussed in Sec. 4.1, reveals that the measured U(r)'s agree with each other to within the variation of the blower capacity for all experiments reported. This gives credence to the results and to the correctness of the flow quantities measured.

2.4.6 Pressure Drop Measurement

The experiment is designed to isolate the parameters ρ_j/ρ_a, U_j and $\dot{M}_j/\dot{M}$ for investigation at a fixed S. Therefore, the implicit assumption is made that either the pressure drop along the test section has very little effect on the flow phenomenon or different density jets do not significantly affect the pressure drop behavior in the flow region of interest. It is reasoned that since the swirl number of the flow is very high, the pressure field immediately downstream of the swirler is dominated by the swirling motion. Jets with small mass and axial momentum fluxes added to the flow will not be able to affect the flow to such an extent that the resultant mean overall pressure drop is significantly different from the case without a center jet. Also, viscous effects near the wall should remain relatively unaffected by the jets in a distance of $x \simeq 3\ D_T$, especially when the jet velocity is high. If this is the case, then the measured pressure drop along the tube wall should be approximately the same for both helium and air jets set at the same velocity. Increasing the jet velocity would affect the level of the pressure drop; however, the basic trend should remain the same as the case without a center jet.

In order to verify this conjecture, the axial wall pressure drop along the tube is measured for $U_j = 0$ and all the experimental conditions listed in

Table 8. The pressure drop is measured with reference to the static pressure upstream of the swirler. A pitot-static tube located at $x/D_T = -2$ is used to provide the reference static pressure, and the pressure drop is normalized with respect to U_o measured by the pitot-static tube. The results are presented in Figure 17. It can be seen that the pressure drop behavior in the first 8 D_T is essentially dominated by the swirling motion. Therefore, the axial pressure drop behavior is not an important parameter in the flow under investigation. The parameters of importance remain to be U_j, ρ_j/ρ_a and $\dot{M}_j/\dot{M}$. In the next section, a program of experiments is outlined to study the effects of these parameters on isothermal mixing in a swirling environment.

3. THE EXPERIMENTAL PROGRAM

For the sake of clarity, the discussion of the experimental program is divided into five parts. The first deals with the characterization of the confined swirling flow, while confined jets is the topic of the second part. This is followed by a discussion of the test conditions for jets in swirling flow. The fourth part deals with air jets in swirling flow. Finally, helium/air jets in swirling flow constitutes the last experiment in this program.

3.1 Confined Swirling Flow

This experiment is carried out to study isothermal flow characteristics downstream of the swirler (Figure 5). The center jet is turned off, so the flow in the test section (Figure 2) is purely a confined swirling flow. This and subsequent swirling flow experiments are conducted at a fixed upstream flow condition. The flow distribution upstream of the swirler is shown in Figure 10. Therefore, the Reynolds number based on U_{av} and D_T is 5.49×10^4. The measured turbulent intensity in the tube core of the upstream flow is ~ 5.5%. Hence the flow approaching the swirler is fully turbulent.

Since the test section is less than five tube diameters long, the swirl decay would not have been significant (Yajnik and Subbaiah 1973). However, as can be seen from the measured results (Table 3(a-d)), the turbulence field has undergone substantial change. Therefore, this set of data can be used as a basis for comparison with subsequent experiments on jets in confined swirling flow, and would allow the turbulent interaction effects between swirling flow and jets of different density gases to be delineated. Profile measurements of U, W, u' and w' are made at x/D_j = 1, 2, 3, 5, 7, 10, 14, 20, 28 and 40. This choice of x locations is selected so that they cover a tube distance of 2.75

D_T, approximately half the length of an actual combustor. The x distance is normalized with D_j for easy comparison with subsequent measurements. In addition, the centerline velocities such as U_o, u'_o, w'_o, at x/D_j = 1, 1.5, 2, 2.5, 3, 4, 5, 6, 7, 8, 9, 10, 12, 14, 16, 18, 20, 24, 28, 32, 36 and 40 are measured. For subsequent swirling flow experiments, if possible, the centerline and profile measurements are carried out at the same x/D_j locations.

In this and all subsequent experiments with swirl, W_o, the centerline circumferential velocity, is not measured, since it is identically zero. Another reason for not measuring W_o is the difficulty of locating the laser measuring volume exactly at r = 0, because the accuracy in the r location measurement is r $\pm$ .75 mm. Since the slopes of U, u', w' at r = 0 are essentially zero for axisymmetric flows, such an error in r has little effect on the measured U, u', w' near the centerline. However, the same is not true for W because of the rapid change with respect to r in the core flow.

The results for U_o, u'_o, w'_o are reported in Table 2, while the profile measurements are listed in Table 3(a-d).

3.2 Confined Jets

The confined swirling flow experiment may provide a basis for evaluating the difference in flow behavior in the region of the tube away from the core. However, this knowledge alone is not sufficient to delineate the turbulent interaction effects between the jet and the swirling flow. Therefore, a knowledge of the behavior of isothermal confined jets in the present test section (Figure 2) is also required. In anticipation of the fact that gas jets of air and helium/air in confined swirling air flow are to be

investigated, three confined jet experiments are performed. One is with air and two are carried out with helium/air issuing into stationary air in the test section. The conditions for the air jet experiment are: U_j = 66.8 m/s, $Re_j = 3.78 \times 10^4$; while those for the helium/air jets are: U_j = 16.8 and 36.5 m/s, ρ_j/ρ_a = .31 and .228, $Re_j = 1.50 \times 10^3$ and 2.97×10^3, respectively. As explained in Sec. 2.4.2, the jets are fully turbulent in spite of the low Re_j. This fact is borne out by the measurements reported in Tables 4-7. The two helium/air jet experiments also give some insight into the penetration of a lighter jet into a heavier fluid medium.

Only U, u' and U_o, u_o' are measured in the confined jet experiments and these are obtained in the same x/D_j locations as before. If the jet terminates at a distance less than $x/D_j = 40$, the measurements are carried out to the point of termination only. The results for the air jet are reported in Tables 4 and 5, while the helium/air jet measurements are tabulated in Tables 6 and 7.

3.3 Test Conditions for Jets in Confined Swirling Flow

The primary purpose of the present experiment is to study the effect of density difference on turbulent mixing in a swirling environment. In order to achieve this objective, it is important to maintain all parameters, other than ρ_j/ρ_a, constant. This way, the effects due to density difference can be examined in detail. Air and helium are chosen for their large density difference. The geometry of the test facility is fixed and so is the swirl number. In a follow-on investigation, the swirl number will be changed to give the effects of swirl. As discussed in Sec. 2.4.2, the jets are made fully turbulent so as to eliminate the jet Reynolds number dependence. Also,

the upstream flow Re is maintained constant for all experiments. Since it is not possible to maintain both U_j and $\dot{M}_j/\dot{M}$ constant for different density gas jets, it is decided to configure the air and helium/air jet experiments so that in one case the U_j's are maintained approximately the same, while in another case, the ratio $\dot{M}_j/\dot{M}$ is set as close to each other as possible for both air and helium/air jets. The different conditions for both sets of experiments are summarized in Table 8. These experiments are all carried out at room temperature.

3.4 Air Jets in Confined Swirling flow

Three air jet experiments are carried out. The conditions are listed in Table 8. For the U_j = 25.4 m/s case, the $\dot{M}_j/\dot{M}$ ratio is the same as the helium jet experiment with U_j = 66.8 m/s. These jet velocities are chosen to minimize the Mach number effect. For the highest jet velocity investigated, the jet Mach number is close to .45. However, this case is only chosen to illustrate the dependence of the initial jet decay on the $\dot{M}_j/\dot{M}$ ratio. As a result, jet development in the x-direction is not investigated fully.

The other two cases, U_j = 25.4 and 66.8 m/s, are studied in detail and the measurements include both U, W, u', w' and U_o, u'_o, w'_o at the x/Dj locations picked out for the confined swirling flow experiment. Tabulated results are given in Tables 9-11. The U_o, u'_o measurements for the U_j = 152.8 m/s case are given in Table 9b while the profile measurements of U, u' at x/D_j = 2.9 and 27.4 are reported in Table 12.

3.5 Helium/Air Jets in Confined Swirling Flow

Only two experiments are carried out for the helium/air jet. The U_j's

chosen are 16.8 m/s and 36.5 m/s, respectively. Out of these two cases, one case has a $\dot{M}_j/\dot{M}$ ratio equal to 1/2 of the air jet experiment. Therefore, the effect of density on turbulent mixing in a swirling environment can be examined in detail. The measurements of U, W, u', w' and U_o, u_o', w_o' are again obtained at the same x/D_j locations, and the results are reported in Tables 13-15.

4. DISCUSSION OF RESULTS

The present study is the first part of a more complete investigation on isothermal mixing in an axisymmetric combustor. Therefore, it only reports on the fluid dynamics of the mixing phenomenon. Concentration distribution and the various turbulent flux measurements will be the subject of subsequent reports. The fluid dynamic properties reported in this study include both the mean flow behavior and the turbulent normal fluxes. These are limited to the measurements in the axial and circumferential directions only. Radial measurements are not made and therefore are not reported. In anticipation of the fact that these measurements could also be used to correlate turbulence models formulated for combustor flows, care is taken to report sufficient data at the inlet to the test section as well as at the outlet. However, due to test facility and diagnostic instrument arrangement, it is not possible to make measurements at x/D_j less than 1. Consequently, all measurements are made from $x/D_j = 1$ to $x/D_j = 40$. The last location is chosen because it corresponds to $x/D_T = 2.75$, which is about one-half the length of an actual gas turbine combustor. In a combustor, practically all reactions are completed at this point. Therefore, it is important to understand the mixing phenomenon at this location.

The objective of this study is not on confined jet mixing with stationary environment. Therefore, detailed study of this phenomenon has not been carried out. Whatever measurements made will only be used to help explain the effect of density difference on mixing in a swirling environment. As such, the data obtained on confined air and helium/air jets will not be examined separately. Rather, they will be examined in conjunction with the data on jets in confined swirling flow.

With this in mind, a clear presentation and discussion of the results can be made by dividing them into three separate sections: (1) confined swirling flow, (2) air jets in confined swirling flow and (3) helium/air jets in confined swirling flow.

4.1 Confined Swirling Flow

Measured U velocity profiles at different x/D_j stations, including the upstream location (Figure 10), are integrated across the tube to give the total volume flow rate at each location. Since there are no measurements closer to the tube wall than r = 59.5 mm for data downstream of the swirler, and r = 57.5 mm for data upstream, the integration is performed by assuming a linear velocity profile from this last point to U = 0 at the wall. Continuity is found to satisfy to within 7%. The average velocity, $\bar{U}$, determined for the upstream flow is 6.8 m/s, while for the downstream flow, it varies from a low of 7.06 m/s to a high of 7.65 m/s. This gives an average $\bar{U}$ of 7.04 m/s. This discrepancy between the measured $\bar{U}$'s could be due to variation in blower capacity. An effort has been made to determine the variation in blower capacity. It is found that the blower volume flow varies by as much as $\pm$ 8% about its nominal value over a period of one week. The nominal volume flow corresponds to a nominal U_{av} of 7.26 m/s. Given this condition, the variation in measured $\bar{U}$ is not too surprising because the upstream flow is obtained at a different date compared to the downstream measurements. It is also possible that the inadequate measurements of U(r) near the wall for the upstream flow is another source of error for this discrepancy. Because of these discrepancies, it is better to present the U(r) velocity profiles in Figure 18 with U(r) normalized by the local $\bar{U}$. Therefore, the integrated volume flow at

each station is normalized to one and continuity is satisfied. The u'(r) and w'(r) profiles are also normalized by the local $\bar{U}$ (Figure 20, 21); however, the W(r) profiles (Figure 19) are normalized with the nominal U_{av} of 7.26 m/s.

The swirler is designed to give a swirling flow with a flow angle equal to 66° immediately downstream of the swirler. This is achieved, as can be seen from Figure 11. Therefore, the swirling flow can be said to be characterized by a swirl number of S = 2.25. This is a very large swirl number and would lead to recirculation regions in the center of the tube. In the region investigated, that is $0 \leq x/D_T \leq 2.75$, two recirculation regions are observed; one very close to the swirler and one further downstream (Figure 18). The one close to the swirler only extends to $x/D_T = .1375$. On the other hand, the second recirculation region starts at about $x/D_T = 1$ and extends to beyond $x/D_T = 2.75$. It is not at all clear why there is no recirculating flow between $.206 \leq x/D_T \leq 1$ (Figure 18). Since the U measurements near the tube center are very small in the region $x/D_T < 1$, it is possible that measurement error could be the reason for the absence of the measured recirculation region in $.206 \leq x/D_T \leq 1$. However, upon repeated checking of the U measurements in this region, essentially the same result shown in Figure 18 is obtained.

Another reason for this behavior could be the presence of the center plate in the swirler, which extends from $r/R \simeq .069$ to $r/R \simeq .42$, and which affects the back pressure behind the swirler. As a result, the decline of U is substantially slowed down at the beginning of the center plate in the swirler (Figure 18). This slowing of the U decline is sufficient to decrease the recirculation region at $x/D_T < .206$ and eliminate it completely in the region $.206 \leq x/D_T \leq 1$. Further downstream, the effect of the plate is not felt by the flow and the recirculation region again appears in the tube

center, as shown by the U(r) profiles at x/D_T = 1.375 to x/D_T = 2.75 (Figure 18). The reverse flow could have originated from downstream infinity. However, this is not the concern of the present investigation, since the test region of interest is ~ 3 D_T long only, corresponding to about one-half the length of an actual combustor.

The fluid inside the test section rotates like a free vortex near the wall and like a solid body near the tube center. As a result, the presence of the center plate has little effect on the mean circumferential velocity (Figure 19) in the tube core ($0 \leq r/R \leq .32$). The slope of the solid-body rotation curve, $C = W/r$, at x/D_T = .069 is determined to be $C \simeq 811\ s^{-1}$ (Figures 19 and 38). However, this decays to $C \simeq 700\ s^{-1}$ at x/D_T = 2.75 (Figures 38). A decrease in C is physically consistent because after the swirl has completely decayed, fluid rotation inside the tube has to be identically zero. The region covered by the measurements is not long enough to allow a decay rate to be established for C. But, judging from the measurements at $x/D_T \cong .069$ and 2.75, one can conclude that the decay of C is quite rapid, at least in the initial period. This result does not agree with the measurements of Weske and Sturov (1974); however, in their experiment, the swirl is one of solid body rotation from tube wall to tube center.

The turbulence field produced by the swirler is not uniform. It has a peak at $r/R \simeq .75$ and a plateau in the region $.5 < r/R < .64$ (Figures 20, 21). The plateau, of course, is the consequence of the center plate in the swirler. As the flow evolves downstream, the initial change in slope of the U(r) profiles at $r/R \simeq .42$ leaves a permanent mark on the turbulence field and the plateaus in the turbulence distributions eventually evolve into local maxima. Although the mean flow swirling motion is responsible for mixing the highly turbulent fluid near the wall with the fluid in the tube center and produces a

fairly uniform turbulence field at $x/D_T = 2.75$ (Figures 20, 21), the peaks in u' and w' are still evident. This is probably due to excessive local production of turbulent energy arising from the rapid change in slope of the U(r) profile at or near $r/R \simeq .42$.

Nearly isotropic turbulence is produced by the swirler (Figures 20, 21). This is true for the greater part of the test section except in the region $x/D_T < .206$. The reason is the immediate downstream effect of the center plate on u. This anisotropic behavior decreases as the flow moves downstream. At $x/D_T = 2.75$, the data show that $u' \simeq w'$ over the region $0 \leq r/R \leq 1$.

4.2 Air Jet Experiments

As mentioned in Sec. 2.4.2, the volume flow through the jet is checked by two independent means. One is by measuring U_j using pitot-static probe at the jet exit plane and the other is obtained through a rotor-meter connected to the compressed air or helium supply line. Both techniques give a jet velocity accurate to $\pm$ 3% of the mean value. Therefore, the volume flow added to the tube due to the jet is fairly constant and ranges from 1.8% of the tube flow for the low velocity jet to 10% for the $U_j = 152.8$ m/s jet. This addition is fairly small and could not contribute to large variations in the volume flow in the tube.

The surprise came when the velocity profiles in the jet experiments are integrated as discussed in Sec. 4.1 to give the volume flow and hence $\bar{U}$ at each measuring station. It is found that $\bar{U}$ for the $U_j = 25.4$ m/s case varies from a low of 6.23 m/s to a high of 7.79 m/s, a variation of 11% about the average value of 6.89 m/s. On the other hand, the maximum and minimum values for the $U_j = 66.8$ m/s case are 8.20 m/s and 6.57 m/s, respectively. This

gives a variation of 11% about the average value of 7.27 m/s. The variation is larger than the observed blower variation of $\pm$ 8% about the mean, and cannot be explained away by the jet flow addition to the tube. However, repeat measurements give the same trend for the data but not necessarily the same values. Consequently, it is concluded that the volume flow variations have little effect on the trend of the data, except to change the level of the U(r) distributions. This difference in levels can be made to disappear if the normalized U(r) profiles are compared. Shown in Figure 37 are the $U(r)/\bar{U}$ profiles, at x/D_j = 1 and 40 for the air jet experiments. It can be seen that, except in the jet region, the profiles are in excellent agreement with each other. In view of this, the U(r), u'(r), w'(r) profiles are again normalized with the local $\bar{U}$ before presenting in Figures 28, 30-32, 34, 35. As for the W(r) profiles, they are again normalized with respect to the blower nominal U_{av} of 7.26 m/s. These are shown in Figures 29 and 33.

Before presenting the results of the air jet in swirling flow experiments, it is instructive to examine the behavior of the confined air jet. For confined jet flows, two limiting behaviors can be identified dependent on the test facility geometry. If the jet is issued into a confinement the cross-sectional area of which is not too large compared to the jet cross-sectional area, then the resultant flow downstream of the jet exit can be expected to resemble that found in flow through a sudden expansion (Eaton and Johnston 1980; Janjua et al 1983). As a result, recirculation regions would occur near the corners and flow reattachment is expected at ~ 10 step height downstream. No definitive value of the confinement to jet area ratio has been determined for such flow to occur. However, from the recent study of Janjua et al (1983), it seems that an area ratio as large as 4 still gives rise to a flow behavior similar to that found in sudden expansion. On the other hand,

if the area ratio is very large, the flow behavior downstream of the jet exit should resemble that of a free jet. The jet growth, of course, will be affected by the resultant axial pressure gradient created as a result of the confinement. However, the general features of the jet should be quite similar to those of free jets. One point is not clear though. That is, at what area ratio can one expect the flow behavior inside the confinement to change from sudden expansion flow to free jet flow. The confined air jet results are studied with this in mind.

The measured U(r) and u'(r) are shown in Figures 22 and 23. It can be seen that the jet-like behavior disappears quickly in the flow inside the tube, and a fairly uniform U profile is obtained at $x/D_j = 14$ (Figure 22). A recirculation region is observed between $x/D_j = 3$ and 10. Therefore, the flow behavior resembles that of a sudden expansion flow, even though in this case the area ratio is ~ 206. The turbulence intensity u' also decays quickly to a fairly uniform distribution at $x/D_j = 14$ (Figure 23), which is indicative of a sudden expansion flow.

The reason for this behavior is not quite clear. However, the following explanation can be offered for consideration. Stationary fluid inside the tube is being pushed by the incoming jet fluid. Because of the confinement and the large amount of fluid to be pushed by the jet, the resistance encountered by the jet is very large. As a result, the jet has to do work on the body of stationary fluid and its momentum is quickly dissipated. The body of fluid is set into motion by the action of the jet and at some distance downstream, the fluid in the tube would achieve a velocity equal to U_j/area ratio. For the present experiment, that velocity would be ~ .32 m/s. This is essentially achieved in the region measured (Figure 22). The highly dissipative nature of the flow is also reflected in the u' measurements. In

spite of the high turbulent energy production associated with the large U(r) gradient, the turbulence intensity is seen to decay very quickly. Therefore, the dissipation rate of k has to be much larger than the production rate of k. It is this highly dissipative behavior that distinguishes the present confined jet flow from a sudden expansion flow or a free jet flow.

The decay of U_o in the presence of external swirl for the U_j = 0, 25.4, 66.8, 152.8 m/s cases are shown in Figure 24. Shown also for comparison is the decay of the confined air jet in the absence of external swirl. It can be seen that the jet decay is very rapid and is substantially different from that of a free jet. A potential core region, where U_o is essentially constant, is practically non-existent for all the jets tested with or without external swirling flow. However, the decay of the jet in the absence of external swirl is quite a bit slower than in the presence of external swirl, at least in the region, $x/D_j < 10$, of the jet. The reason for this is rather clear. When swirl is present, the core flow rotates like a solid body and hence offers even more resistance to the jet flow. This increase in resistance leads to an even more rapid dissipation of the jet momentum and, in turn, leads to a faster disappearance of the jet. Therefore, the flow behavior is highly dissipative and the turbulence field of the swirling flow is not expected to be substantially affected by the jet. The reverse flow region near the tube center has completely disappeared (Figure 24). This result is not surprising, because the introduction of the jet is equivalent to adding more axial momentum to the swirling flow. The effective swirl number in the flow therefore decreases and this, in turn, leads to the disappearance of the recirculation region. Of course, the added mass flux of the jet will increase U_o of the swirling flow.

A more precise way of examining the decay of the jets is to replot the

results as shown in Figure 25. Here, U_j/U_e is plotted versus x/D_j. With the exception of a region bounded by $0 \leq x/D_j \leq 2$, the jet decay is essentially inversely proportional to x/D_j, or $U_e \alpha x^{-1}$. The slope of the curve U_j/U_e vs x/D_j for the jet in the absence of external swirl is clearly seen to be smaller than the cases with external swirl. However, its slope is seen to increase rapidly after $x/D_j = 10$. Jet decay in the presence of external swirl can be divided into two regions. The first is an initial region common for all jet velocities and the extent is a function of the jet velocity, U_j, or the ratio $\dot{M}_j/\dot{M}$. Of course, the larger U_j or $\dot{M}_j/\dot{M}$, the longer is this region because it would take longer to dissipate the initial momentum of the jet. The second region has a much smaller slope because the flow is essentially one of swirling flow in a tube for the two cases of U_j = 25.4 m/s and 66.8 m/s. Within experimental measurement error, it can be seen that the slope of the decay curve, U_j/U_e vs x/D_j, for the second region is the same for the two cases tested. Again, the extent of this region is a function of the jet velocity. For a given external swirling flow, the jet velocity or momentum essentially controls the jet decay behavior and the extent in which this behavior would last.

If the aforementioned conjecture concerning the highly dissipative nature of the flow is true, then one would expect u_o' and w_o' to decay rapidly to the confined swirling flow level in a fairly short distance. The results for u_o' and w_o' are presented in Figures 26 and 27, respectively, and they clearly show the rapid decay anticipated. For u_o', the distance taken by u_o' to reach the level typical of the confined swirling flow is dependent on the initial U_j or $\dot{M}_j/\dot{M}$ (Figure 26). Also, u_o' decays much faster in the presence of external swirl. Again, the reason is due to the increased resistance of the flow

arising from the solid-body rotation behavior. As a result, the flow is even more dissipative. For jets with very large U_j or $\dot{M}_j/\dot{M}$, u_o' decays to the level of the confined swirling flow at $x/D_j \simeq 40$ or $x \simeq 3D_T$.

While the decay of u_o' is a function of U_j, the decay of w_o' is not (Figure 27). The results show that for both the U_j = 25.4 m/s and 66.8 m/s jets, w_o' decay is complete at ~ 20 D_j. This is not true for the mean velocity U_o, though, because at x/D_j = 20, the jets are still in the second stage of decay (Figure 25). The jet-like behavior in the tube center disappears for all jets tested at $x/D_j \simeq 30$ (Figures 28, 32, 36). Therefore, it can be observed that the jet effects are practically negligible by the time the flow reaches $x/D_j \simeq 30$, in spite of the fact that u_o' for the U_j = 152.8 m/s jet is slightly higher than the u_o' of the confined swirling flow. However, u'(r) at $x/D_j \simeq 27$ (Figure 36) is fairly uniform and resembles that shown in Figure 20.

The normalized profiles of U(r), W(r), u'(r) and w'(r) for the two U_j = 25.4 m/s and 66.8 m/s jets and the dimensional profiles of U and u' for the U_j = 152.8 m/s jet are presented in Figures 28-36. Mean U(r) and the turbulence profiles are normalized with the local $\bar{U}$ determined from the U(r) measurements at each x/D_j locations. It can be seen that the recirculation region in the tube core has completely disappeared even for the case where $\dot{M}_j/\dot{M}$ = .071. This shows that a small amount of axial momentum (7% or less) applied in the form of a concentrated jet is enough to eliminate the recirculation region in a high swirl number flow (Figures 28 and 32). The finite U velocity at the centerline of the tube is just a consequence of the added mass flow introduced by the jet. Except for variations in the region around the jet, the normalized U(r) profiles at different x/D_j locations for the three cases, U_j = 0, 25.4, 66.8 m/s, are essentially identical (Figures 18, 28, 36). A comparison of the profiles at x/D_j = 1 and 40 is more clearly shown in Figure

37. Not only does Figure 37 show the invariant nature of the flow in the tube, it also gives credence to the claim that the measurements are very repeatable.

When the jet momentum is only ~ 7% of the swirling flow axial momentum, the jet has little effect on the W(r) distributions. The slopes of the W(r) = Cr curves in the core still decays from C $\simeq$ 811 s^{-1} at x/D_j = 1 to C $\simeq$ 700 s^{-1} at x/D_j = 40 (Figures 19, 29, 38). Once $\dot{M}_j/\dot{M}$ gets up to about .5, the solid-body rotation behavior in the inner region of the core is substantially affected by the jet (Figures 33 and 38). However, this effect altogether disappears when the flow reaches x/D_j = 40 (Figure 38). The reason for this is the strong axial momentum of the fluid at the tube center which acts to prevent the fluid from rotating. This, of course, violates the inner boundary condition for an axisymmetric swirling flow and leads to the near infinite slope for the W = Cr curve very near the center of the tube. Far away from the tube center, W = 811r can again be used to describe the solid-body rotation at x/D_j = 1. The extent of the jet influence is not large. It varies from $0 \leq r/R < .15$ at x/D_j = 1 to essentially zero at x/Dj = 28 (Figure 33).

The behavior of the turbulence field can be clearly identified into two regions for discussion; a jet region that extends to r/R $\simeq$ .25 and a tube region bounded by $.25 < r/R \leq 1$ (Figures 30, 31, 34, 35, 39, and 40). It seems that the jet has little or no effect on the flow in the tube region because the turbulence levels and the isotropic behavior of the turbulence field in this region are preserved. Therefore, irrespective of the amount of jet momentum input to the swirling flow in the tube, the turbulence field in the tube region remains unaffected. This is ample evidence that the flow is highly dissipative. Of course, the flow and turbulence field in the jet region are very much dependent on the initial jet momentum. Even then, the

jet region completely disappears by the time the flow reaches $x/D_j = 14$. This behavior is very similar to the confined jet behavior observed earlier. After $x/D_j = 14$, complete similarity of the turbulence field is observed for all air jet experiments. Not only that, the isotropic behavior of the flow is also very evident with or without the center jets. The repeatability of the turbulence measurements at $x/D_j = 1$ and 40 is agian demonstrated by the results shown in Figures 39 and 40. These results are very comforting because they reassure the accuracy of the present measurements and the technique used.

4.3 Helium/Air Jet Experiments

If the average swirler upstream velocity is taken to be 6.8 m/s as discussed in Sec. 4.1, the mass flow rate through the test section in the absence of any jet is ~ 103 gm/s. The mass flux addition to the test section due to air jets are respectively 4.8 gm/s and 1.8 gm/s for $U_j = 66.8$ m/s and 25.4 m/s. For helium/air jets, the mass fluxes are .50 gm/s and .31 gm/s, respectively, for the high and low jet velocities. In view of this small mass flux addition to the entire flow, the continuity check in the helium/air jet experiments is performed without taking this mass flux addition into account. The high, low and mean $\bar{U}$ found for the $U_j = 16.8$ m/s helium/air jet is 7.70 m/s, 6.75 m/s and 7.05 m/s, respectively. For the $U_j = 36.5$ m/s helium/air jet, the corresponding values are 7.83 m/s, 6.57 m/s and 6.97 m/s, respectively. These results are quite consistent with the air jet experiments. Consequently, the helium/air jet U(r) measurements are normalized in the same manner as discussed in Sec. 4.1 and are shown in Figures 47 and 51. Distributions of u'(r) and w'(r) normalized by $\bar{U}$ and W(r) profiles, normalized by $U_{av} = 7.26$ m/s are shown in Figures 48-50 and 42-54.

Comparison plots are given in Figures 55-57.

Before analyzing the behavior of the helium/air jet results, it is informative to estimate the importance of buoyancy in the present experiment. In the presence of swirl, the buoyant acceleration of a fluid particle is countered by a centrifugal acceleration. Since the former is only 9.8 m/s^2 while the latter is approximately 600 m/s^2 (assuming $W \simeq 6$ m/s) near the tube center, the ratio of these two accelerations is ~ 1/60. Therefore, buoyant effects can at most be ~ 2% of the centrifugal effects. Another indication that buoyancy is not important in the present experiment can be obtained by estimating the axial distance taken by a jet fluid particle to rise from the tube center to the wall. This distance can be approximated by $x = U_j t$. The time t is given by

$$(\rho_h + \frac{1}{2}\rho_a)\frac{d^2r}{dt^2} = g(\rho_a - \rho_h) \quad , \tag{9}$$

where g is the gravitational constant and the virtual mass dragged along by the helium particle is assumed to consist of air particles only. Therefore, solving (9) gives

$$\frac{x}{D_j} = \frac{U_j(R/.67g)^{1/2}}{D_j} \quad . \tag{10}$$

Since x is linearly proportional to U_j, buoyancy will be less and less important as U_j increases. If $U_j = 16.8$ m/s, $x/D_j \cong 190$ is obtained, or, in 40 D_j the helium particle will only rise by ~ .21R. Based on these estimates, it can be concluded that whatever resultant behavior the confined helium/air jet has in the presence of swirl, buoyancy is not the primary cause of this behavior.

If buoyancy effects are important, they would be most pronounced in the case of a low velocity confined helium/air jet. On the other hand, if the

highly dissipative nature of the confined jet flow dominates, then the jet would have disappeared long before the buoyancy effects could have taken hold on the flow according to (10). Therefore, in the confined helium/air jet experiment, the flow phenomenon could be further complicated by the introduction of buoyant acceleration. In order to maximize the effects of buoyancy and at the same time decrease the dissipation rate, it is decided to investigate the U_j = 16.8 m/s helium/air jet in detail rather than the high velocity helium/air jet. The results are shown in Figures 41 and 42. In spite of this, the centerline decays of both jets are also measured. Centerline measurements of U_o and u'_o are shown in Figures 43-45.

It can be seen that the jet centerline velocity decreases rapidly from 16.8 m/s at $x/D_j = 0$ to about 1 m/s at $x/D_j = 10$; the same kind of rapid decay is observed in the air jet experiment (compare Figure 41 to 22). This is too short a distance for the buoyancy effects to take hold on the fluid. Consequently, increased mixing due to buoyancy is not observed and the turbulence intensity of the jet decreases rapidly as a result of high dissipation in the flow (Figure 42). This rapid decrease in u' is clearly shown along the jet centerline (Figure 45). Basically, therefore, the behavior of the confined helium/air jet is similar to that of the confined air jet even though there is a large density difference between the jet and the surrounding fluid. In the case of the air jet, the final velocity attained by the fluid inside the confinement is U_j/(area ratio). For a helium/air jet, this velocity is further reduced by the density ratio so that it becomes approximately $U_j(\rho_j/\rho_a)$/(area ratio). If U_j = 16.8 m/s, the final velocity of the air inside the tube is ~ .025 m/s. At x/D_j = 16, the measured U_o is ~ .043 m/s, or about twice the terminal velocity. For the confined air jet experiment, U_o at x/D_j = 16 is ~ 1 m/s (Figure 24), which is about three times the terminal

velocity of .32 m/s. Since the jet momentum in the air jet experiment is ~ 53 times that of the helium/air jet experiment, it is reasonable to expect a longer decay to terminal state for the air jet experiment. The centerline measurements shown in Figure 43 for the helium/air jet at U_j = 36.5 m/s also reveal that it takes longer for this jet to decay to the terminal state.

Centerline velocities of the helium/air jets are shown in Figure 43. The results for the helium/air jets in confined stationary air are also presented for comparison. Unlike the results shown in Figure 24 for the air jets, the helium/air jets actually decay faster in the absence of swirl. This behavior can be explained by the following physical reasoning. In the presence of swirl, the lighter helium/air mixture is confined by heavier swirling air. An inward radial pressure gradient acts on the fluid particle to balance the outward angular momentum. Thus, a helium particle displaced outward to the surrounding air and carrying with it the original angular momentum will be prevented by the radial pressure gradient at the new location from further migration outward. As a result, mixing is hindered. Such a mechanism is not present in the absence of external swirl. This, therefore, accounts for the slower decay of helium/air jets in the presence of swirl.

In order to compare the helium/air jet decay to that of the air jets, the U_o data are replotted to show U_j/U_o vs x/D_j in Figure 44. Shown also are the two decay curves for the air jets. The helium/air jets also decay in two stages. The decay in both regions again obey the law $U_o \alpha x^{-1}$ and the slopes of these decay curves, to within experimental measurement error, are essentially the same for both the 16.8 m/s and 36.5 m/s jets. However, the slopes of the curves for both the first and second stages of decay are substantially smaller than the corresponding slopes for the air jets. One could possibly argue that the slower decay is due to the much smaller jet

momentum injected into the swirling flow. This, in turn, leads to less dissipation of the jet. However, this line of reasoning is not quite valid, because the helium/air jet with about the same momentum as the air jet still decays at a slower rate than the air jet. The same is also true of helium/air and air jets with about the same jet velocity. Therefore, the only physical reason that can account for this difference in behavior between the helium/air and air jets is the combined action of swirl and density difference. It is also interesting to note that the decay rate of helium/air jets in the absence of swirl is essentially the same as the initial decay rate of the confined air jet investigated (compare Figures 25 and 44).

Another consequence of the decrease in mixing between the jet fluid and surrounding air is the eventual levels of u_o' and w_o' reached by the 16.8 m/s and 36.5 m/s helium/air jets (Figures 45 and 46). Unlike the air jet cases, the eventual levels reached by u_o' and w_o' are not the same for all jets tested. The result actually reflects the continued presence of the jet in the flow because u_o' and w_o' for the high velocity jet is 50-100% higher than those for the low velocity jet. In spite of this, the near isotropic behavior of the turbulence field in the central core of the swirling flow is still preserved (Figures 49, 50, 53, 54).

Unlike the case of the air jets, the jet-like behavior of the flow in the tube core is clearly visible for both 16.8 m/s and 36.5 m/s helium/air jets (Figures 47 and 51). In addition, recirculating flow region is observed between the jet region and the external swirling flow. The existence of this region does not seem to depend on the initial jet velocity or momentum, and the size of this region is about the same as that found in confined swirling flow without any central jet. It seems that the recirculating flow region is being displaced by the jet from the tube center to the edge of the jet. This

observed behavior is a strong indication that jet mixing with the surrounding air is very much impeded. The controlling mechanism is, of course, due to the combined effects of density difference and swirling motion of the air particles. The behavior seems to be independent of the jet velocity or momentum. Of course, the swirl number, S, and the density ratio, ρ_j/ρ_a, are important parameters. For small S and large ρ_j/ρ_a, one would expect the jet velocity or momentum would also become an important factor in determining the resultant flow field. Another consequence of the strong swirl and small ρ_j/ρ_a is the near constant width of the jet after $x/D_j \simeq 20$. As a matter of fact, the jet width first increases and then decreases until the width becomes constant (Figures 47 and 51). Therefore, the main factors that cause the difference in behavior between the air and helium/air jets are those due to S and ρ_j/ρ_a. One could thus speculate that, for a given S, the jet would dissipate faster if $\rho_j/\rho_a > 1$, compared to the air jet case where $\rho_j/\rho_a = 1$.

The behavior of W(r) seems to depend very much on the jet velocity and not at all on the jet momentum (Figures 48 and 52). While the jet momentum for the 36.5 m/s helium/air jet is ~ 1/2 of that for the 25.4 m/s air jet, the W(r) profiles, especially in the core region where solid body rotation behavior persists, are similar to those obtained for the 66.8 m/s air jet. On the other hand, the W(r) profiles for the 16.8 m/s helium/air jet are very similar to those obtained for the air jet at about the same U_j (compare Figure 52 with 29). In addition, the W(r) profiles at $x/D_j = 40$ for the air jet cases with $U_j = 0$ and 25.4 m/s and for the helium/air jet case with $U_j = 16.8$ m/s are practically identical (Figure 57). In the air jet experiment, the distortions of the W(r) profile in the core region are completely erased by the time the flow reaches $x/D_j = 40$ (Figure 38). However, this is not true for the helium/air jet. Due to the decrease in mixing activity, the

distortion in the W(r) profile is still visible, even at $x/D_j = 40$ (Figures 48 and 57).

The near uniform distributions of u' and w' across the tube in the air jet experiments at $x/D_j = 40$ are not seen in the helium/air jet experiments (Figures 49 and 50). This is a consequence of the decreased mixing between the jet fluid and the surrounding swirling air. As a result, u', w' profiles in the core region resemble those seen in jets, while the profiles far away from the core resemble those found in wall flows; that is u', w' reach a maximum near the tube wall and decrease away from the wall. In the present results, the tube region with the lowest level of u' w' corresponds to the location where the center plate is found in the swirler (Figures 49 and 50). This behavior is seen also, but to a lesser extent, in the 16.8 m/s helium/air jet experiment (Figures 53 and 54). However, the measured u', w' are quite similar and the turbulence field is close to isotropic behavior.

The implication of all this is that, for combustors with swirling flow design, unless something is done to mix the product gases downstream of the first half of the combustor, the temperature and velocity profiles at the combustor exit will not be uniform. Dilution air jets located near the exit end of combustors actually serve two purposes. Besides lowering the gas temperature, they also serve to thoroughly mix the product gases and air and give rise to a uniform temperature and velocity distributions at the combustor exit.

5. CONCLUSION

Based on the results presented in Sec. 4, the following conclusions can be drawn. These are:

(I) Confined Swirling Flow

(1) A recirculation region exists in the core of the tube. For the particular swirl number, S = 2.25, the recirculation region starts at approximately one tube diameter downstream of the swirler.

(2) The swirling flow has very little decay, except in the solid-body rotation core, where the slope of W(r) decreases from 811 s^{-1} at $x/D_j = 1$ to 700 s^{-1} at $x/D_j = 40$.

(3) The initial high turbulence intensities, u' and w', near the tube wall quickly decay to the level in the tube core. This occurs in a distance less than three tube diameters.

(4) Judging from the measurements of u' and w', it can be seen that the swirler produces fairly isotropic turbulence. This isotropic property is preserved through the region measured. In addition, the turbulence becomes fairly uniform at about three tube diameters.

(II) Air Jets in Confined Swirling Flow

(1) Jets in confined flow with large area ratio are highly dissipative. This is because the jet momentum has to work against large resistance in the fluid due to confinement.

(2) Jet decay in a confined swirling flow environment can be delineated into two regions. In both regions, U_o decays like x^{-1}; however, the slopes are different. The initial decay has a much larger slope than the final decay. It is also found that for a given axial momentum of the swirling

flow the extent of each region is a strong function of the jet momentum.

(3) In all air jet cases investigated, the jet is completely dissipated in about 30 jet diameters or about two tube diameters downstream of the swirler. This, however, is independent of the jet momentum.

(4) The jets do not affect the slopes of W(r) in the solid-body rotation core when the jet momenta are small compared to the axial momentum of the swirling flow. This is no longer true when the jet momentum is about one-half of the swirling flow axial momentum. However, after the jet has been completely dissipated, the W(r) slope of the solid-body rotation core becomes the same as the case without any center jet.

(5) The decay of the W(r) slope in the solid-body rotation core from $x/D_j = 1$ to 40 is the same with or without air jets in the tube center.

(6) The jet augments the turbulence field only in a small region surrounding the jet. Beyond this region, the turbulence field is essentially the same as that in the confined swirling flow.

(7) In spite of the large jet momentum imparted to the flow, the turbulence field at $x/D_j = 40$ is essentially the same for all air jet cases investigated. Therefore, dissipation of the turbulence field in the region $1 \leq x/D_j \leq 40$ is very rapid, and is essentially controlled by the extent of the confinement.

(8) For the particular swirler investigated, near isotropic behavior and uniformity of u' and w' at $x/D_j = 40$ for all air jet cases investigated are observed.

(III) Helium/Air Jets in Confined Swirling Flow

(1) Helium/air jets in confined flow are also highly dissipative. However the rate of dissipation is a function of the jet momentum. In the two

cases investigated, the distance the jets take to reach terminal state is $< 30\ D_j$ and is about the same as that observed in confined air jets.

(2) In the presence of external swirl, the jet is preserved to beyond $x/D_j = 40$.

(3) While the recirculation region in the swirling flow is destroyed by the introduction of an air jet along the tube centerline, such is not the case when the jet fluid is lighter than air. Instead, the recirculation region is embedded between the jet and the external swirling flow.

(4) Since all the parameters, except the jet fluid density, governing the flow are the same, the difference in behavior between the air and helium/air jets is directly attributed to the combined action of swirl and density difference between the jet fluid and the external flow.

(5) The major mechanism is the radial pressure gradient which, in the case of a lighter fluid, acts to prevent the light fluid from diffusing outward to mix with the external heavier air. For air jets, since the density of the jet and external fluid is the same, the radial pressure gradient does not hinder mixing of the jet fluid.

(6) This behavior is also observed even when the jet momentum is $< 1\%$ of the swirling flow axial momentum. The predominance of the radial pressure gradient effect on isothermal variable density mixing is borne out.

(7) Because of this effect, uniformity of u' and w' distributions at $x/D_j = 40$ cannot be achieved. As a result, the peaks observed in u' and w' in the jet and near wall regions at $x/D_j = 1$ are also visible at $x/D_j = 40$.

(8) At low helium/air jet velocity, the W(r) distributions in the solid-body rotation core are not affected by the jet. Consequently, they are similar to those measured for the air jet experiments.

(9) At high helium/air jet velocity, the solid-body rotation core W(r) distributions are totally different. The reason for this is not known. It could be due to the hindrance of mixing that prevents the initially disturbed W(r) from recovering to the confined swirling flow W(r) distribution at $x/D_j = 40$.

(IV) Overall

(1) Swirling motion is an effective way of promoting mixing and this is especially the case for flows with a large swirl number. Therefore, the concept is most suitable for combustor design.

(2) However, uniform mixing can only be achieved if, and only if, the mixing gases have the same density.

(3) Since the density of the combustion products in a combustor is usually much lighter than that of the surrounding air, the present results show that uniform mixing in a combustor cannot be achieved without the help of strategically located dilution air jets in the combustor.

(4) The present investigation offers a reasonable explanation for the observed decrease in combustion efficiency in solid fuel ramjets subject to spin and for the requirement of dilution air jets at the exit end of gas turbine combustors.

6. FURTHER WORK

The present investigation gives a fairly complete and detailed account of the fluid dynamics behavior of different density gas jets in confined swirling flow. However, there are still many questions concerning the turbulence field behavior that need addressing. For example, it would be very beneficial to the present study if the dissipation rate of turbulence can be measured. This knowledge could help explain the highly dissipative nature of the flow observed in the experiments. Turbulent flux measurements of both mass and momentum would provide valuable information on the diffusion process and the effects of ρ_j/ρ_a and S on this process. In addition, the measurements could also be used to evaluate turbulence models for scalar transport and the calculations of swirling flows. The effects of varying S on the behavior of the helium/air jets are also of interest. In view of this, the following program of work is presently being carried out as a continuation of this study.

(1) A similar experiment is underway with a different swirler, where $S < 1$.

(2) An experiment to measure the concentration field in the present set-up is also underway. Quantities to be measured include the statistics of the concentration plus its probability density function. The present results are used to guide the selection of measuring locations for the concentration experiment.

(3) Having determined both the velocity and concentration field characteristics, the measurement of the turbulent mass and momentum flux distributions at selected locations will be carried out. The first attempt will

rely on the use of LDA and hot-wire concentration probes. A second attempt will be made with LDA/Raman or LDA/Rayleigh scattering technique.

(4) A fourth experiment is to study the dissipative nature of confined air jets. Hot-wire or LDA technique will be used to measure the terms in the dissipation rate function, in addition to the measurement of turbulent stresses. This experiment will be carried out for at least two different jet velocities.

REFERENCES

Abramovich, G.N., Yakovlensky, O.V., Smirnova, I.P. Sekundov, A.N. and Krasheninnikov, S. Yu. 1969 An investigation of the turbulent jets of different gases in a general stream. Astron. Acta 14, 229-240.

Alpinieri, L.J. 1964 Turbulent mixing of coaxial jets. AIAA J. 2, 1560-1567.

Batt, R.G. 1977 Turbulent mixing of passive and chemically reacting species in a low-speed shear layer. J. Fluid Mech. 82, 53-95.

Becker, H.A., Hottel, H.C. and Williams, G.C. 1967 The nozzle-fluid concentration field of the round, turbulent, free jet. J. Fluid Mech. 30, 285-303.

Birch, A.D., Brown, D.R., Dodson, M.G. and Thomas, J.R. 1978 The turbulent concentration field of a methane jet. J. Fluid Mech. 88, 431-449.

Brown, G.L. and Roshko, A. 1974 On density effects and large structure in turbulent mixing layers. J. Fluid Mech. 64, 775-816.

Buchhave, P. and George, W.K. 1978 Bias Corrections in turbulence measurements by the laser Doppler anemometer. Proceedings of the Third Workshop on Laser Doppler Anemometry, Purdue University, W. Lafayette, Ind. (W. Stevenson ed.).

Buchhave, P., George, W.K. and Lumley, J.L. 1979 The measurement of turbulence with the laser Doppler anemometer. Annual Review of Fluid Mechanics, 11, 443-503.

Cheng, W.K. 1978 Turbulent mixing in swirling flow. MIT GT and PDL Rept. 143.

Chriss, D.E. 1968 Experimental study of turbulent mixing of subsonic axisymmetric gas streams. Arnold Engineering Development Center, AEDC-TR-68-133.

D'Souza, G.J. 1968 Measurement of turbulent correlations in a coaxial flow of dissimilar fluids. NASA CR-960.

Eaton, J.K. and Johnston, J.P. 1980 Turbulent flow reattachment: an experimental study of the flow and structure behind a backward-facing step. Stanford University, Thermoscience Div. Rept MD-39.

Erdman, J.C. and Gellert, R.I. 1976 Particle arrival statistics in laser anemometry of turbulent flow. Appl. Phy. Lett. 29, 408-411.

George, W.K. 1976 Limitations to measuring accuracy inherent in the laser Doppler signal. Proceedings of the LDA Symposium, Copenhagen, P.O. Box 70, 2740 Skovlunde, Denmark, 20-63.

George, W.K. 1978 Processing of random signals. Proceedings of the Dynamics Flow Conference, Marseille, France, 757-793.

Habib, M.A. and Whitelaw, J.H. 1979 Velocity characteristics of a confined coaxial jet. J. Fluids Eng. 101, 521-529.

Habib, M.A. and Whitelaw, J.H. 1980 Velocity characteristics of confined coaxial jets with and without swirl. J. Fluids Eng. 102, 47-53.

Hesel, W. and Rodi, W. 1977 New biasing elimination method for laser Doppler velocimeter counter processing. Rev. Sci. Instru. 48, 910-919.

Janjua, S.I., McLaughlin, D.K., Jackson, T.W. and Lilley, D.G. 1983 Turbulence measurements in confined jets using a rotating single-wire probe technique. AIAA J. 21, 1609-1610.

Johnson, B.V. and Bennett, J.C. 1981 Mass and momentum turbulent transport experiments with confined coaxial jets. NASA CR-165574.

Melinand, J.P. and Charnay, G. 1978 Digital analysis of LDA counter signals in separated boundary layer. Proceedings of the Dynamics Flow Conference, Marseille, France, 909-916.

Reynolds, A.J. 1976 The variation of turbulent Prandtl and Schmidt numbers in wakes and jets. Int. J. Heat Mass Transfer 19, 757-764.

Ricou, F.P. and Spalding, D.B. 1961 Measurements of entrainment by axisymmetrical turbulent jets. J. Fluid Mech. 11, 21-32.

Schetz, J.A. 1980 Injection and mixing in turbulent flow. Progress in Astro and Aero. 68.

Sforza, P.M. and Mons, R.F. 1978 Mass, momentum, and energy transport in turbulent free jets. Int. J. Heat Mass Transfer 21, 371-384.

Stanford, R.A. and Libby, P.A. 1974 Further applications of hot-wire anemometry to turbulence measurements in helium-air mixtures. Phys. Fluids 17, 1353-1361.

Tan, C.S. 1980 An experimental study of the effects of swirl and density difference on mixing in shear flows. MIT GT and PDL Rept. 153.

Vu, B.T. and Gouldin, F.C. 1980 Flow measurements in a model swirl combustor. AIAA Paper No. 80-0076.

Way, J. and Libby, P.A. 1970 Hot-wire probes for measuring velocity and concentration in helium-air mixtures. AIAA J. 8, 976-978.

Way, J. and Libby, P.A. 1971 Application of hot-wire anemometry and digital techniques to measurements in a turbulent helium jet. AIAA J. 9, 1567-1573.

Weske, D.R. and Sturov, G.Ye. 1974 Experimental study of turbulent swirled flows in a cylindrical tube. Fluid Mech. - Soviet Res. 3, 77-82.

Yajnik, K.S. and Subbaiah, M.V. 1973 Experiments on swirling turbulent flows. Part 1. Similarity in swirling flows. J. Fluid Mech. 60, 665-687.

Zakkay, V., Krause, E. and Woo, S.D.L. 1964 Turbulent transport properties for axisymmetric heterogeneous mixing. AIAA J. 2, 1939-1947.

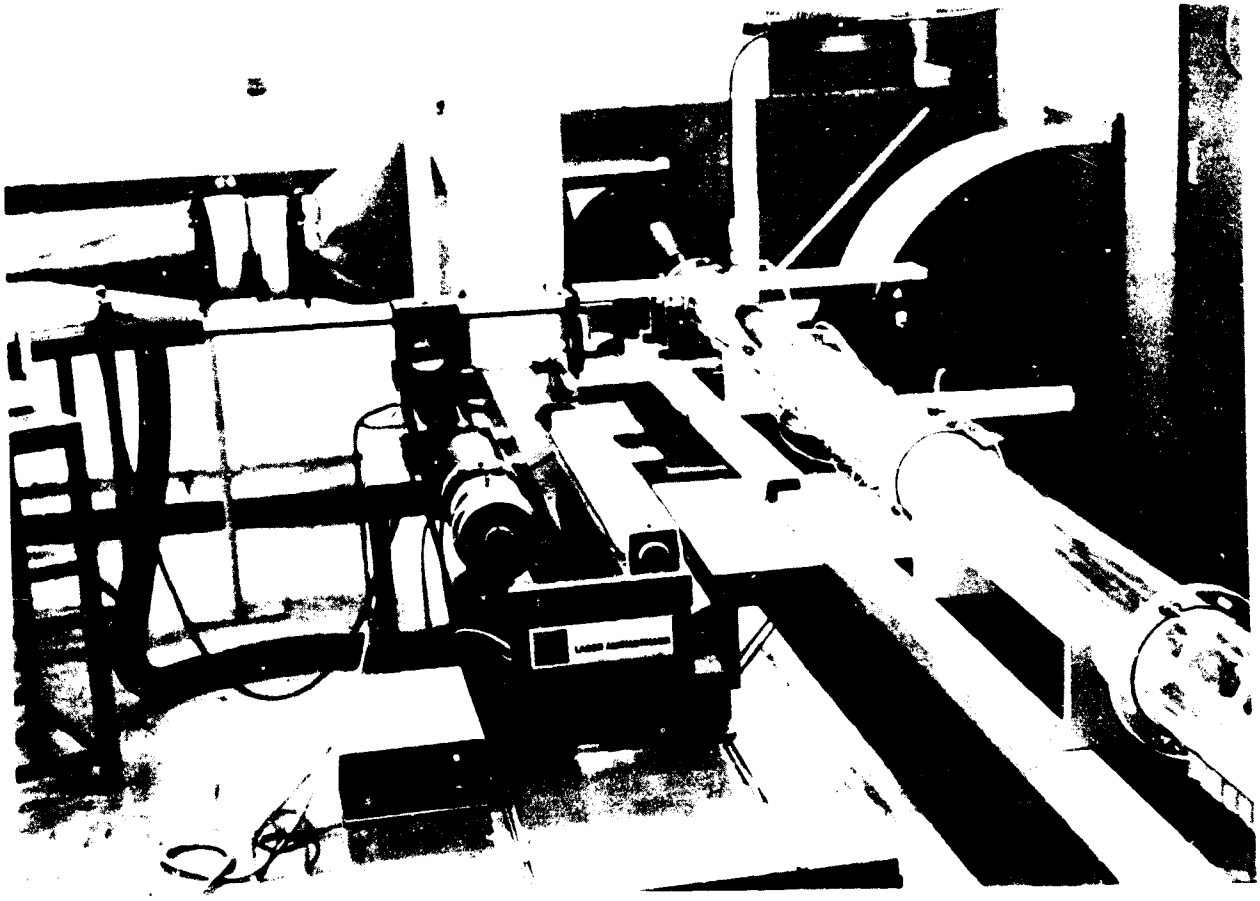

Figure 1. Test Facility Showing LDA Diagnostic and Test Section.

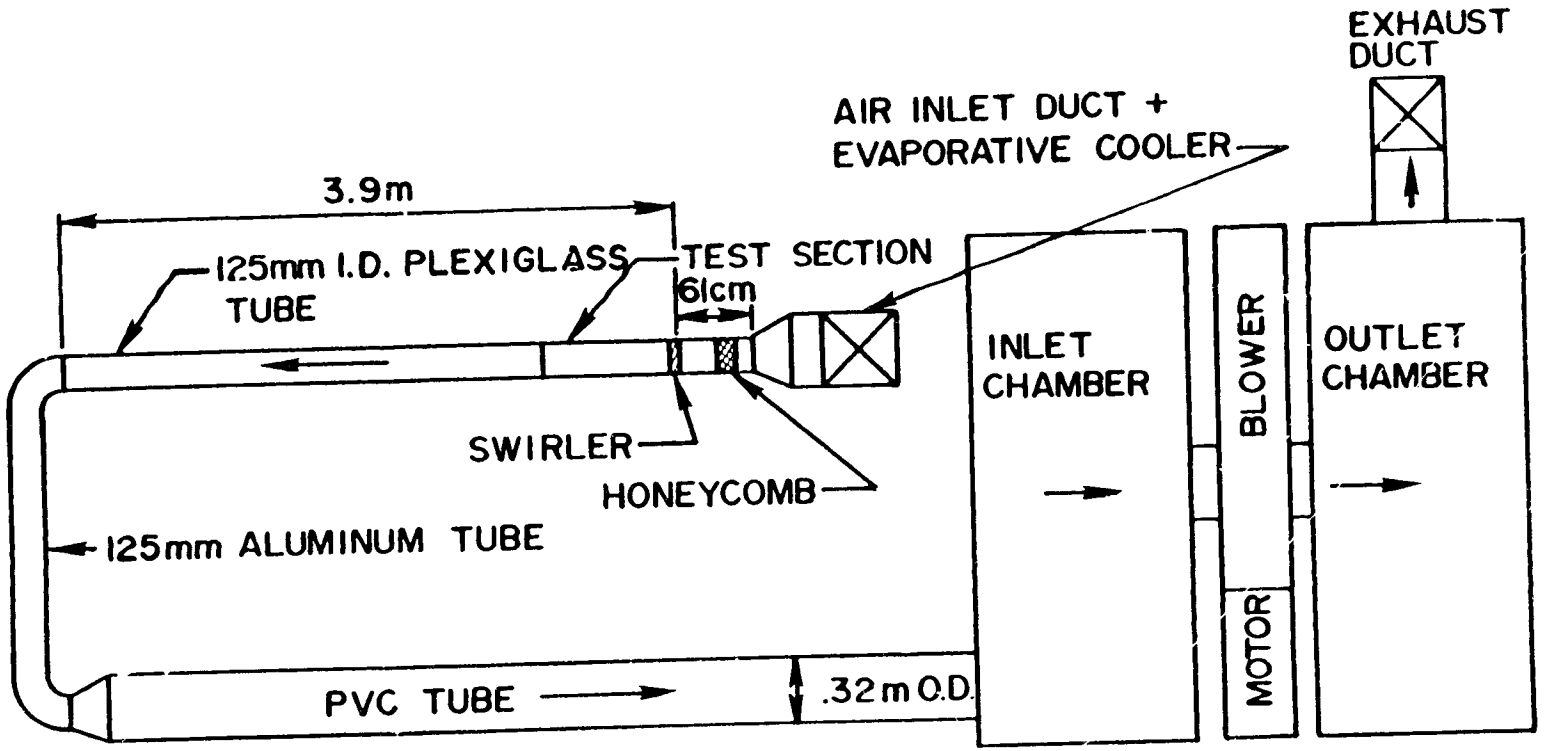

Figure 2. Schematic of Test Facility.

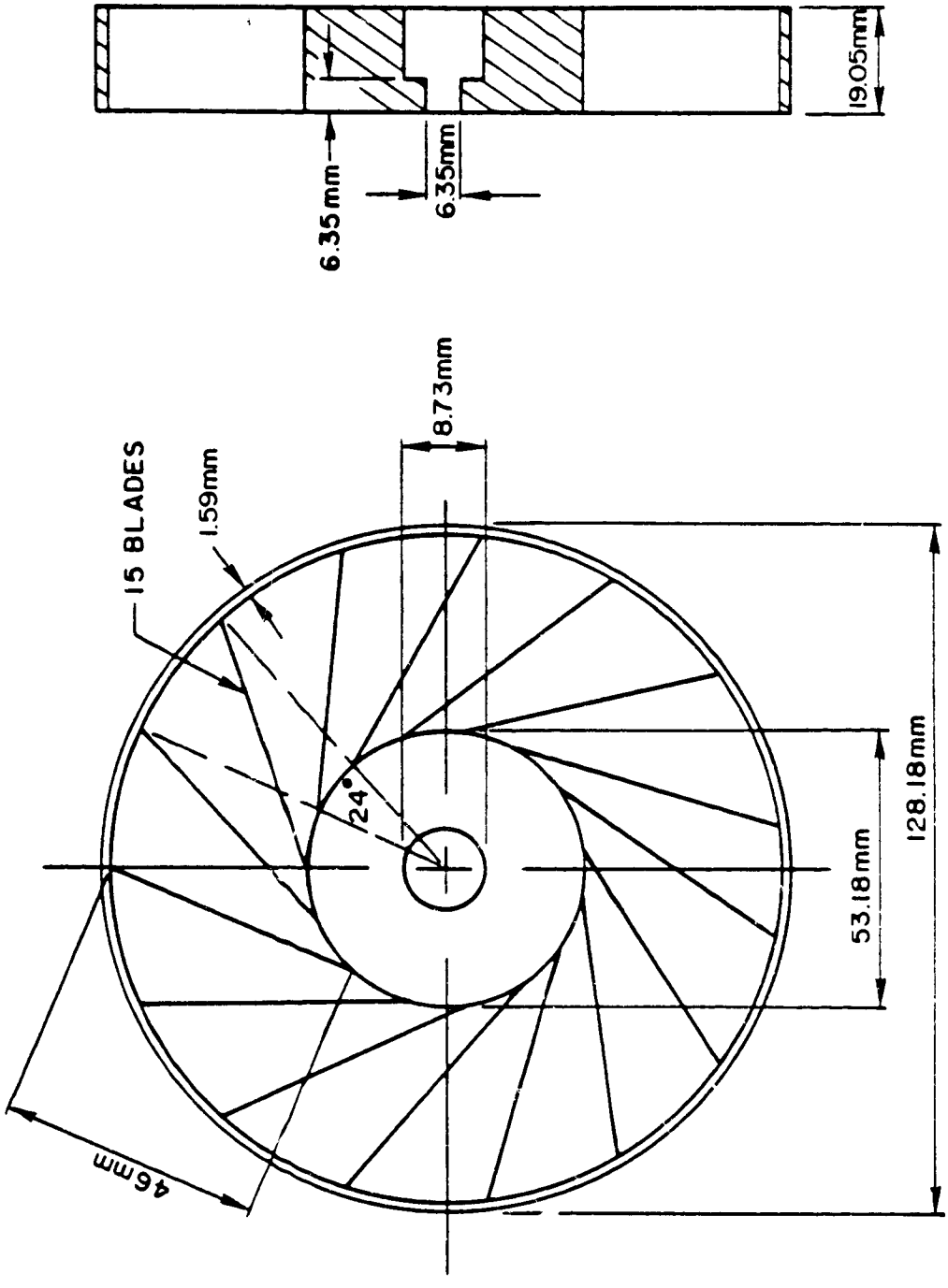

Figure 3. Details of Swirler Geometry.

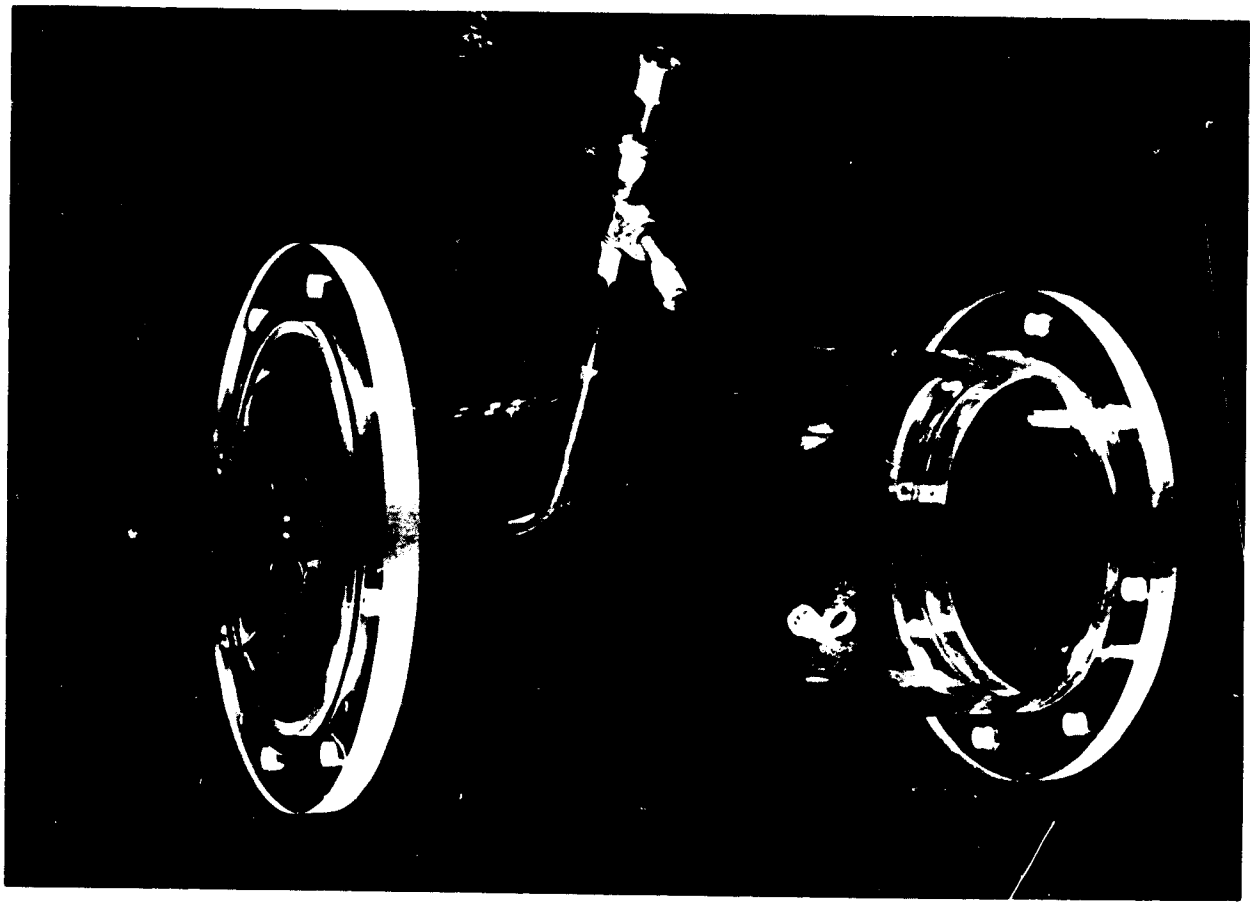

Figure 4. Test Swirler.

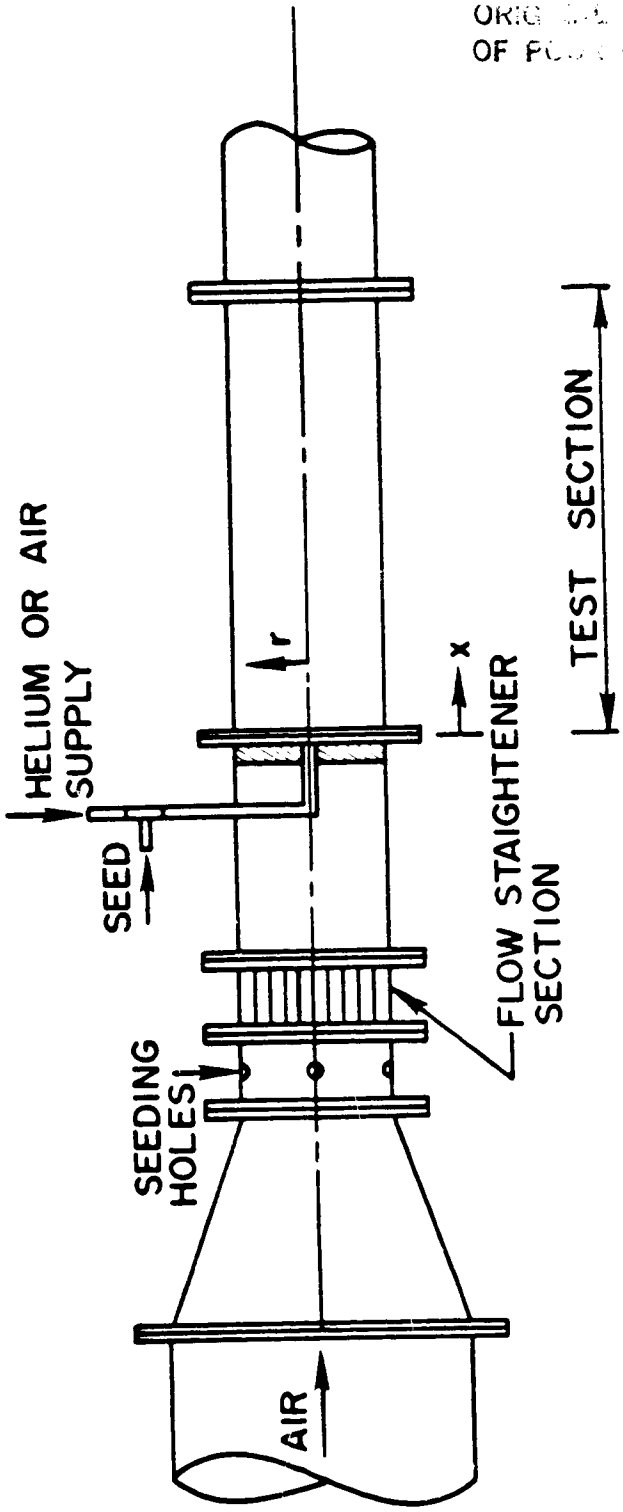

Figure 5. Details of Test Section.

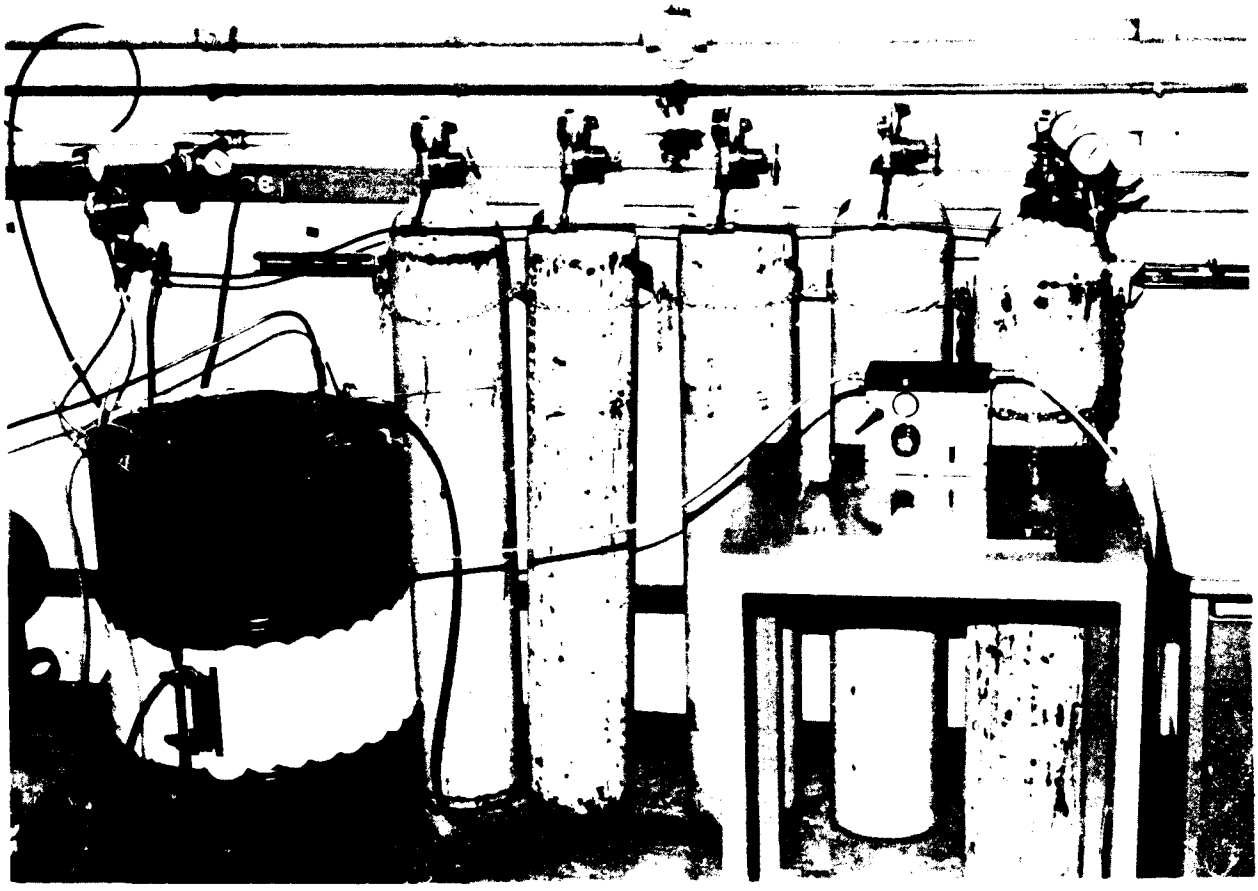

Figure 6. Helium Bottles and Heat Exchanger.

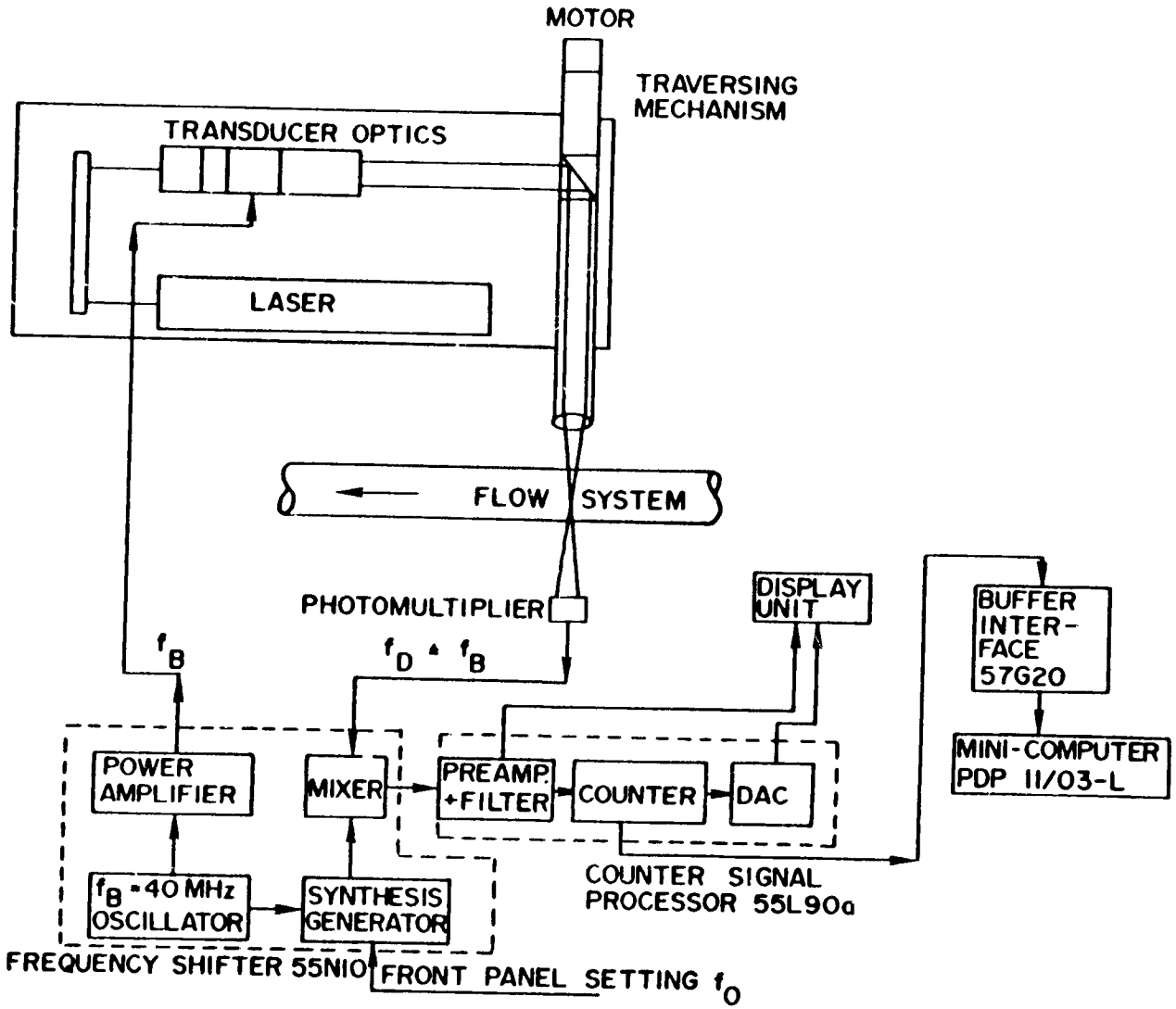

Figure 7. Block Diagram of the LDA and Data Acquisition System.

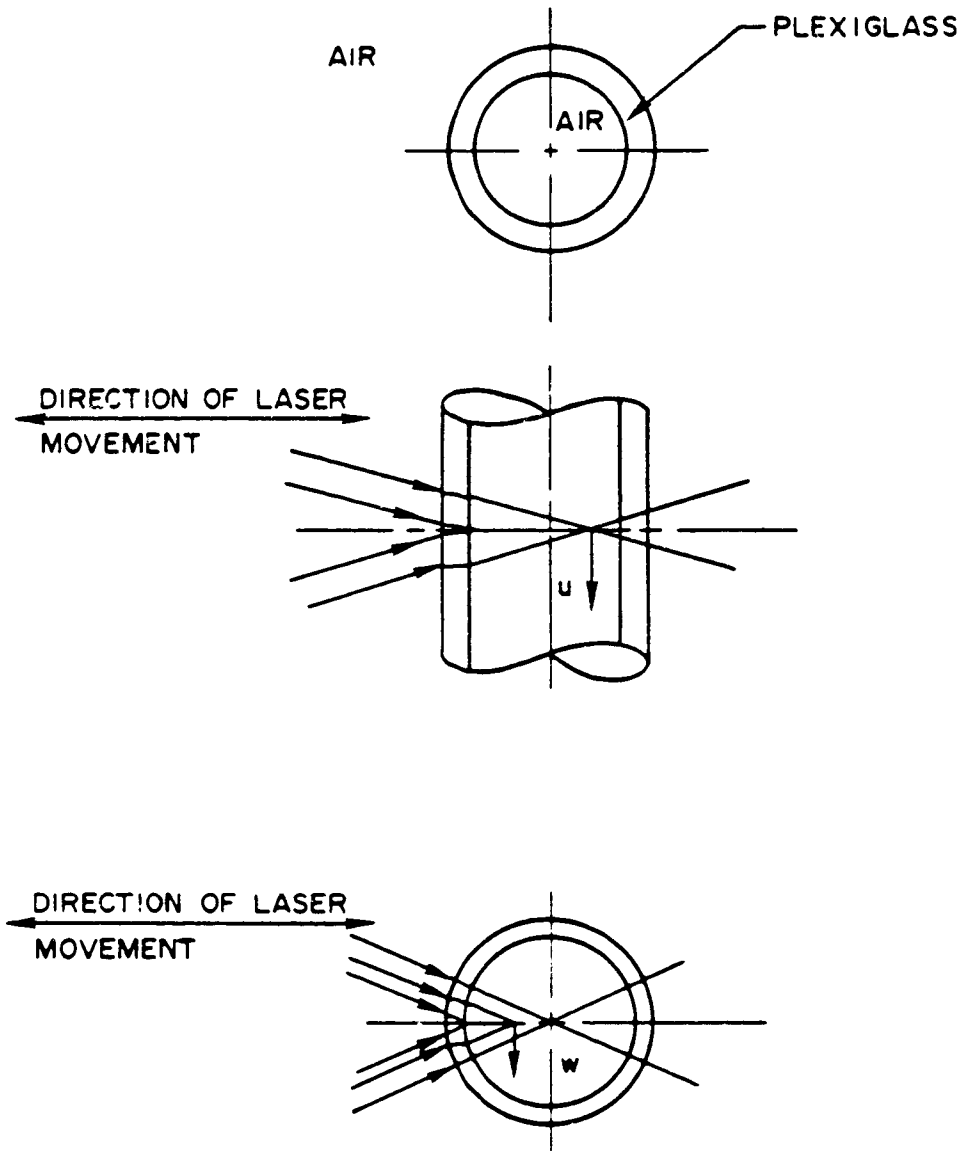

Figure 8. Schematic Showing the LDA Measurement of u and w.

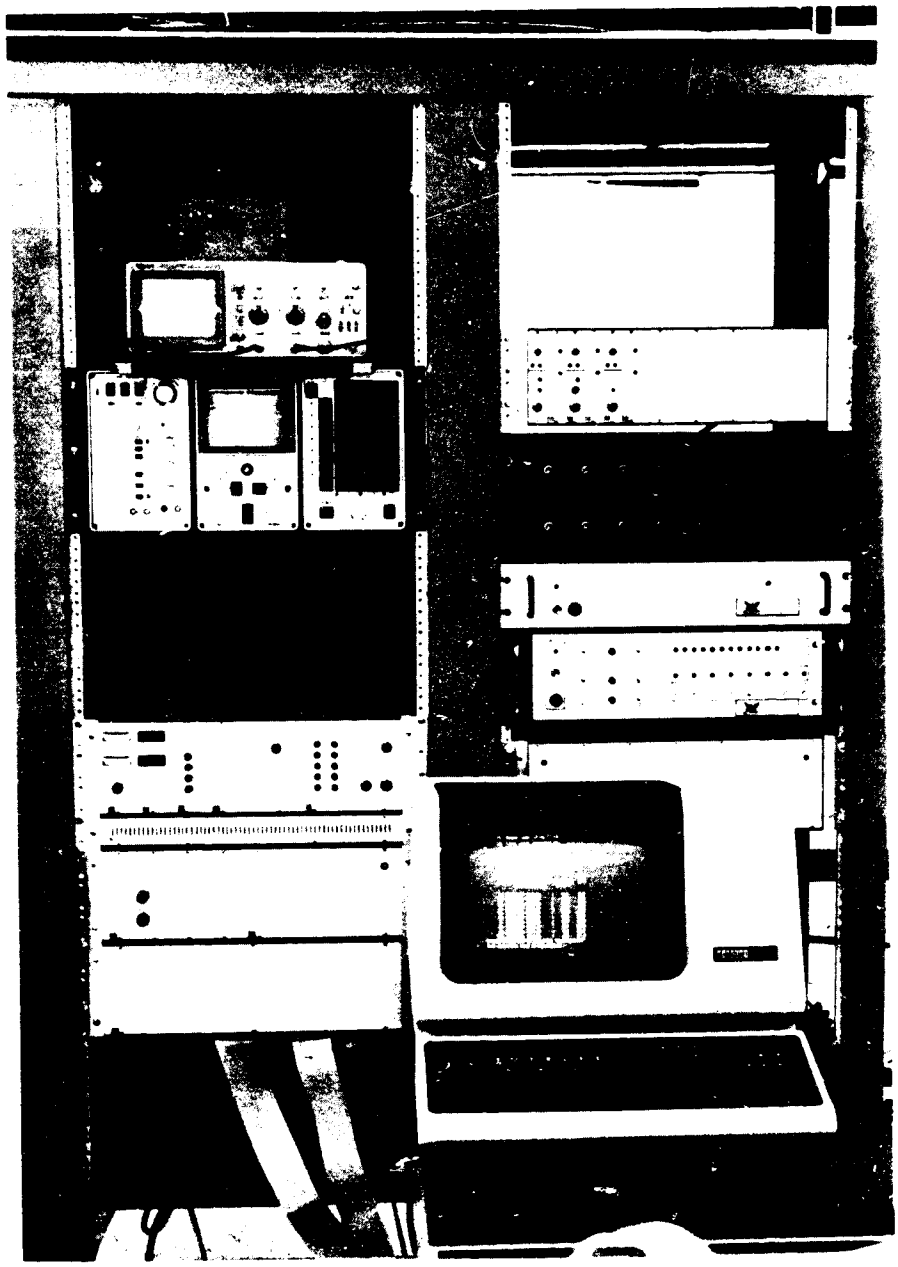

Figure 9. Instrument Panel.

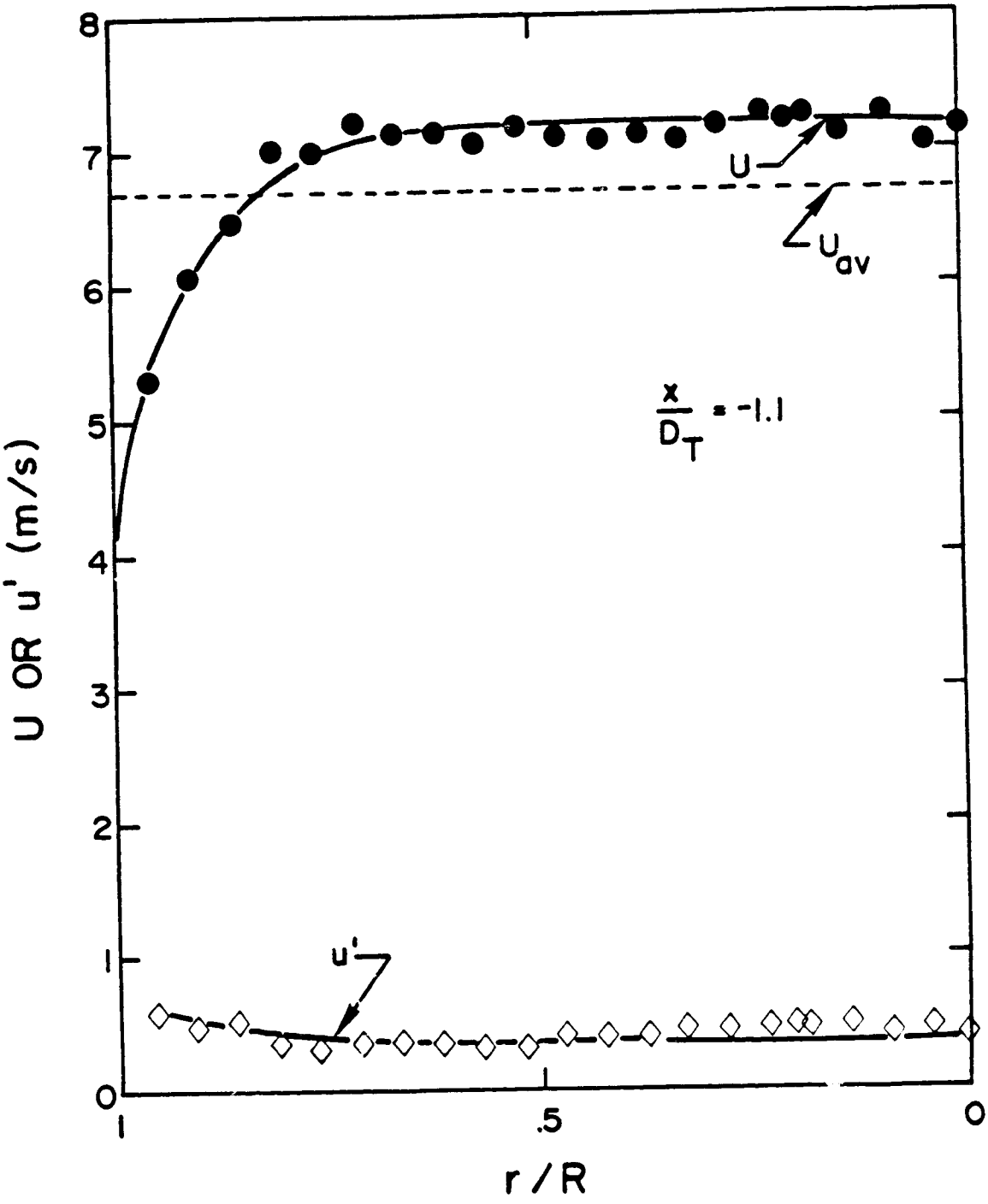

Figure 10. Flow Characteristics Upstream of Swirler.

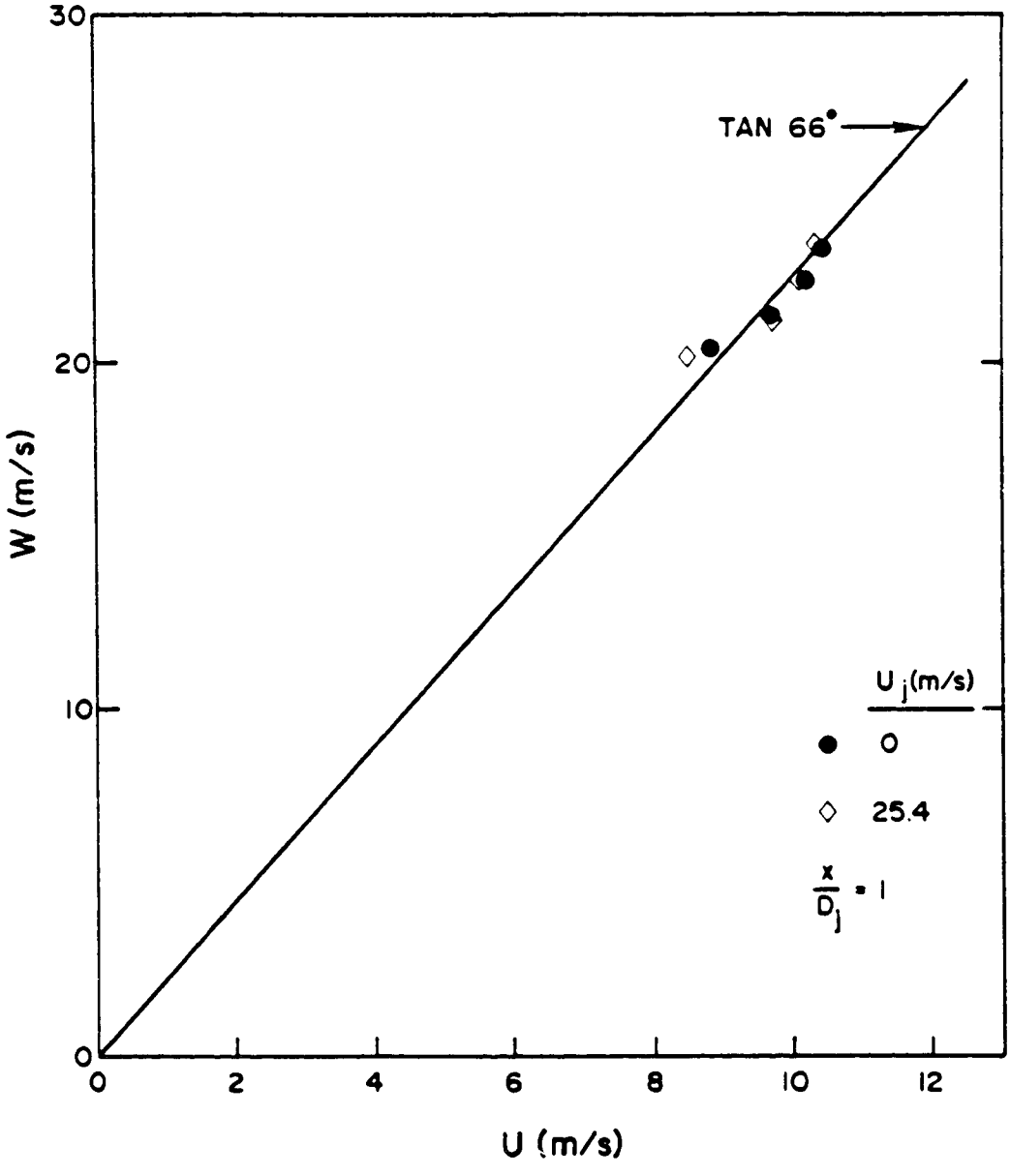

Figure 11. A Plot of W versus U.

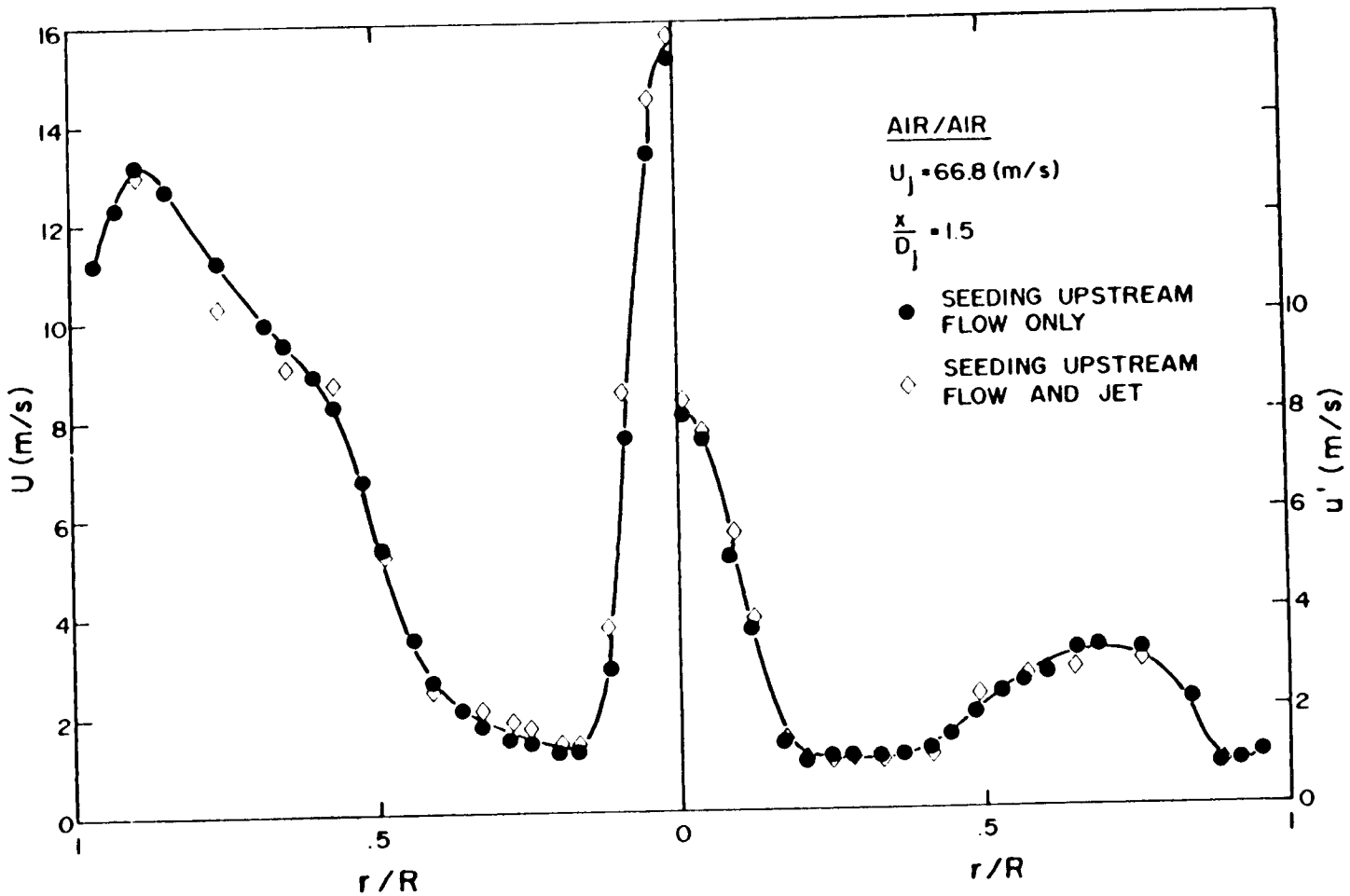

Figure 12. Effects of Different Modes of Seeding on Velocity Measurements.

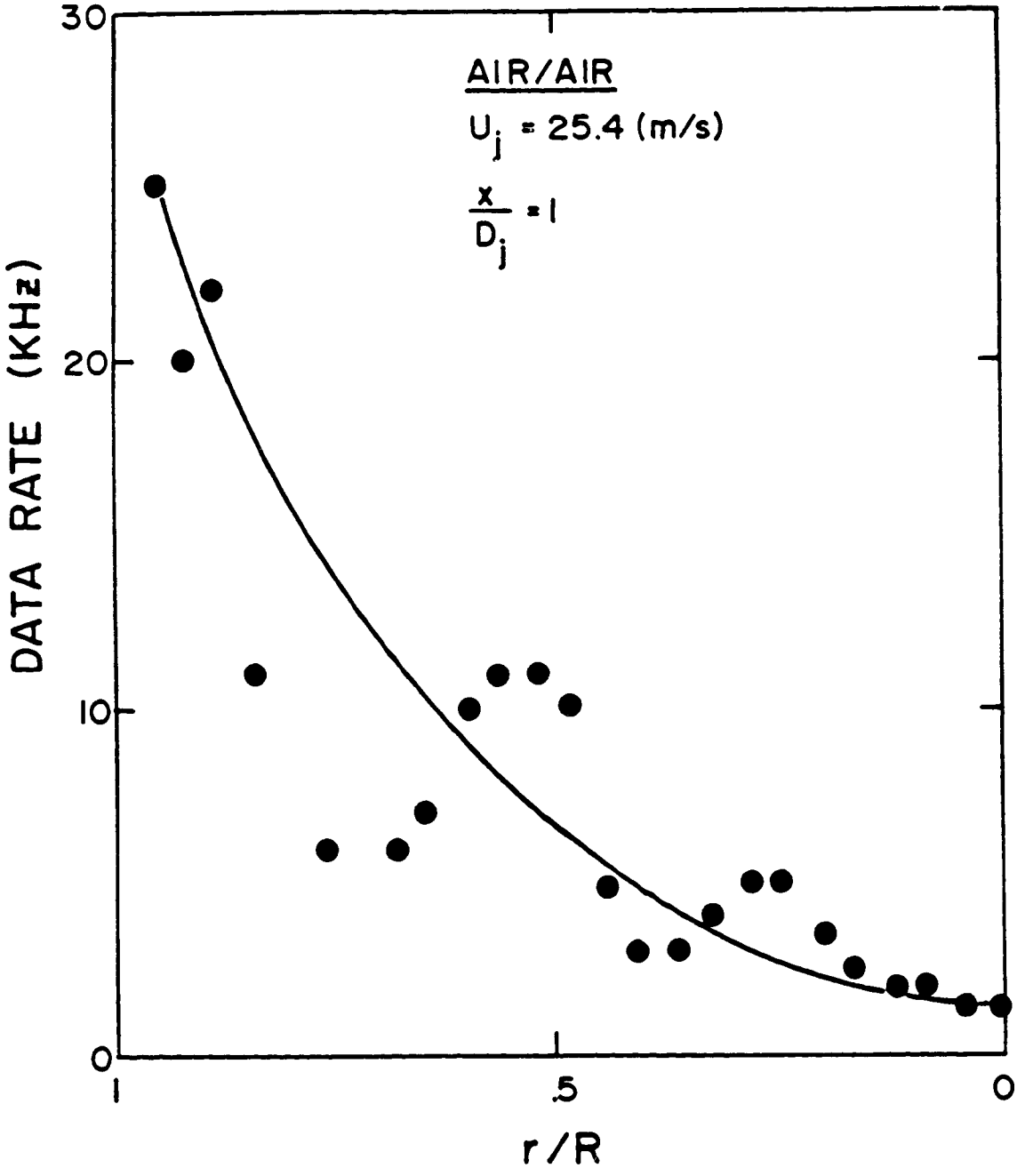

Figure 13. Typical Data Rate Distribution Across Tube Radius.

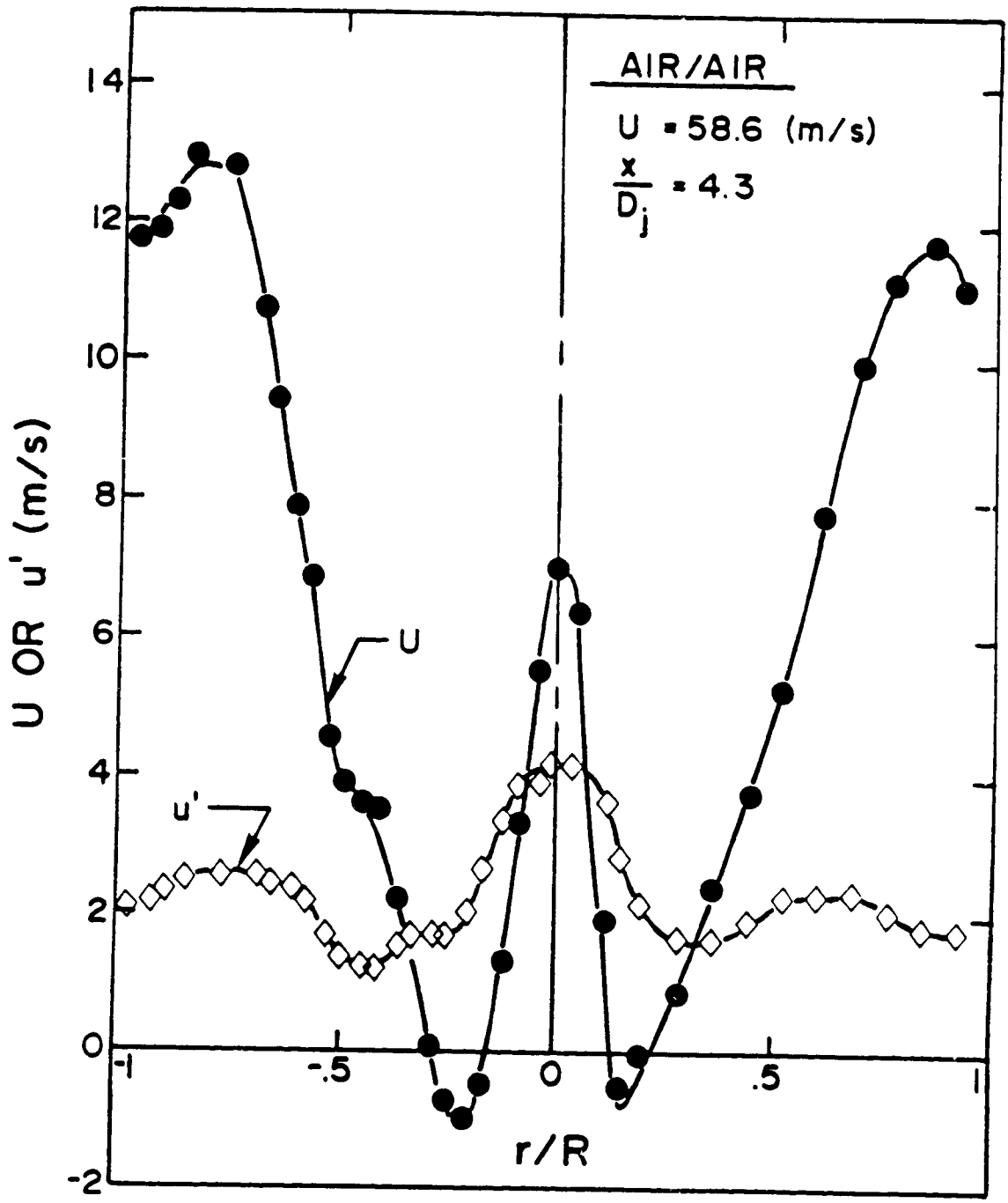

Figure 14. Symmetry Check on Flow and Turbulence Field at $x/D_j = 4.3$; $U_j = 58.6$ m/s.

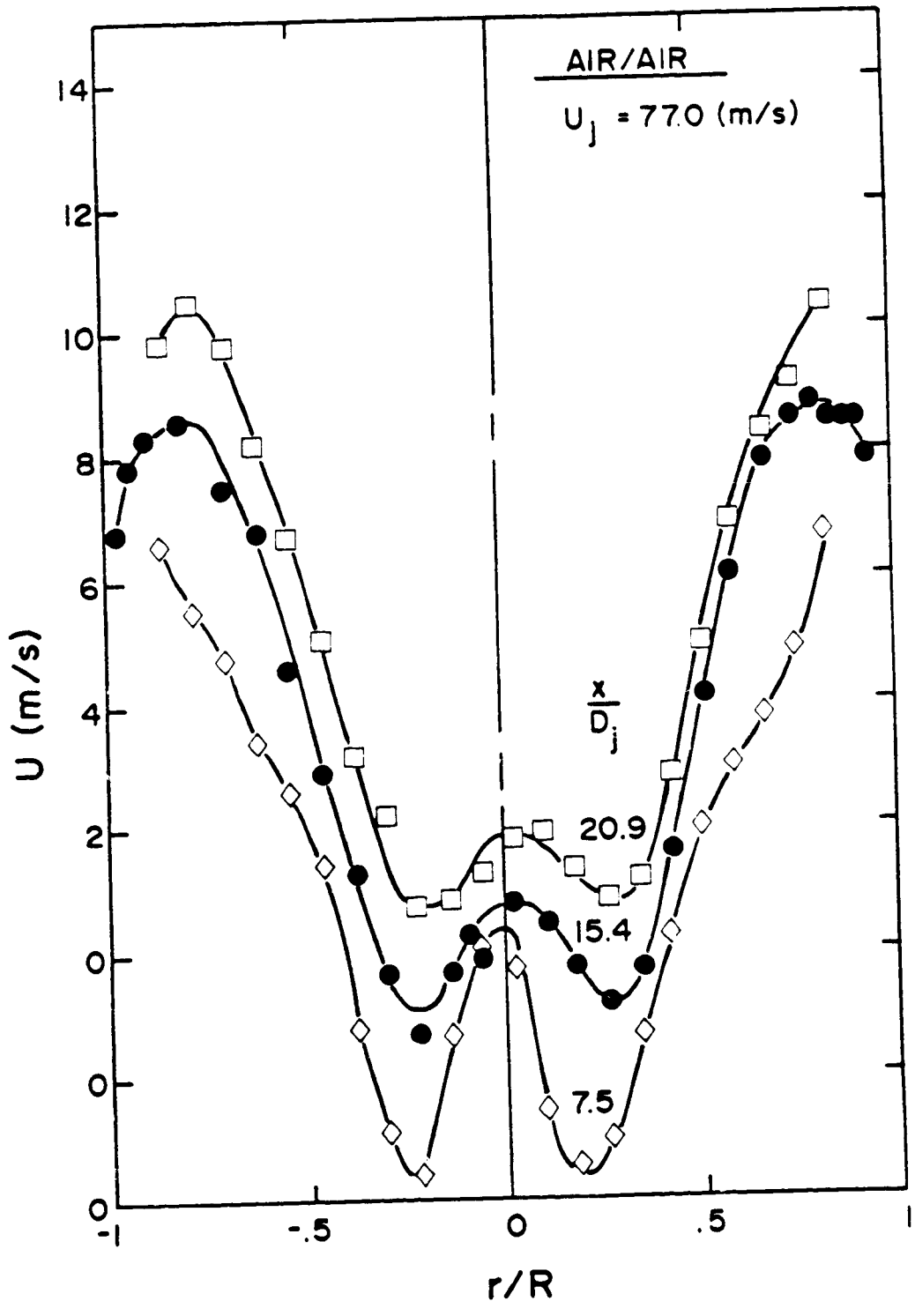

Figure 15. Symmetry Check on Flow at Three Different x/D_j Locations; U_j = 77.0 m/s.

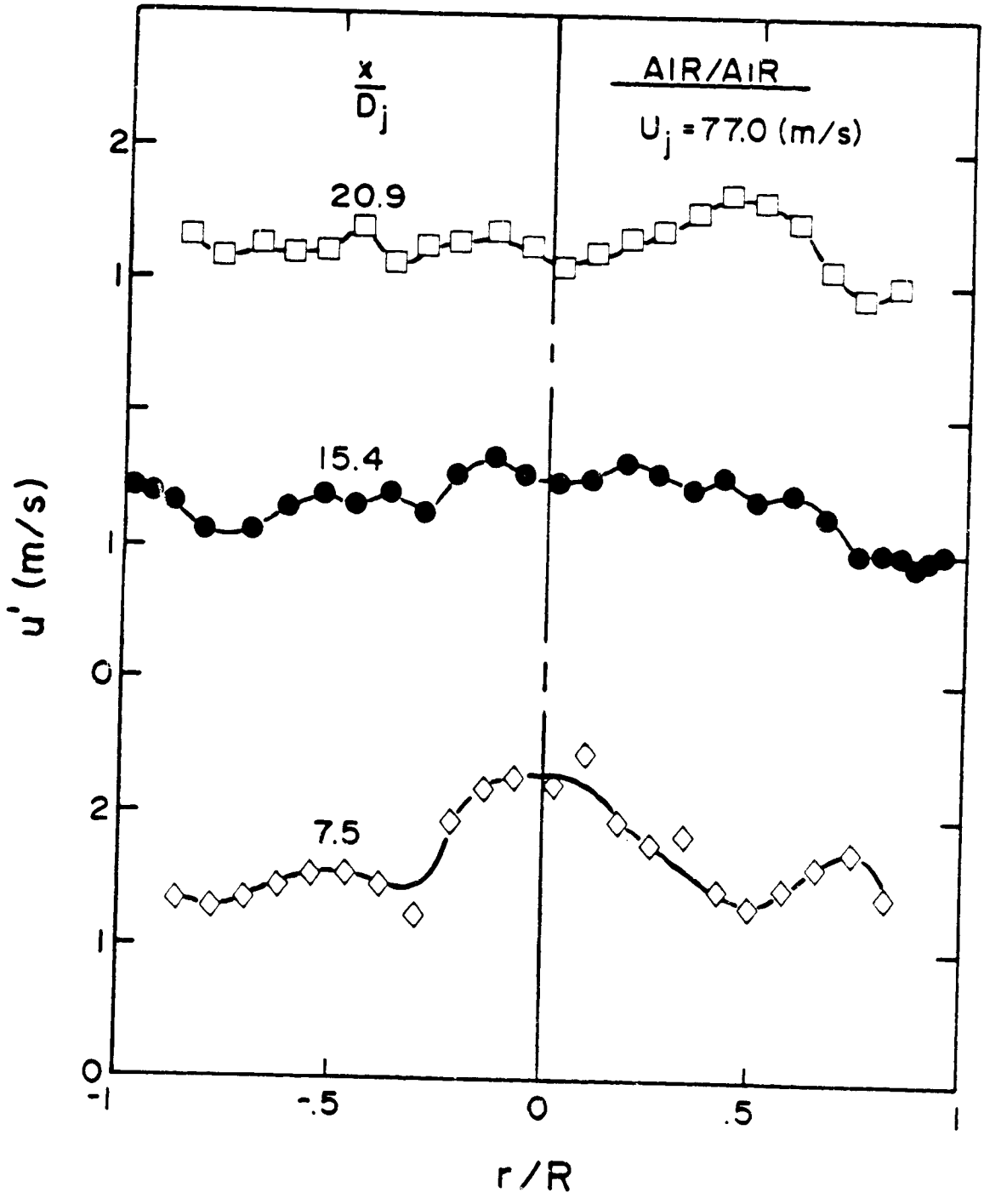

Figure 16. Symmetry Check on Turbulence Field at Same Conditions as Figure 15.

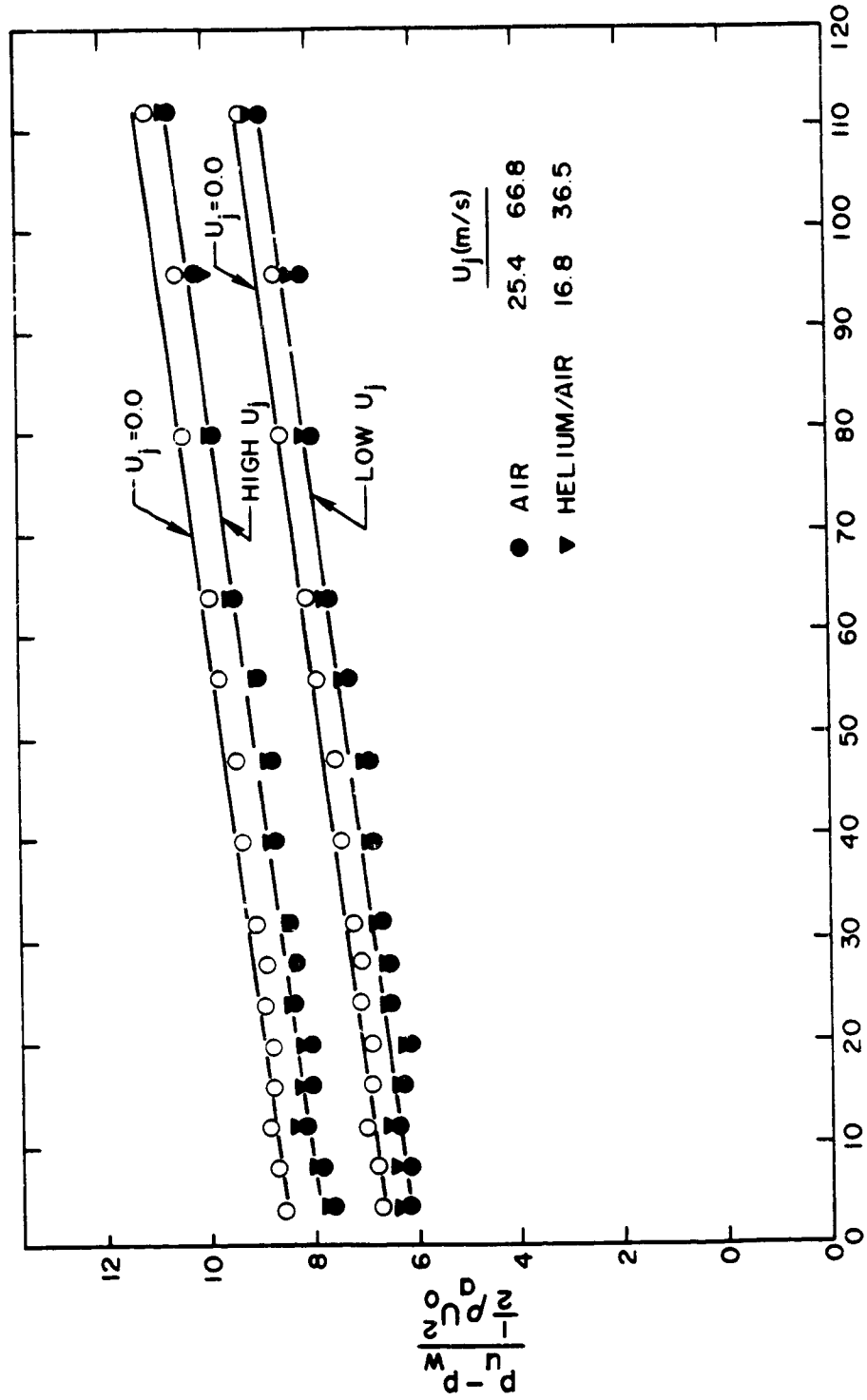

Figure 17. Wall Static Pressure Drop Along Tube Axis.

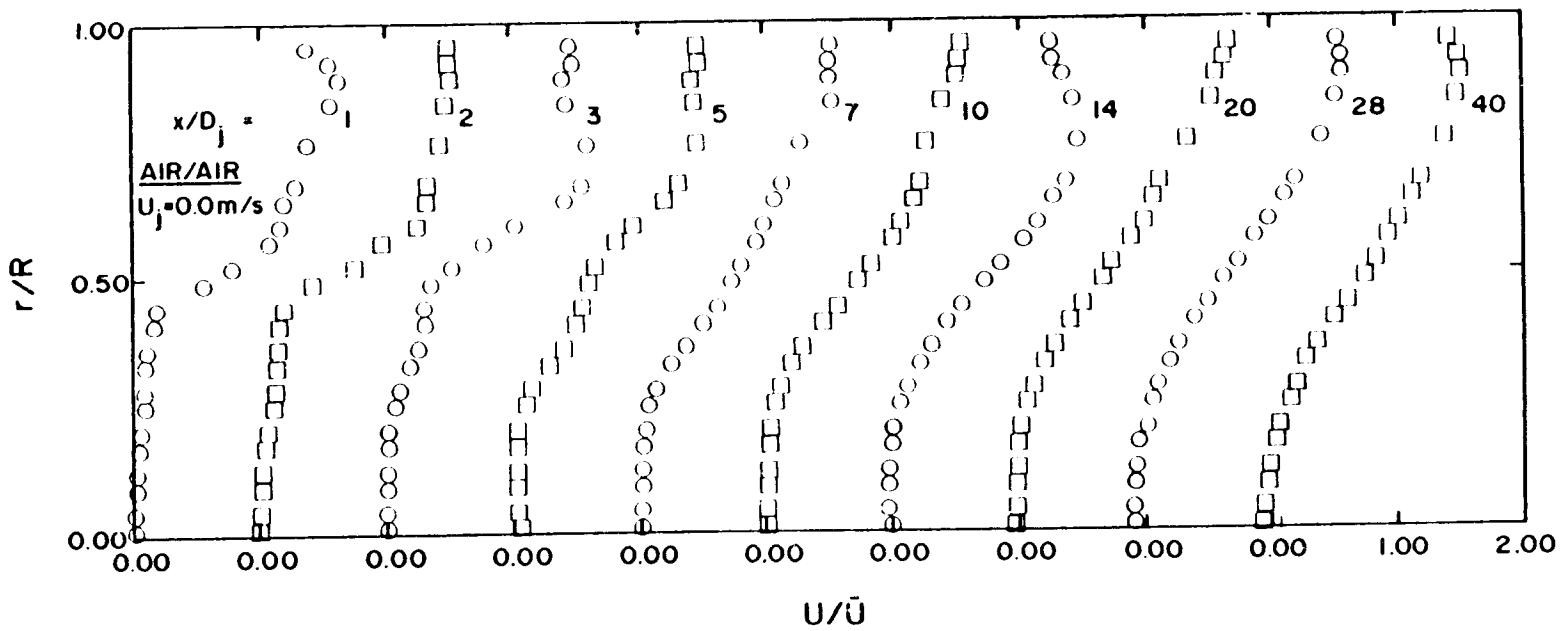

Figure 18. Evolution of U Distributions for the U_j = 0 Case.

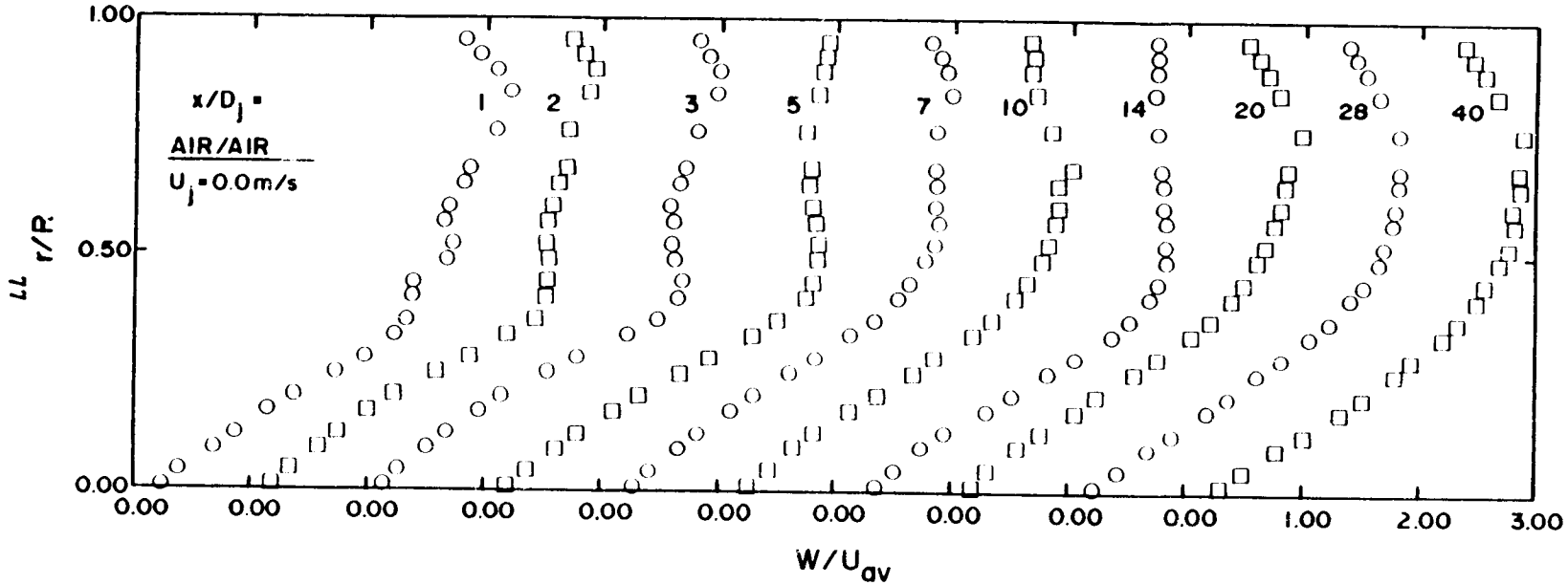

Figure 19. Evolution of W Distributions for the U_j = 0 Case.

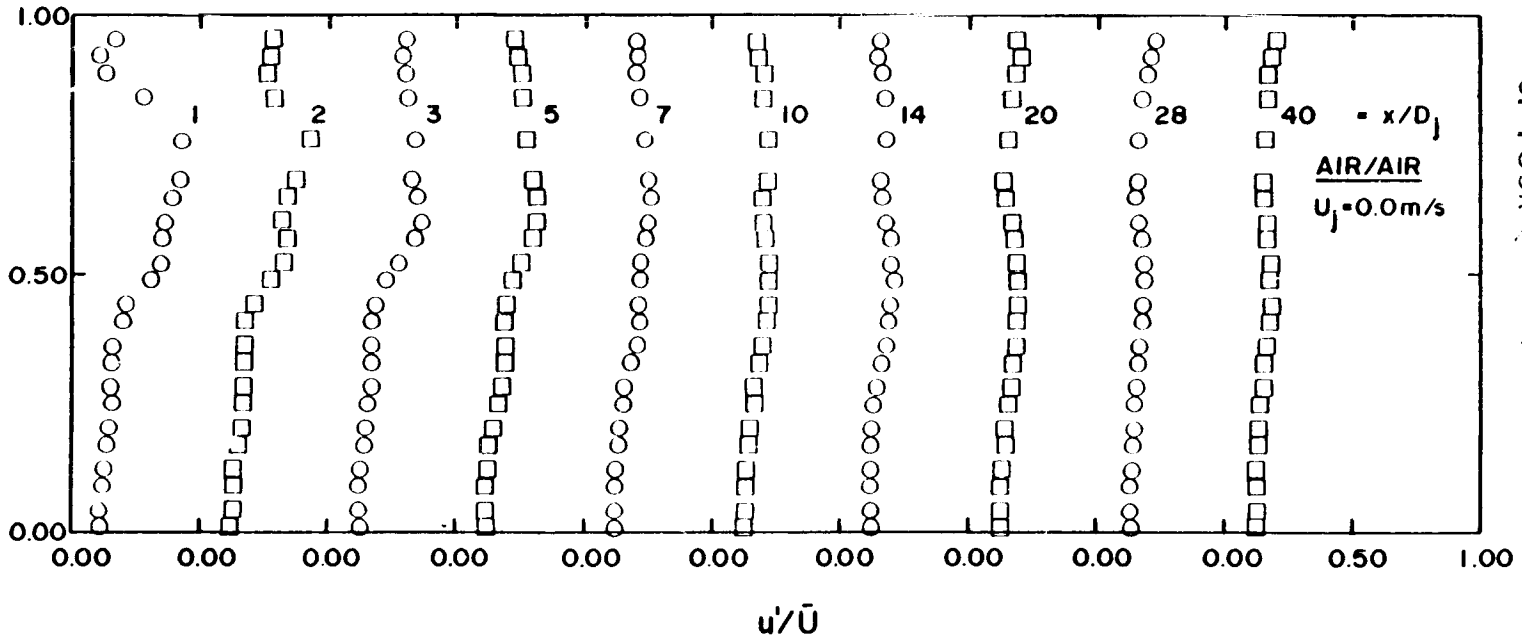

Figure 20. Evolution of u' Distributions for the U_j = 0 Case.

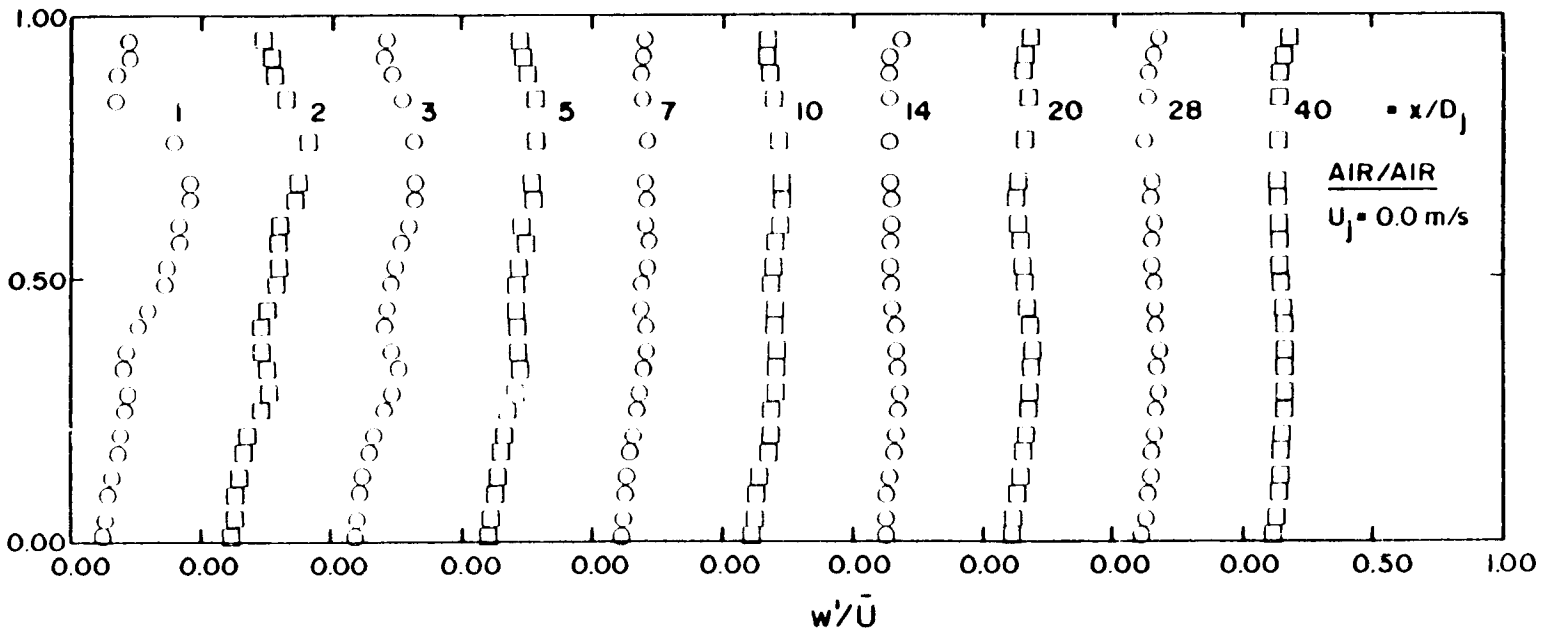

Figure 21. Evolution of w' Distributions for the U_j = 0 Case.

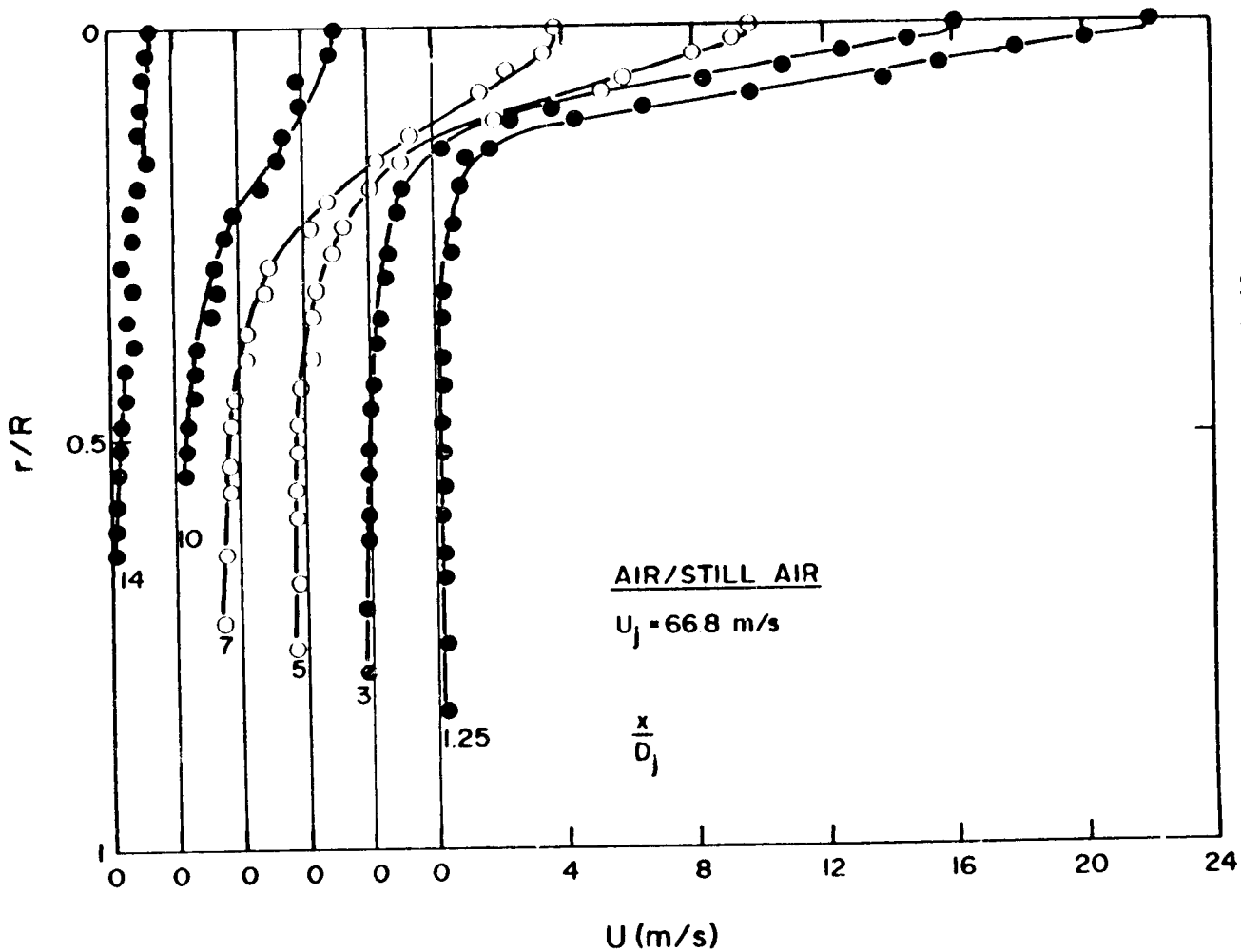

Figure 22. Evolution of U Distributions of Confined Air Jet.

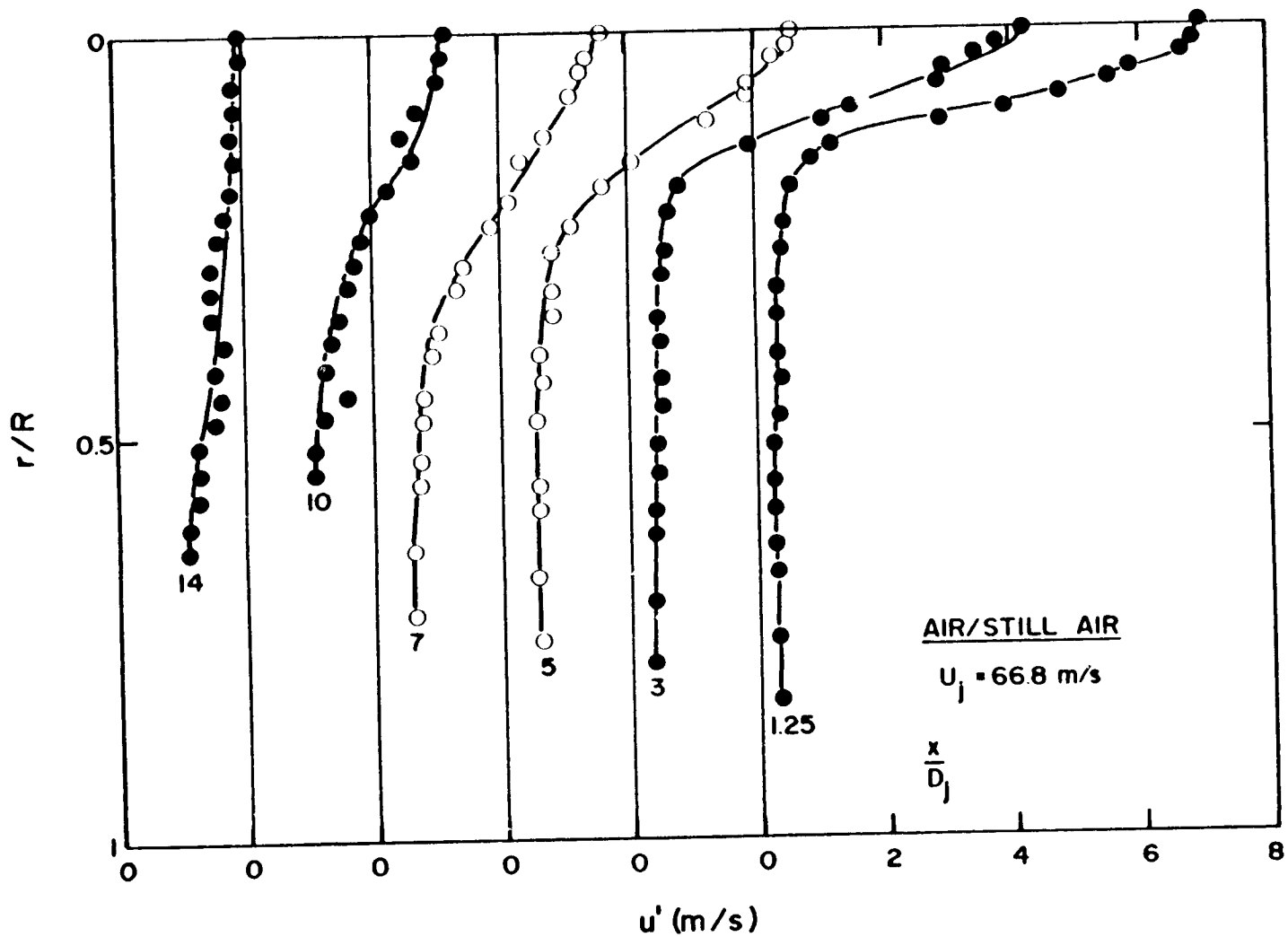

Figure 23. Evolution of u' Distributions of Confined Air Jet.

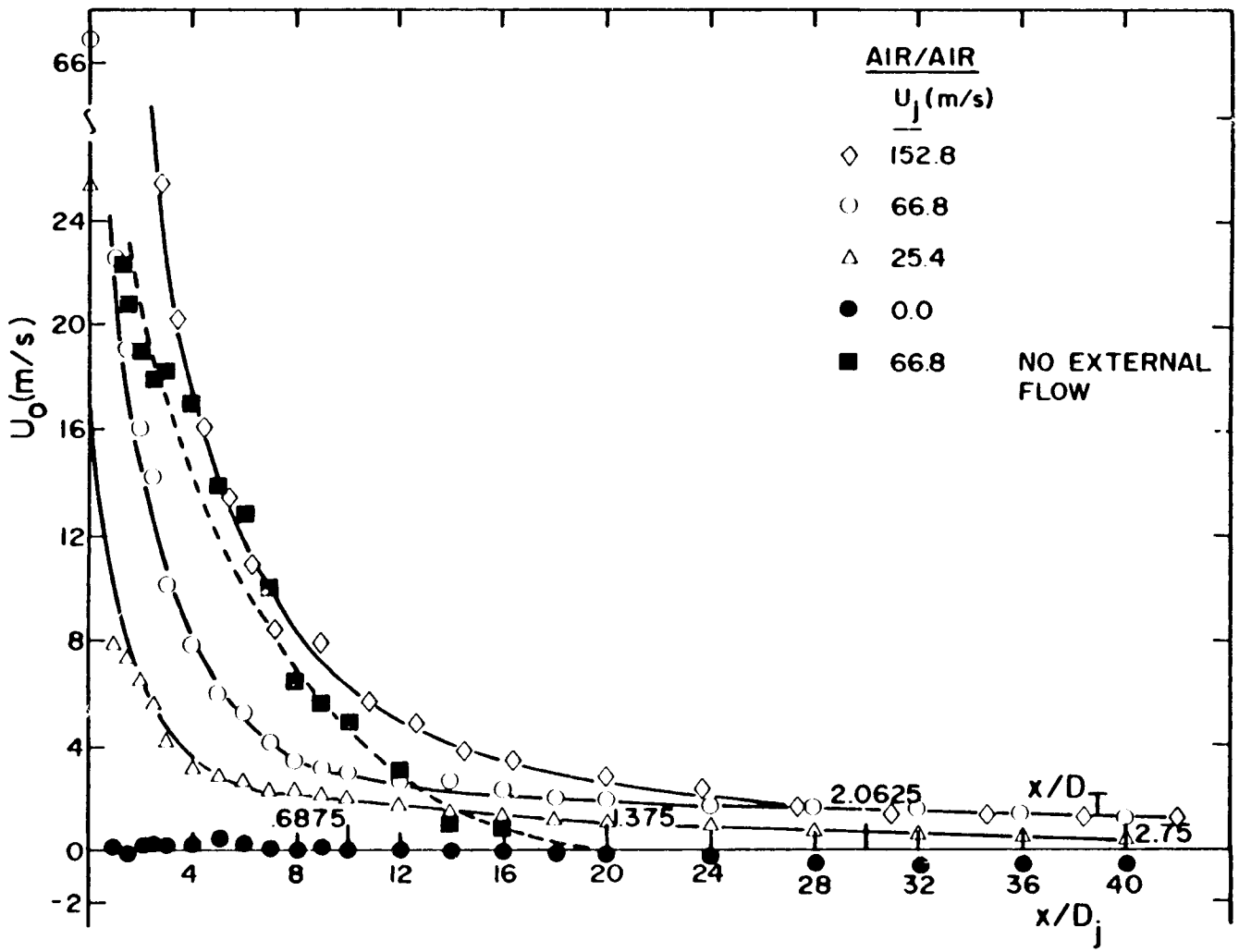

Figure 24. Distribution of Mean Centerline Velocity for the Air Jet Experiments.

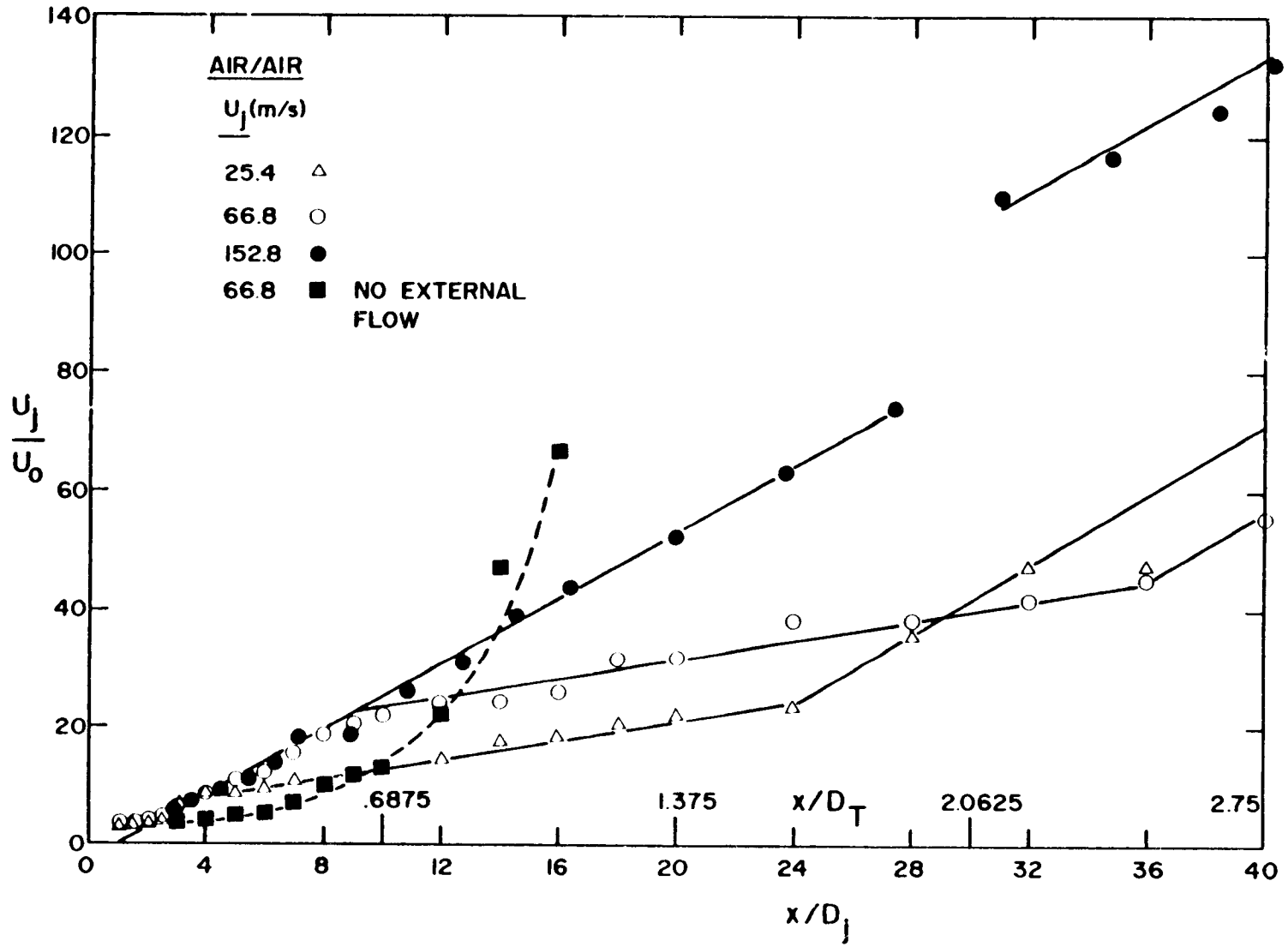

Figure 25. Air Jet Decay in Confined Swirling Flow.

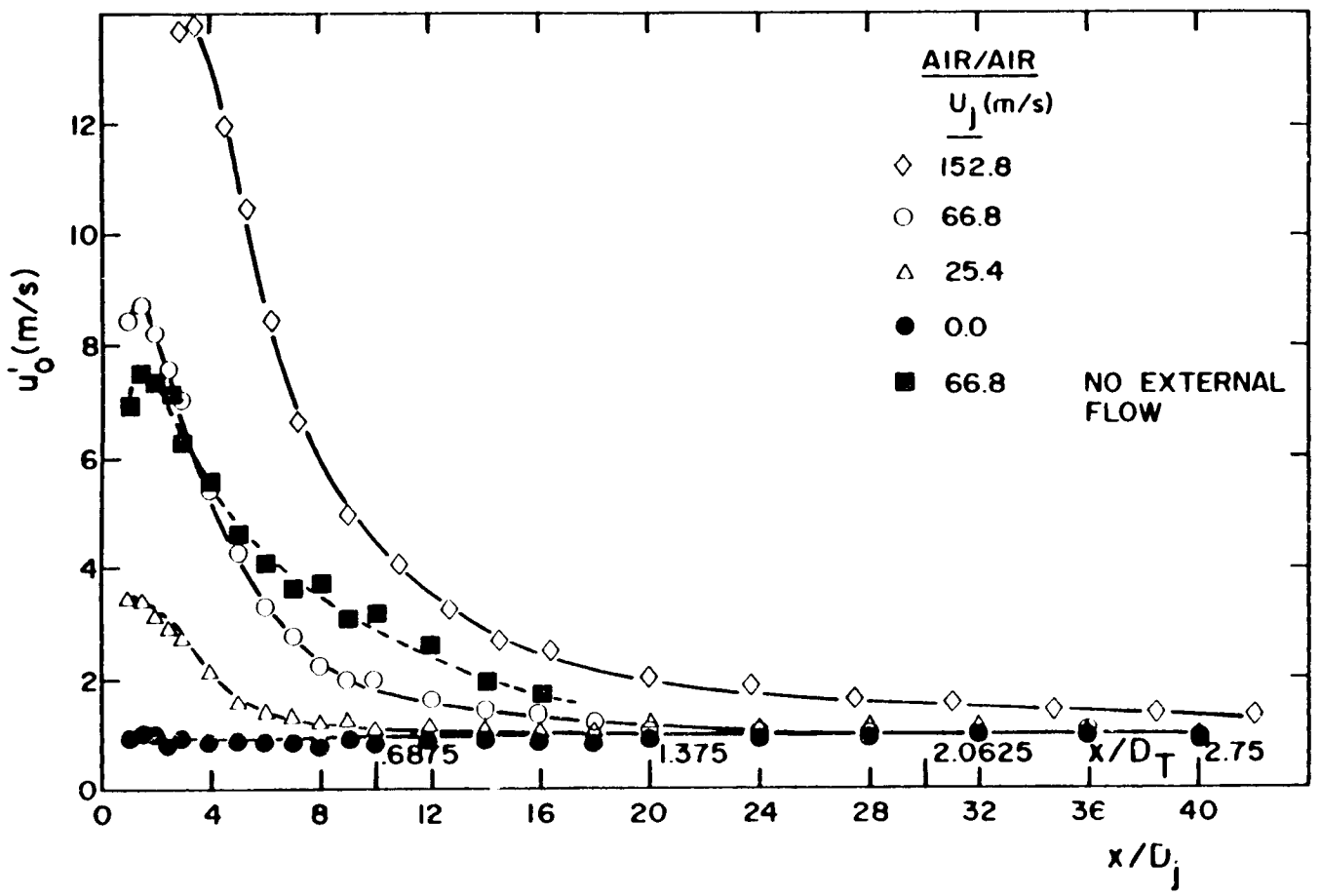

Figure 26. Distributions of Centerline u' for the Air Jet Experiments.

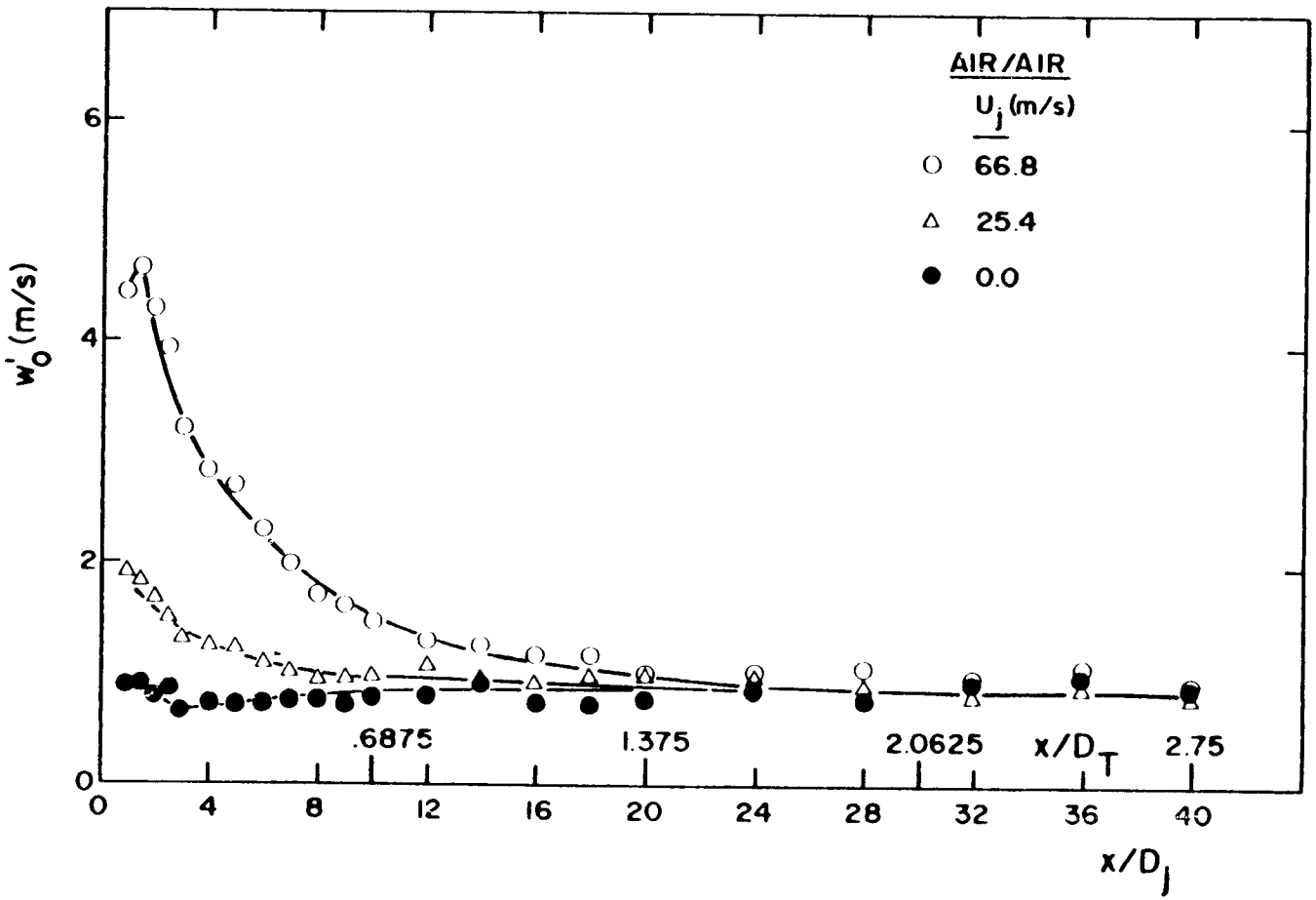

Figure 27. Distributions of Centerline w' for the Air Jet Experiments.

ORIGINAL PAGE IS
OF POOR QUALITY

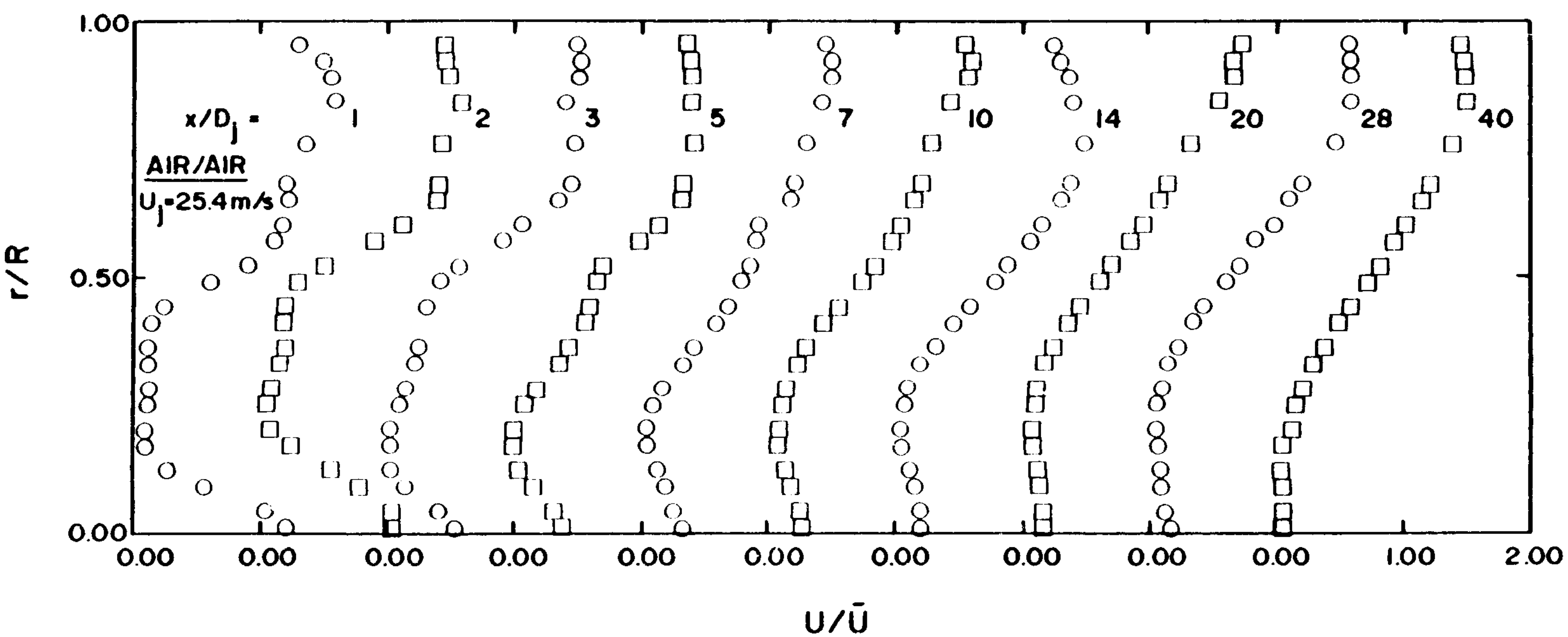

Figure 28. Evolution of U Distributions for the U_j = 25.4 m/s Air Jet Case.

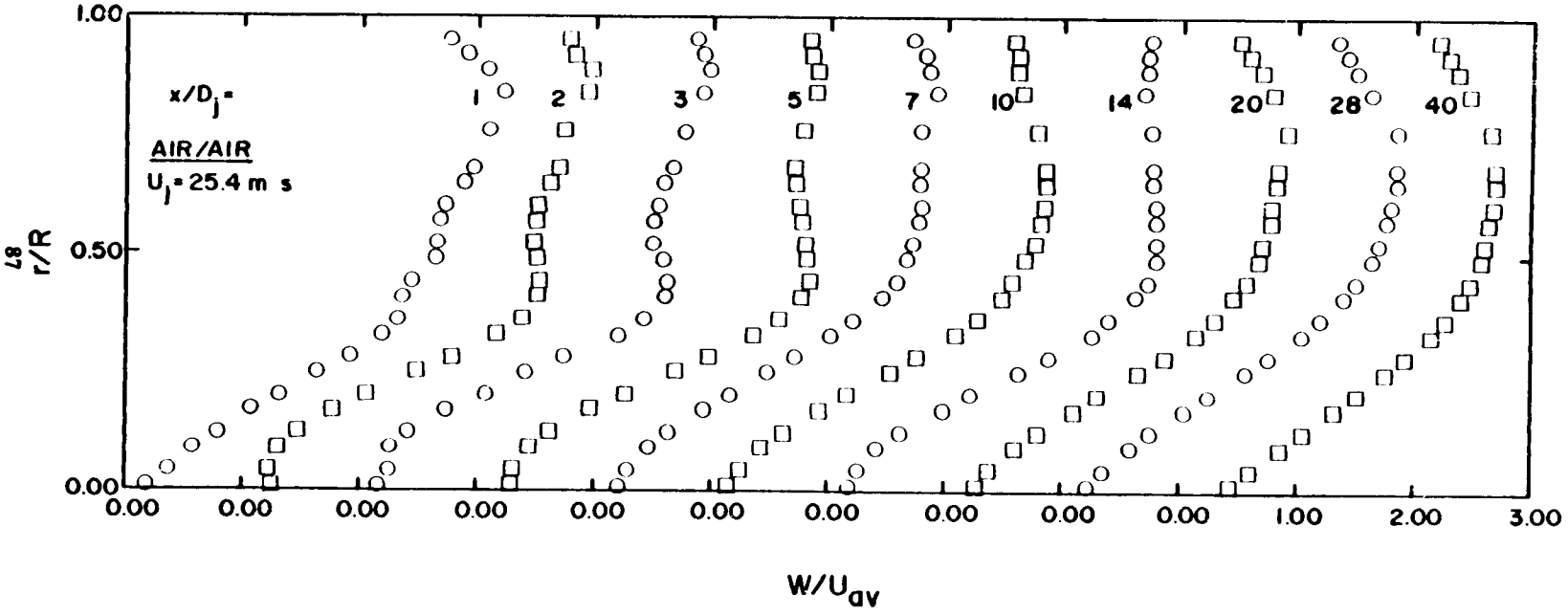

Figure 29. Evolution of W Distributions for the U_j = 25.4 m/s Air Jet Case.

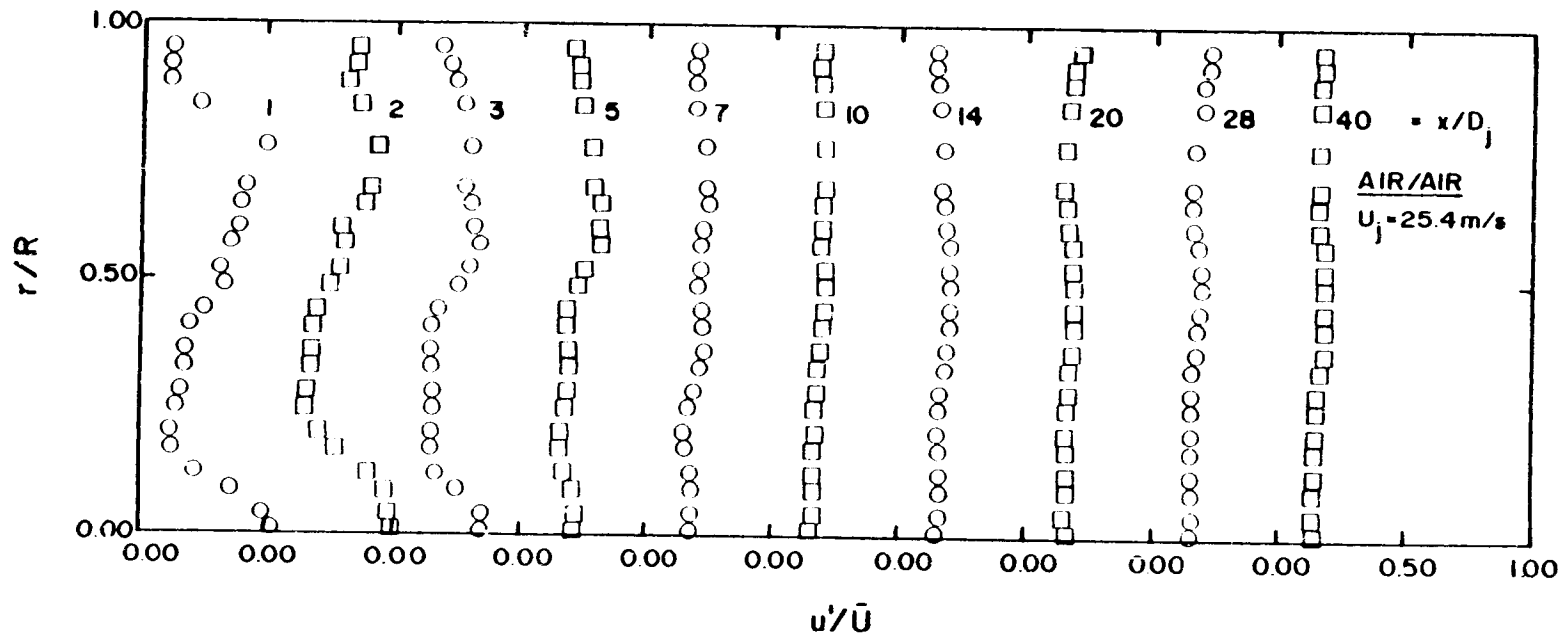

Figure 30. Evolution of u' Distributions for the U_j = 25.4 m/s Air Jet Case.

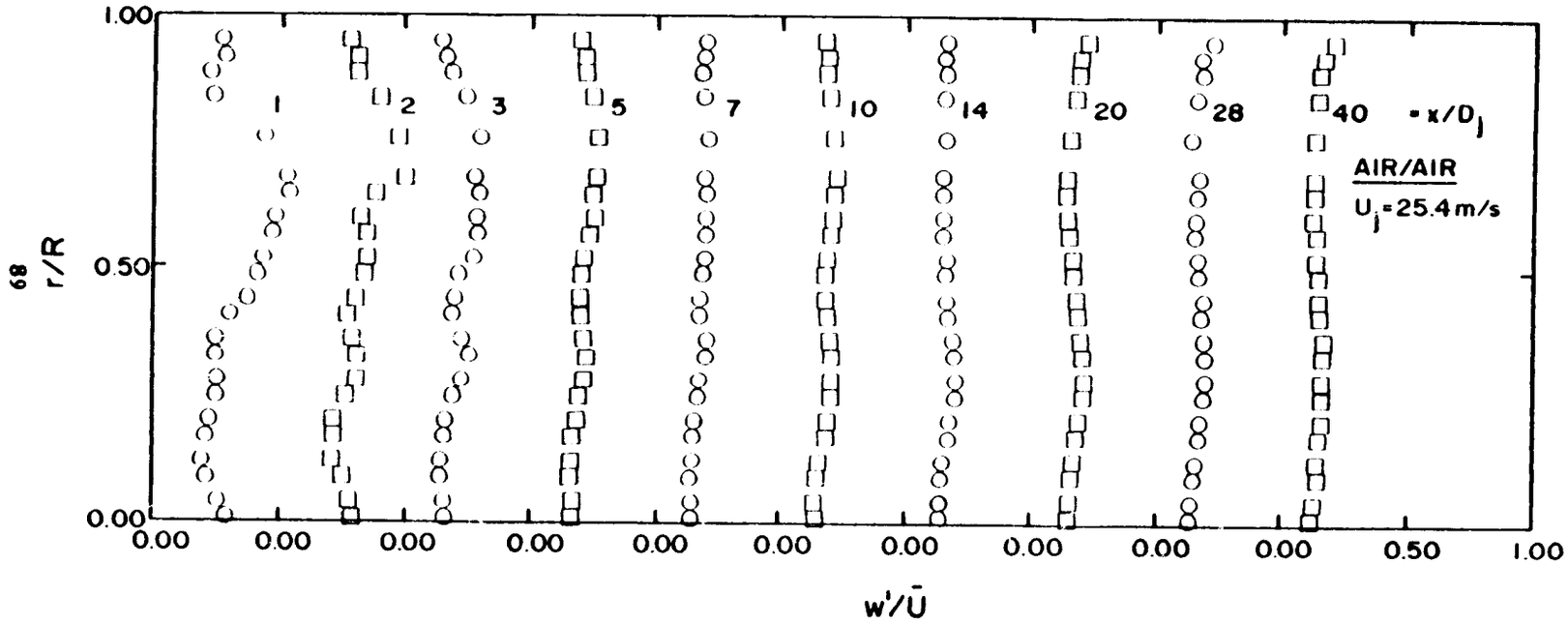

Figure 31. Evolution of w' Distributions for the U_j = 25.4 m/s Air Jet Case.

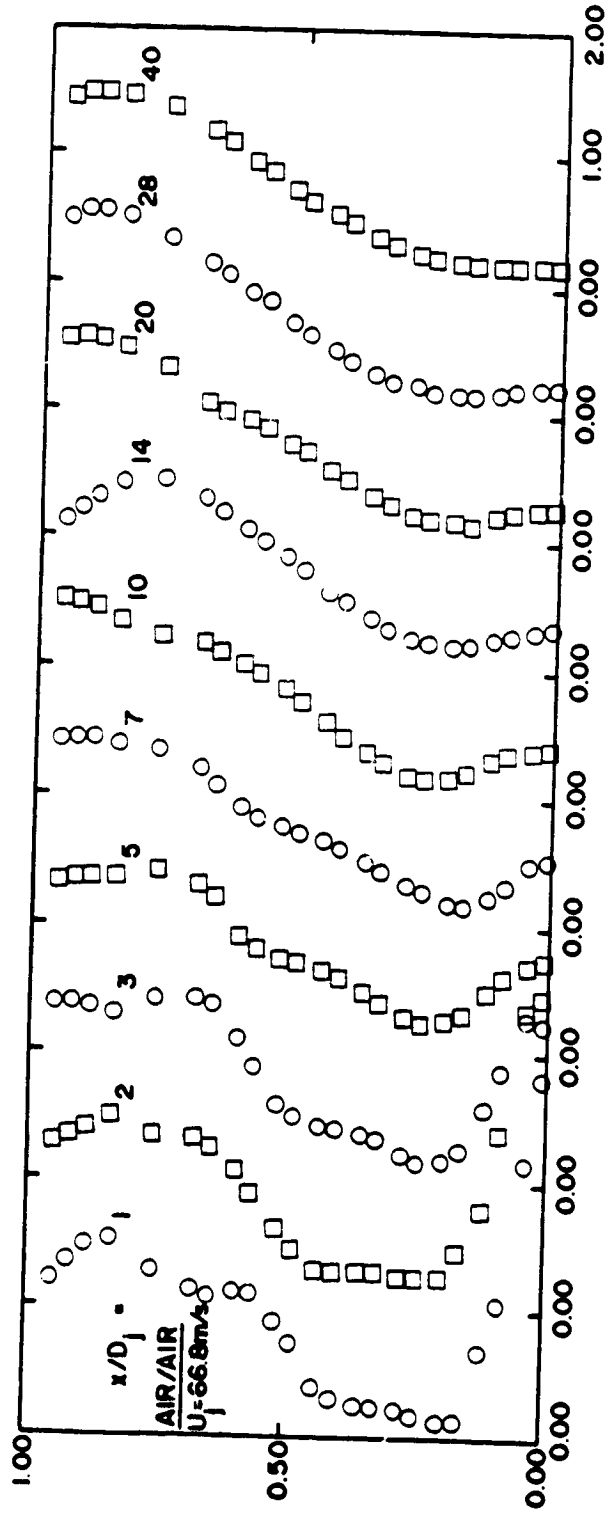

Figure 32. Evolution of U Distributions for the U_j = 66.8 m/s Air Jet Case.

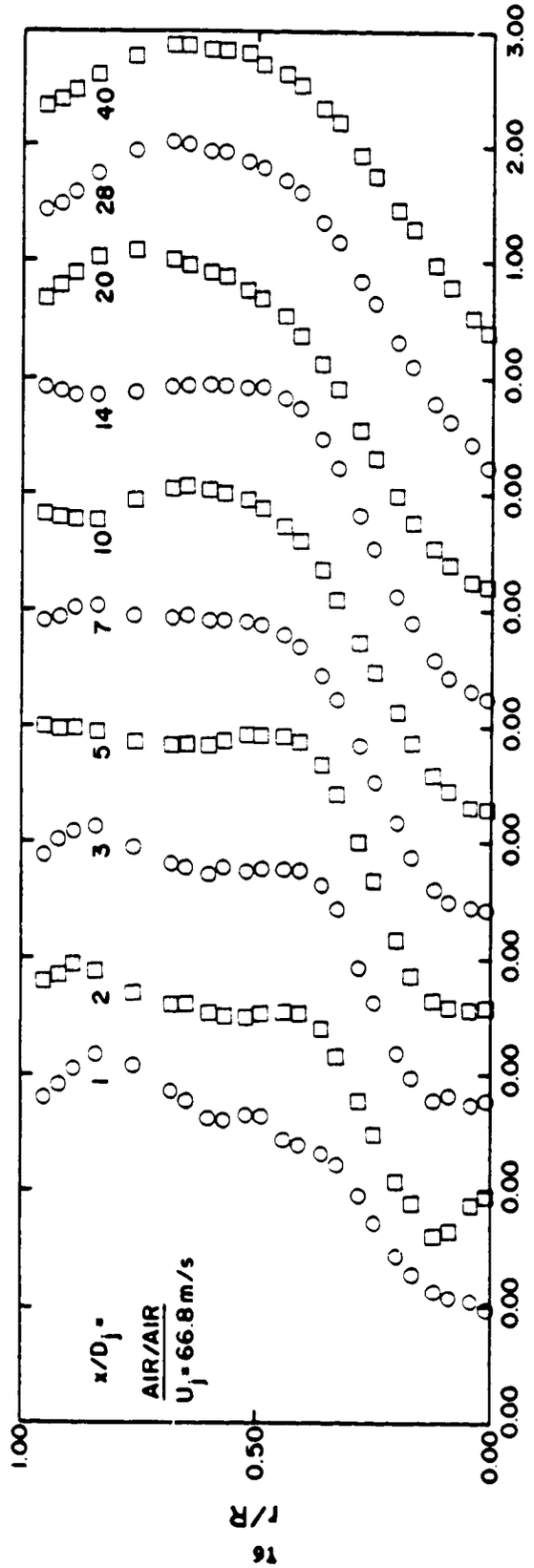

Figure 33. Evolution of W Distributions for the U_j = 66.8 m/s Air Jet Case.

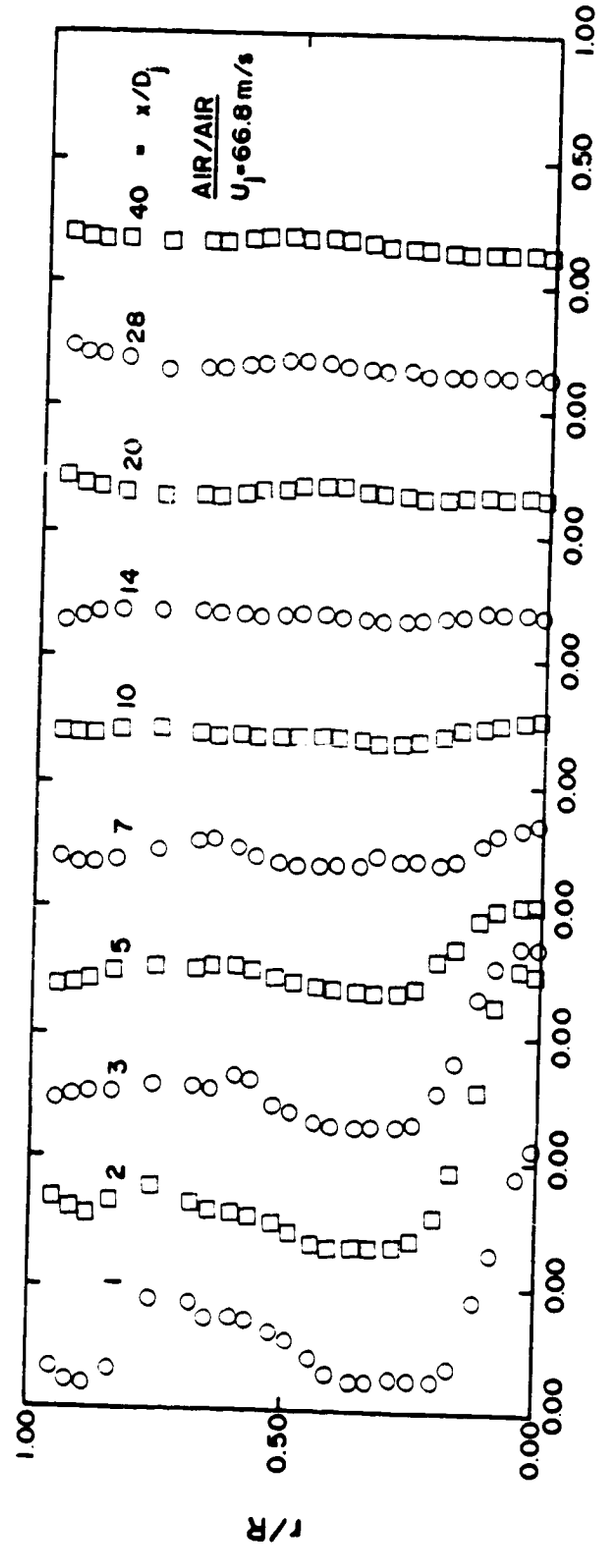

Figure 34. Evolution of u' Distributions for the U_j = 66.8 m/s Air Jet Case.

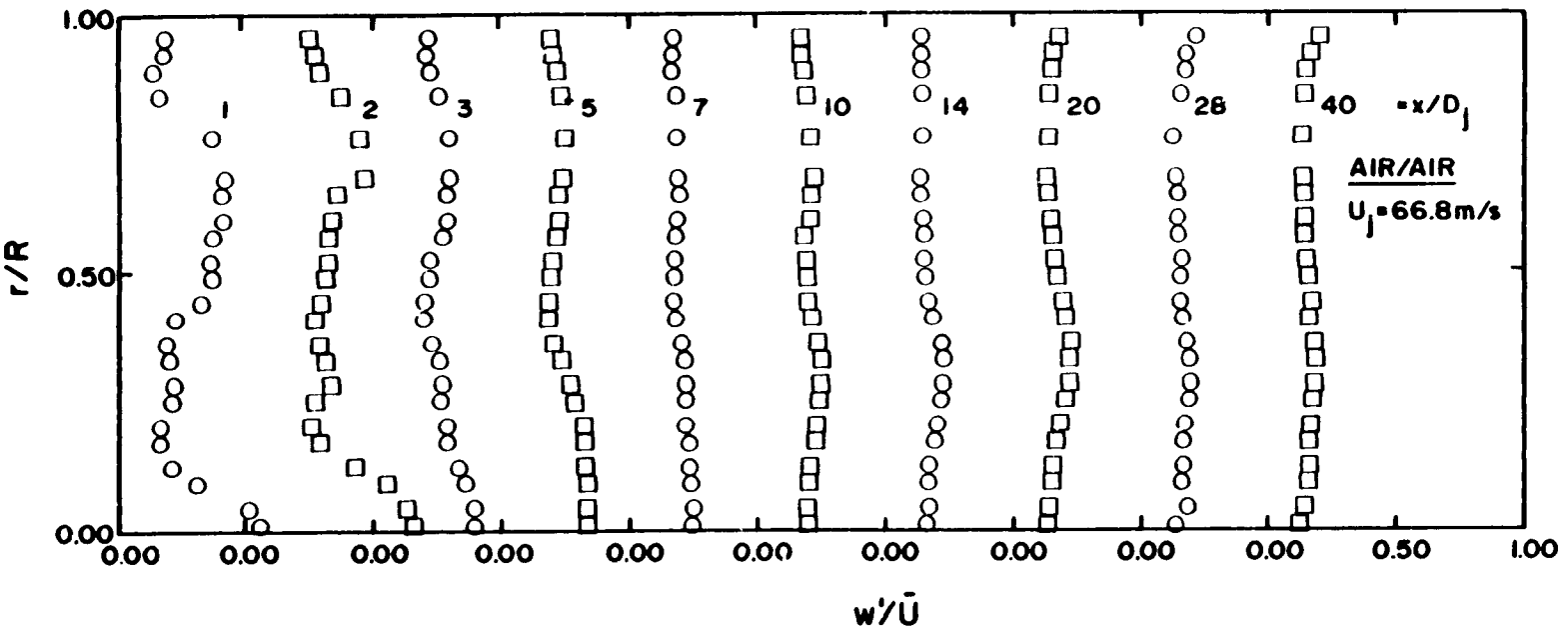

Figure 35. Evolution of w' Distributions for the U_j = 66.8 m/s Air Jet Case.

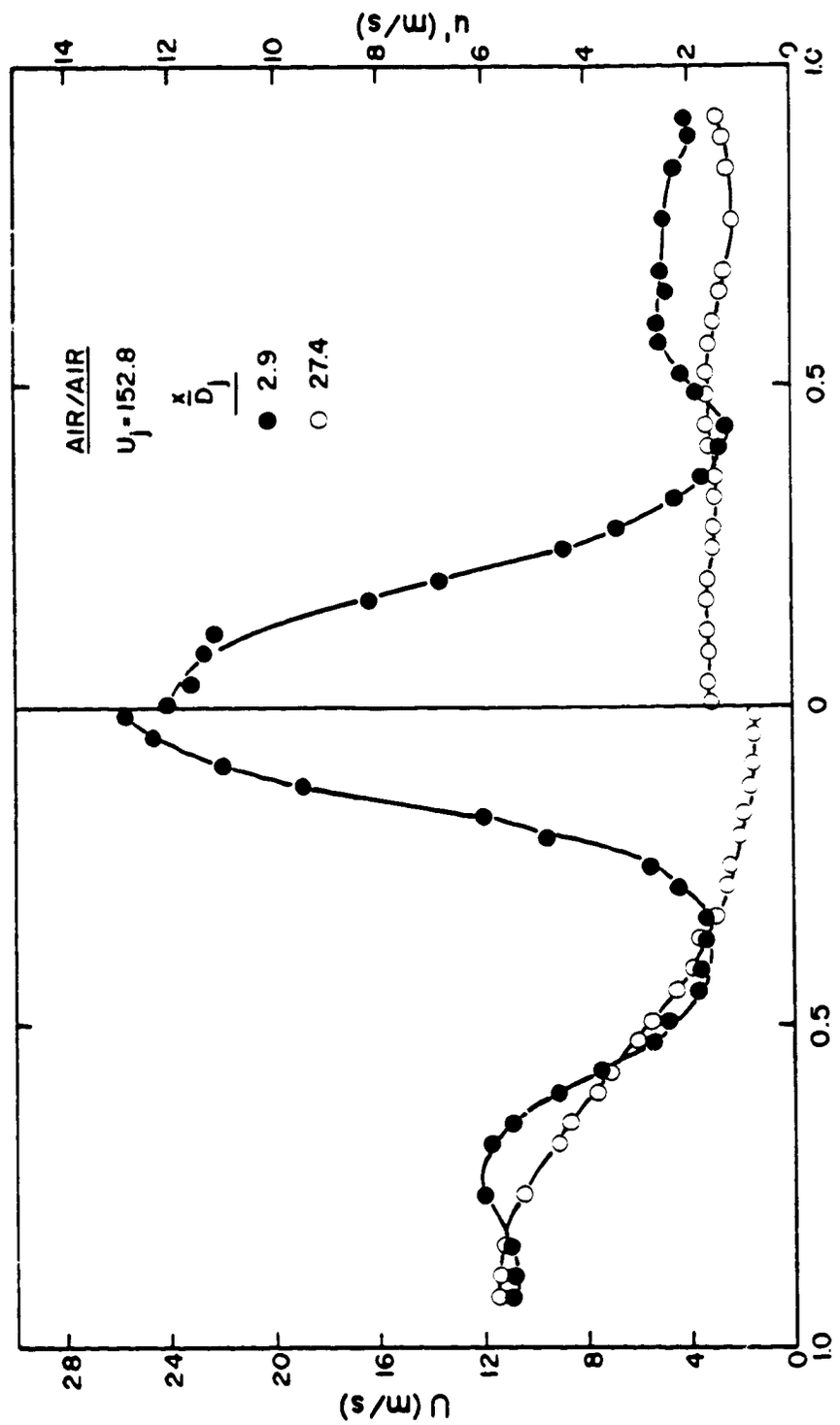

Figure 36. Distributions of U and u' at Two Locations for the U_j = 152.8 m/s Air Jet Case.

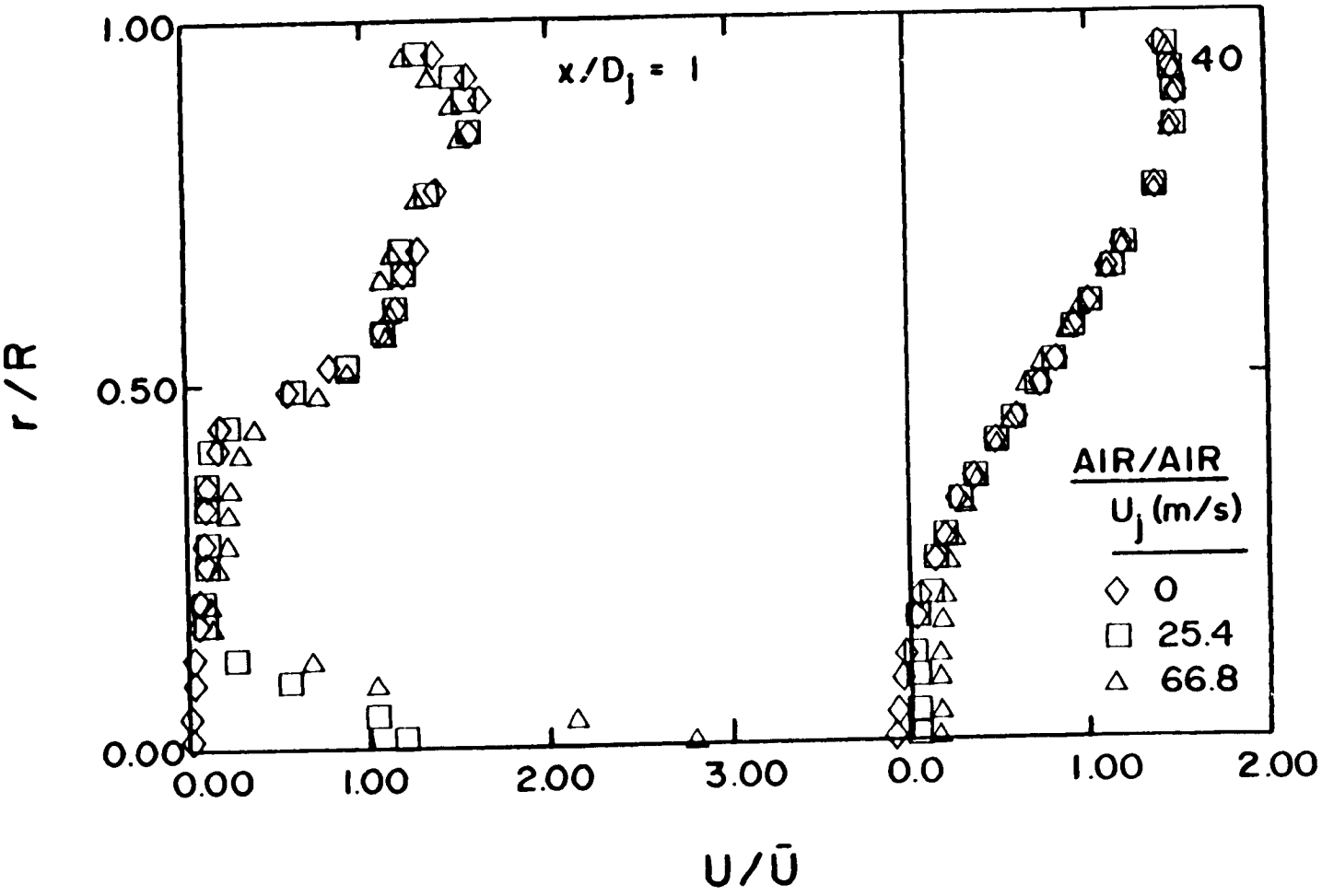

Figure 37. Comparison of U Distributions at x/D_j = 1 and 40 for the Air Jet Experiments.

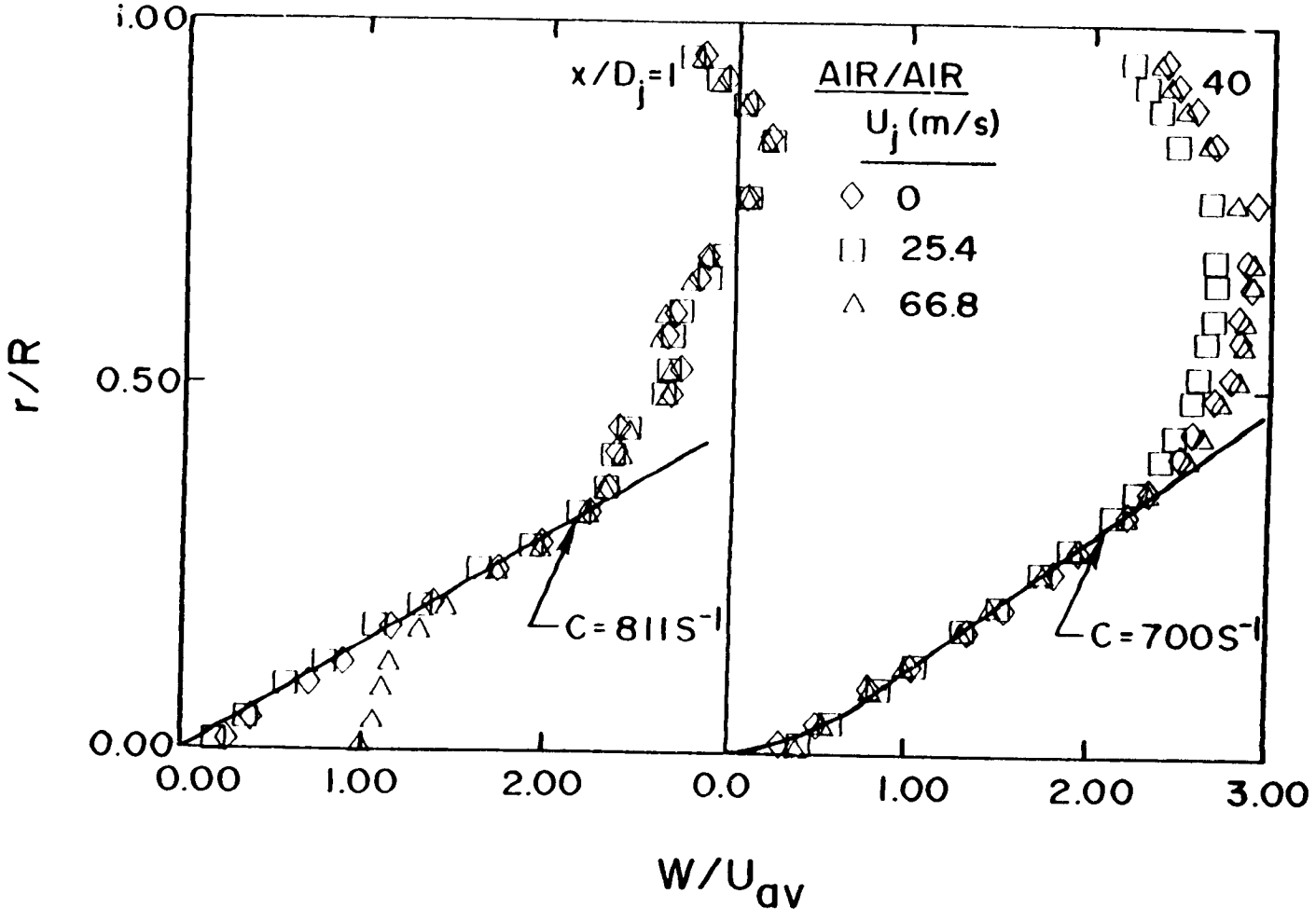

Figure 38. Comparison of W Distributions at x/D_j = 1 and 40 for the Air Jet Experiments.

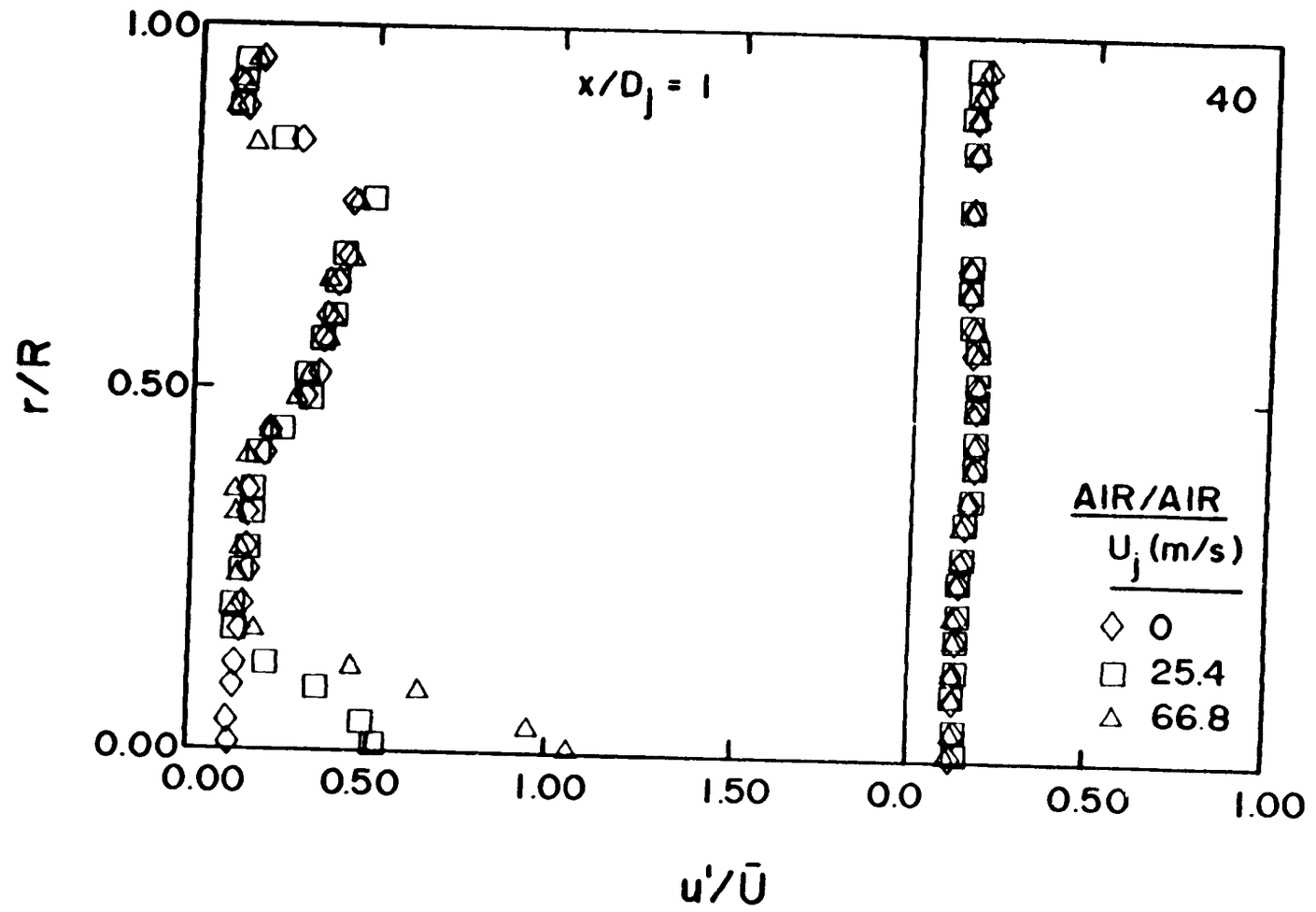

Figure 39. Comparison of u' Distributions at x/D_j = 1 and 40 for the Air Jet Experiments.

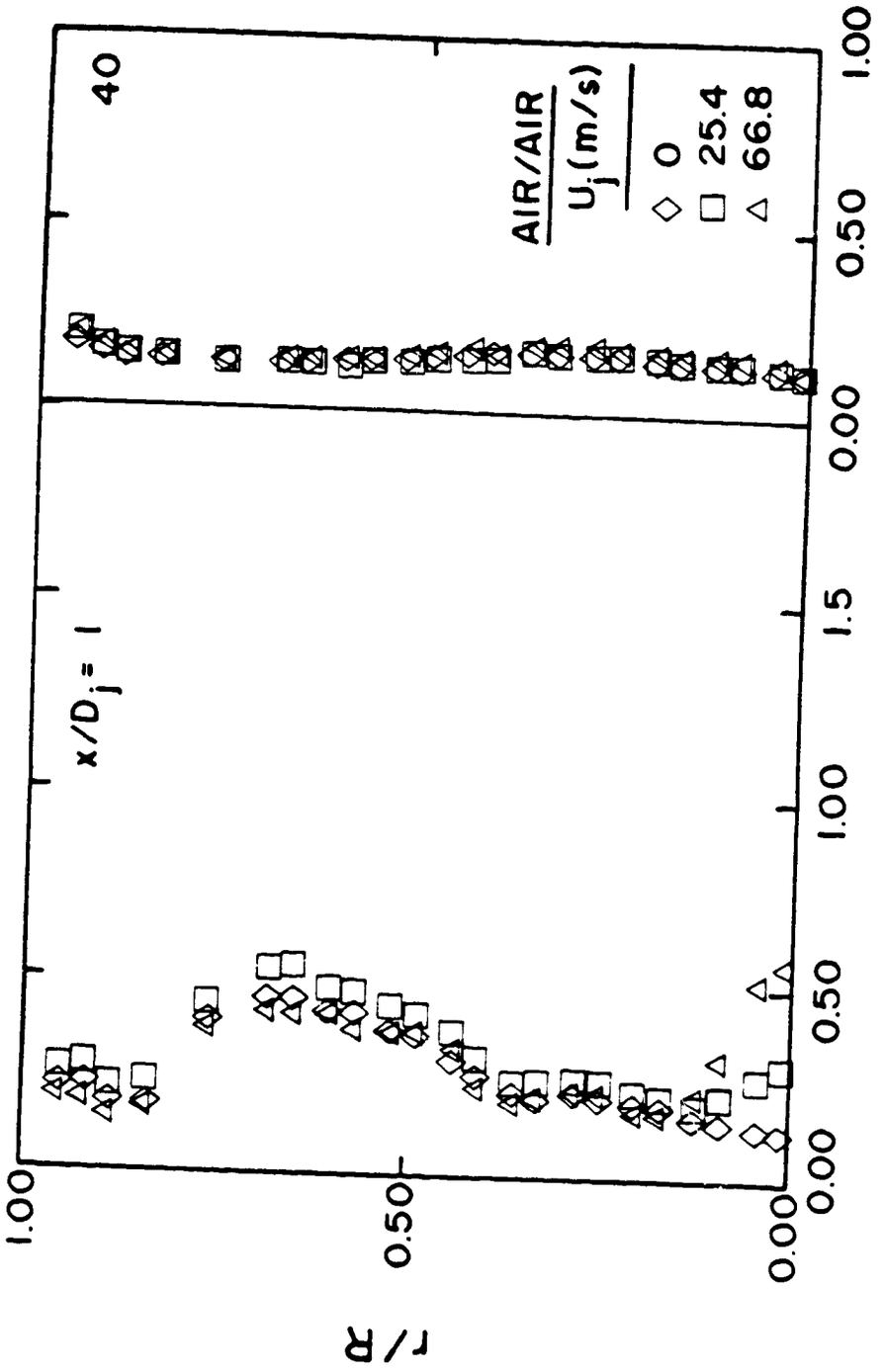

Figure 40. Comparison of w' Distributions at x/D_j = 1 and 40 for the Air Jet Experiments.

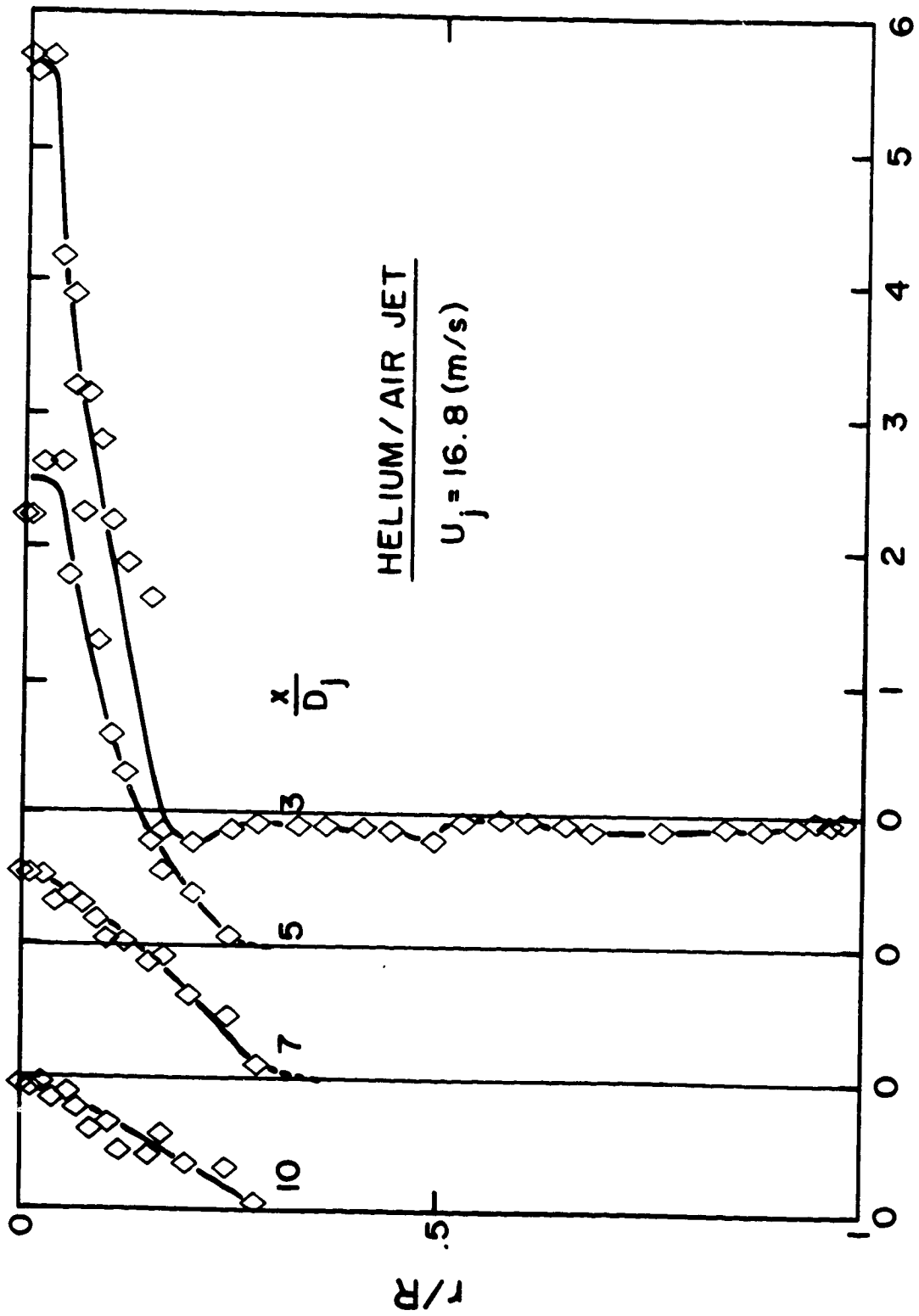

Figure 41. Evolution of U Distributions for the Helium/Air Jet into Still Air Experiment; U_j = 16.8 m/s.

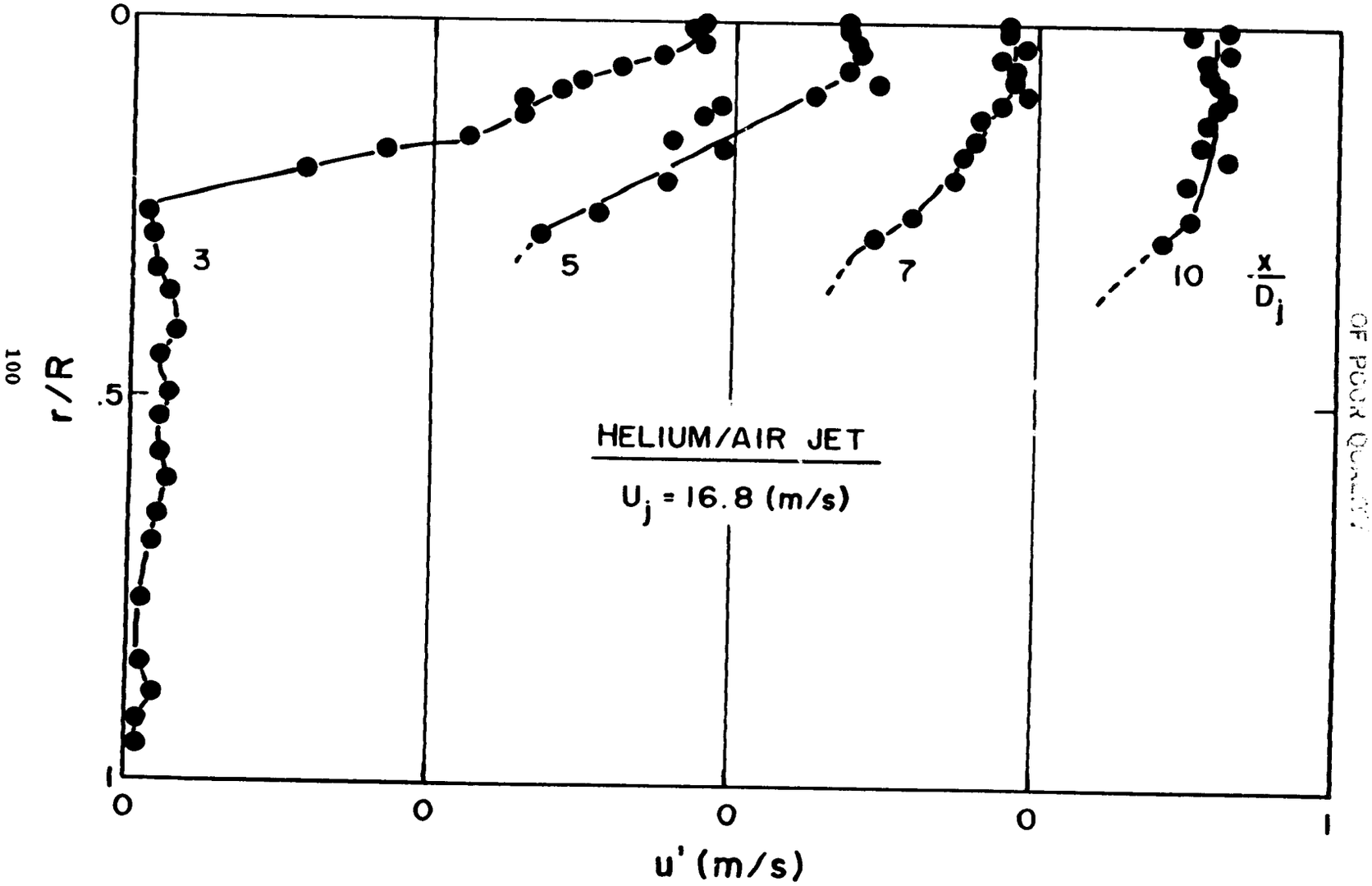

Figure 42. Evolution of u' Distributions for the Helium/Air Jet into Still Air Experiment; U_j = 16.8 m/s.

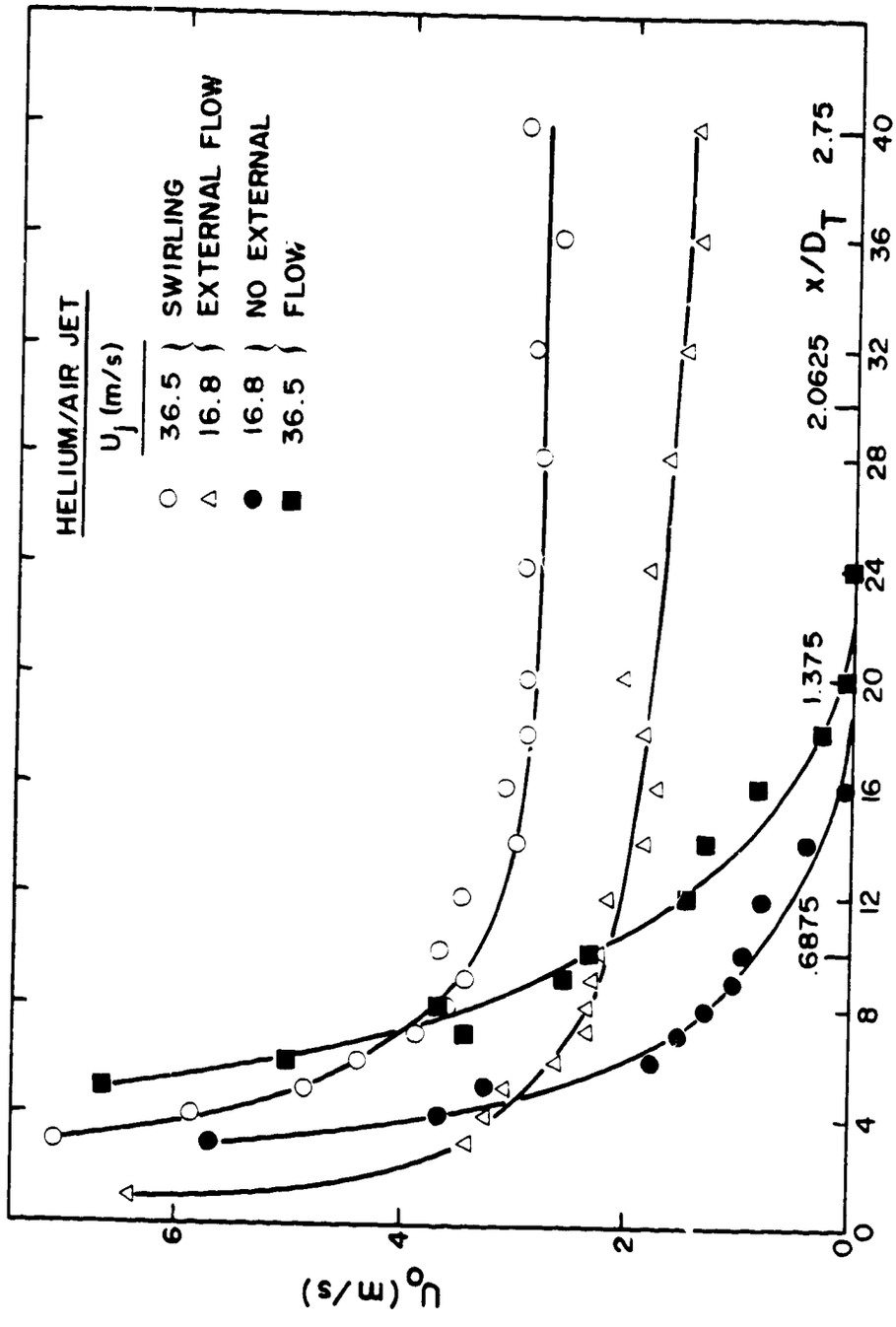

Figure 43. Distributions of Mean Centerline Velocity for Helium/Air Jet Experiments.

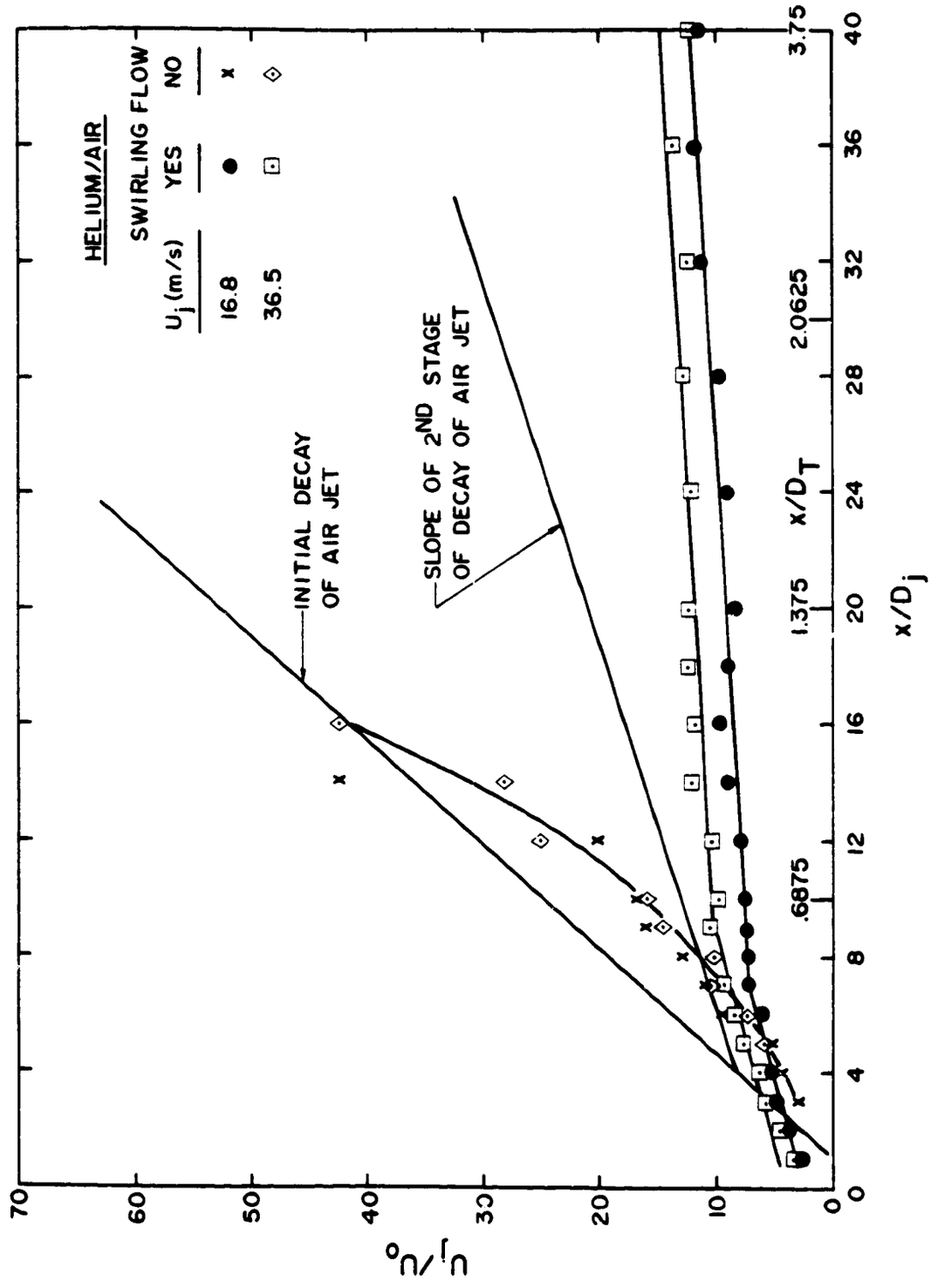

Figure 44. Helium/Air Jet Decay in Confined Flow.

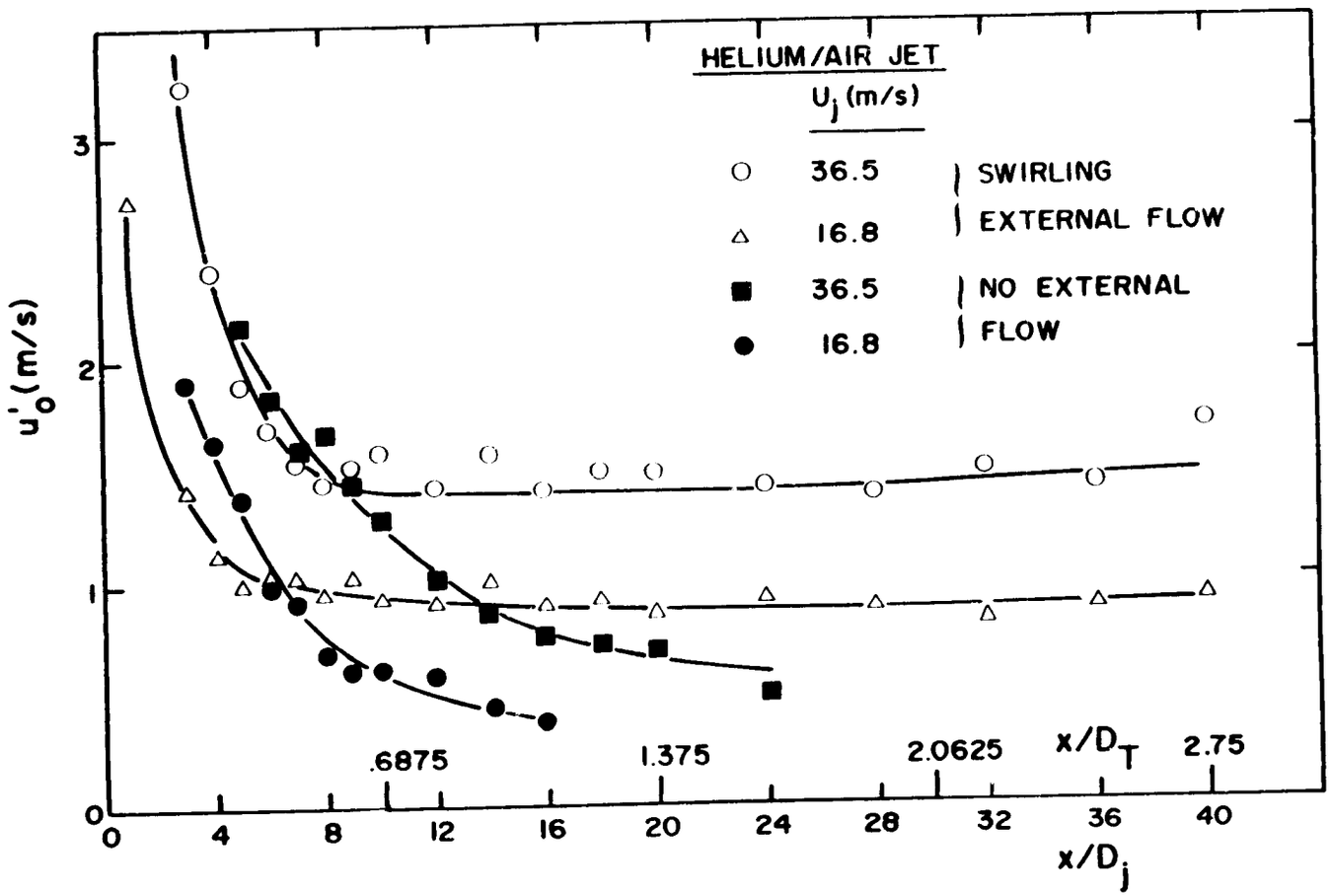

Figure 45. Distribution of Centerline u' for Helium/Air Jet Experiments.

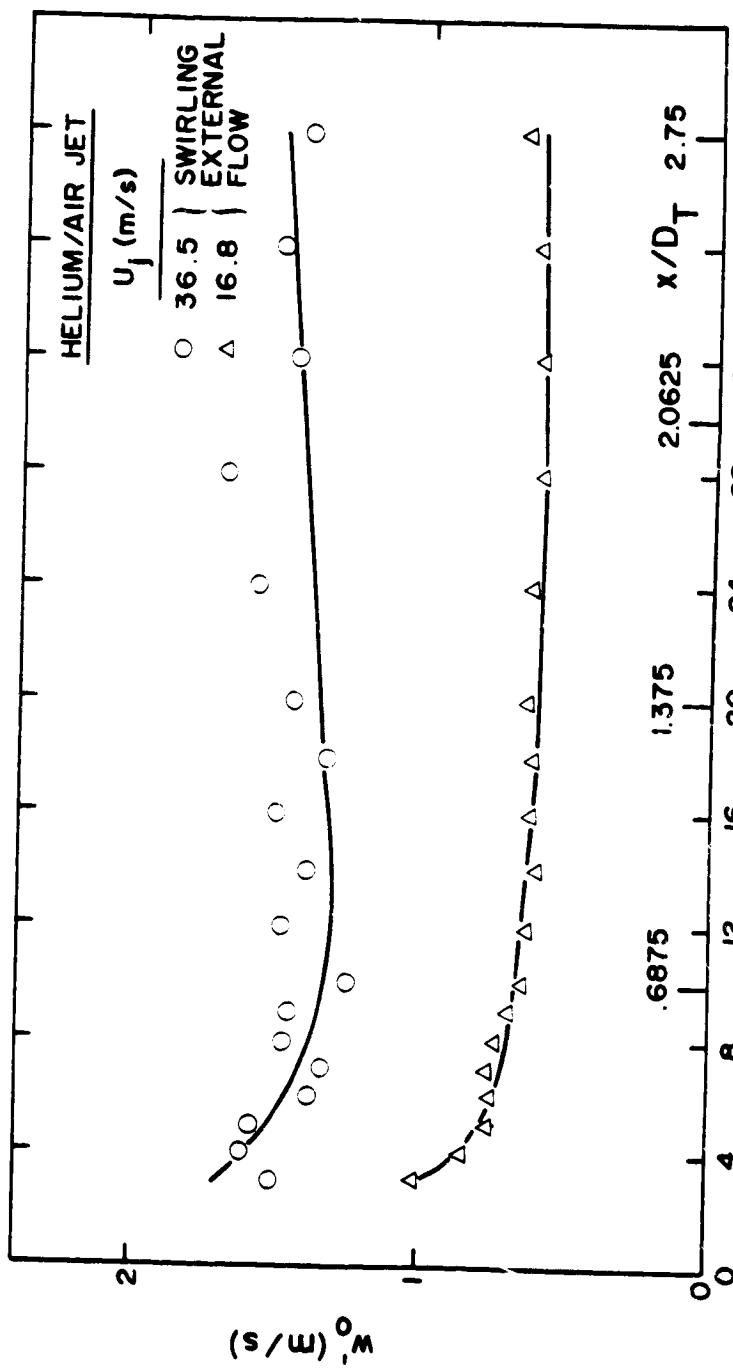

Figure 46. Distribution of Centerline w' for Helium/Air Jet Experiments.

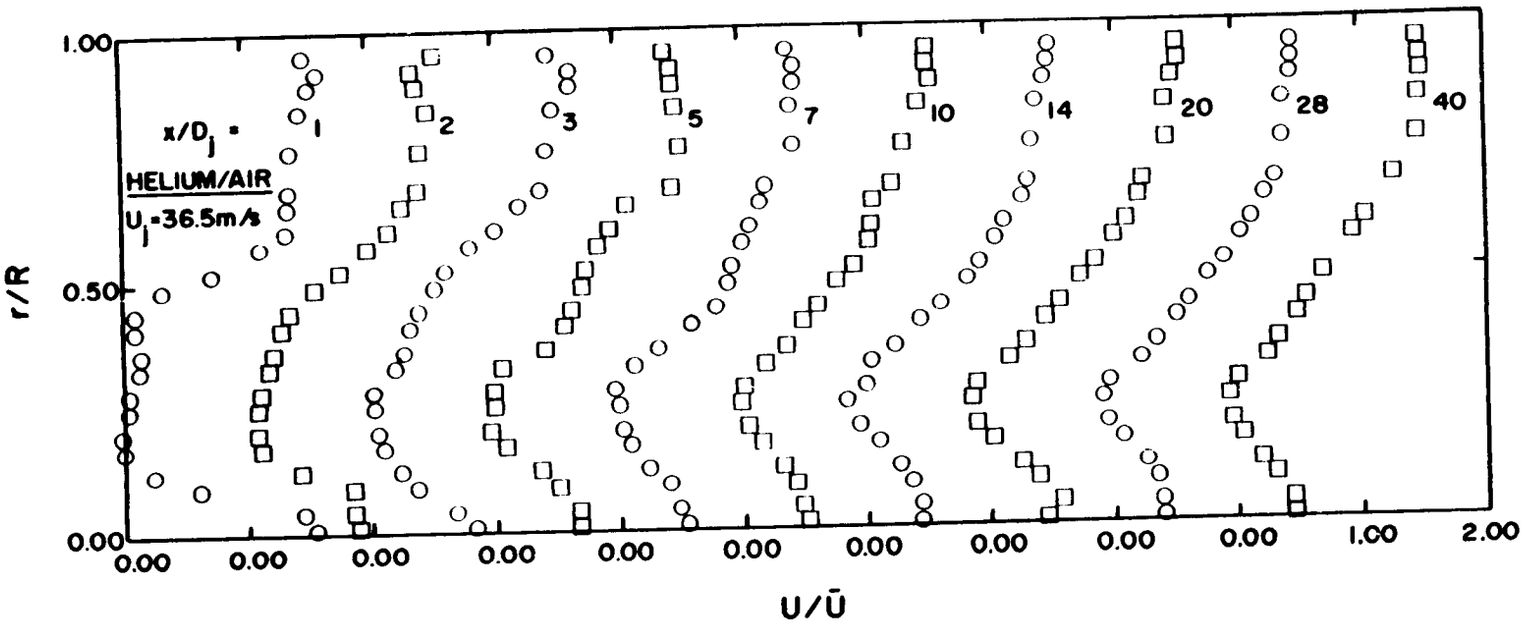

Figure 47. Evolution of U Distribution for the U_j = 36.5 m/s Helium/Air Jet Case.

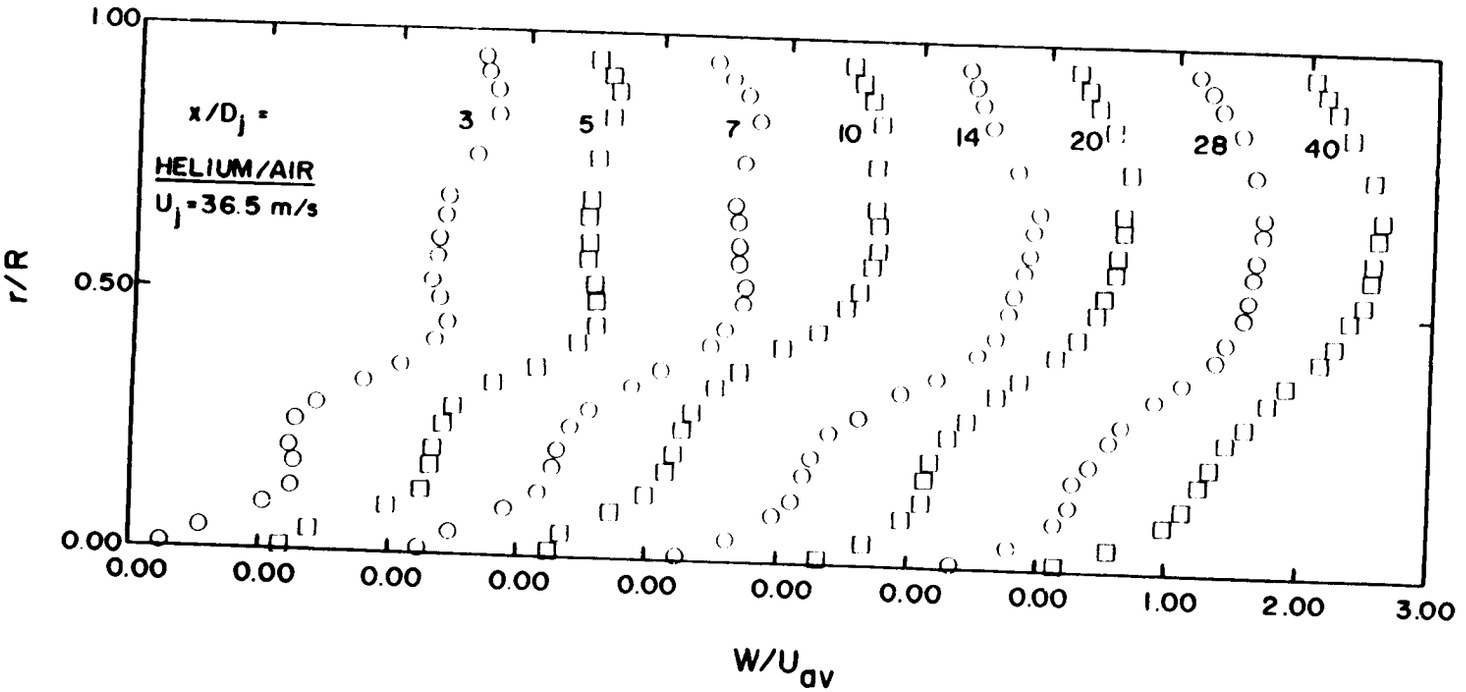

Figure 48. Evolution of W Distribution for the U_j = 36.5 m/s Helium/Air Jet Case.

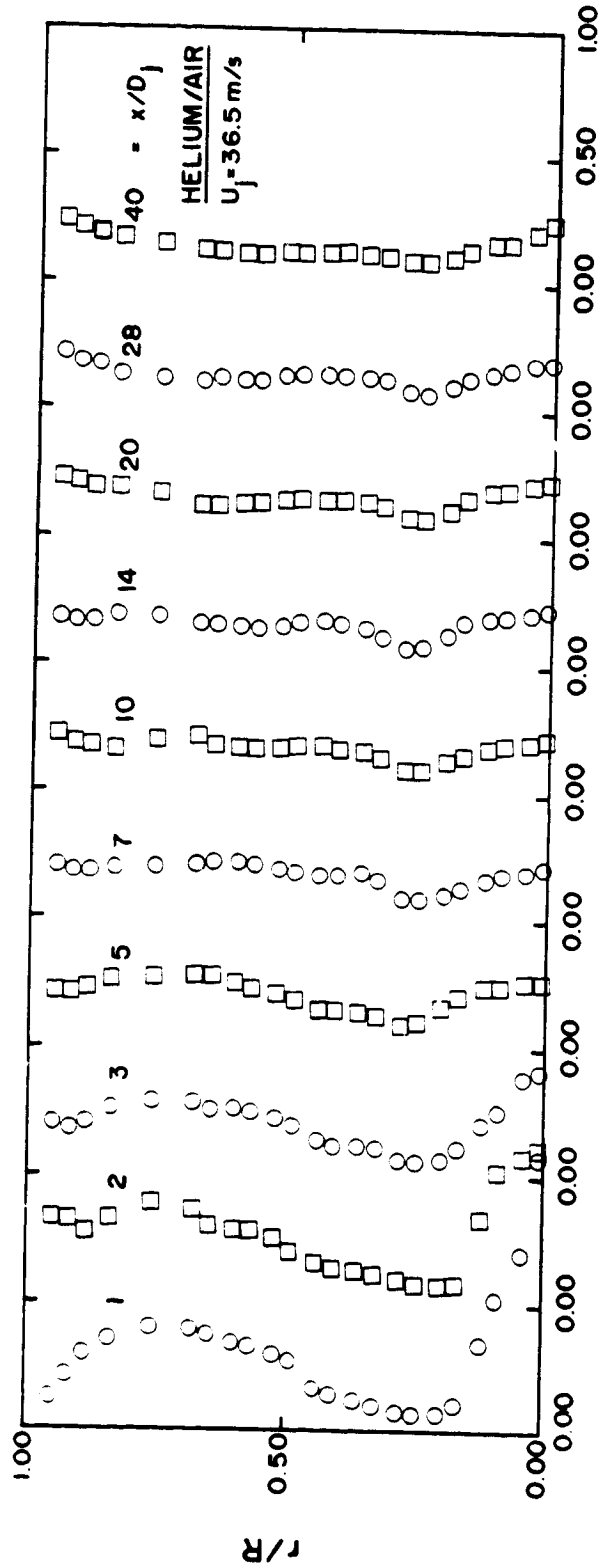

Figure 49. Evolution of u' Distribution for the U_j = 36.5 m/s Helium/Air Jet Case.

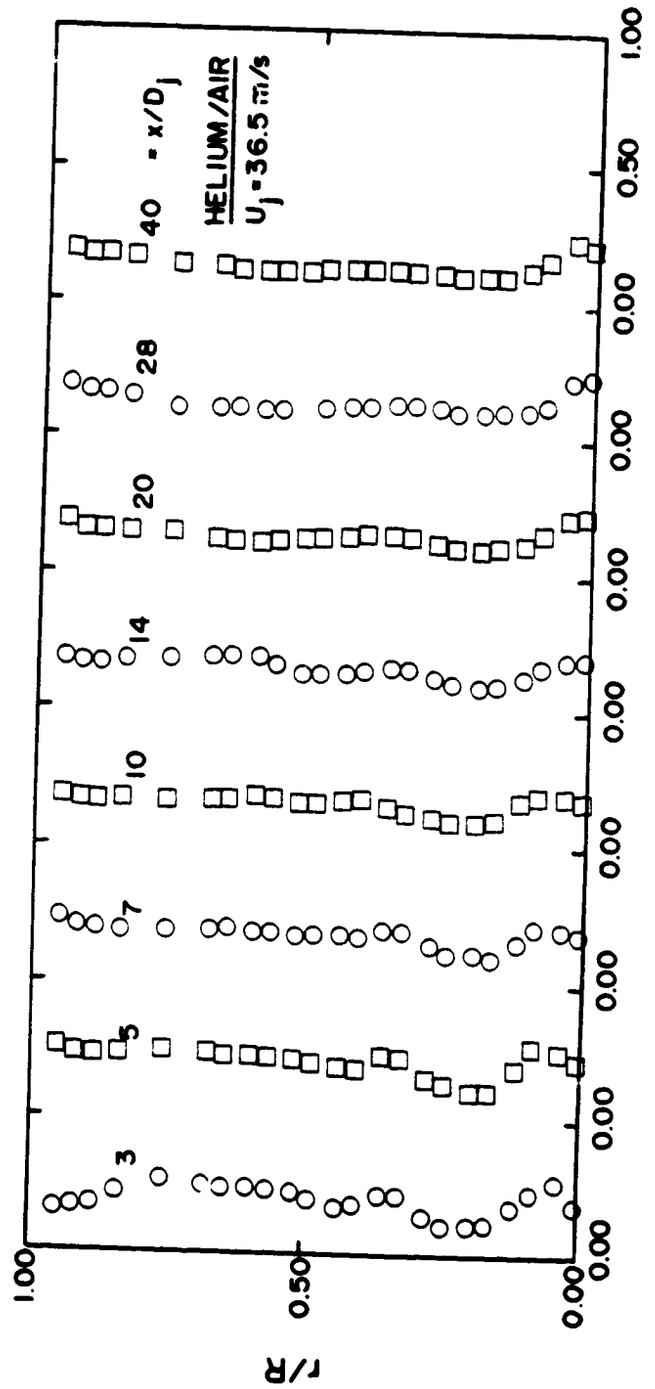

Figure 50. Evolution of w' Distribution for the U_j = 36.5 m/s Helium/Air Jet Case.

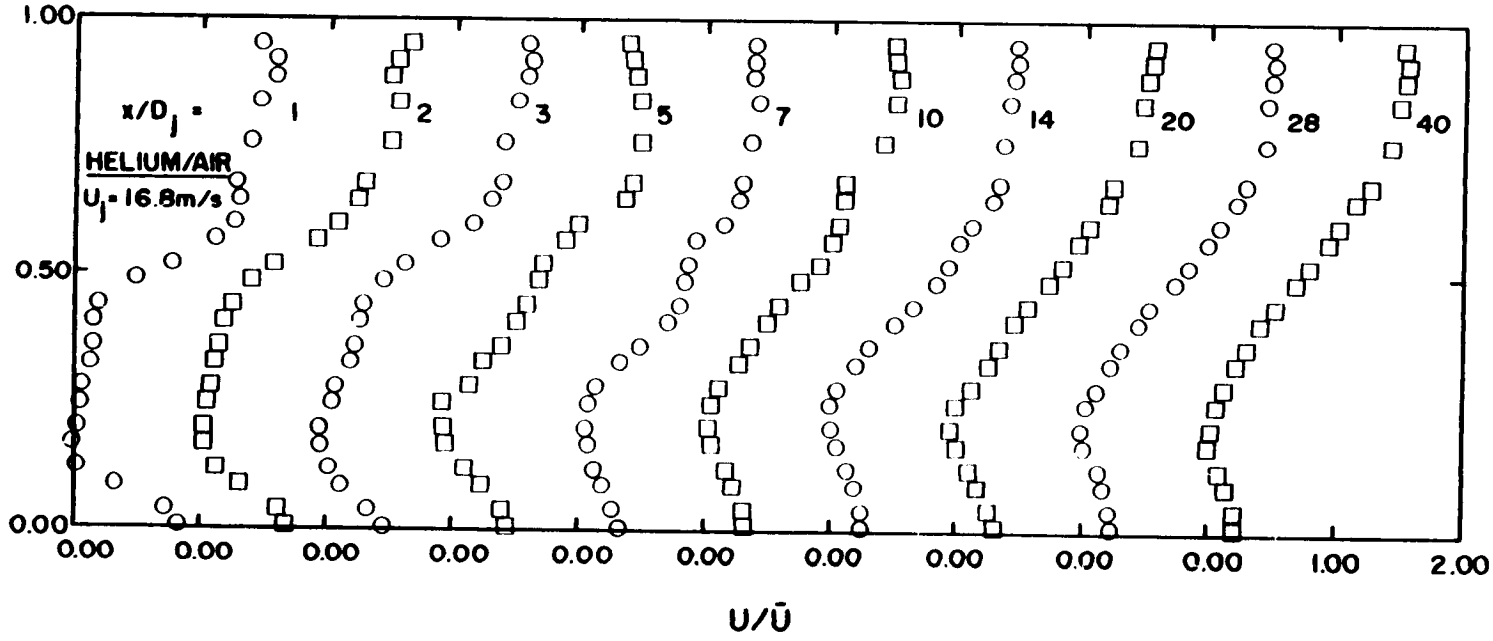

Figure 51. Evolution of U Distribution for the U_j = 16.8 m/s Helium/Air Jet Case.

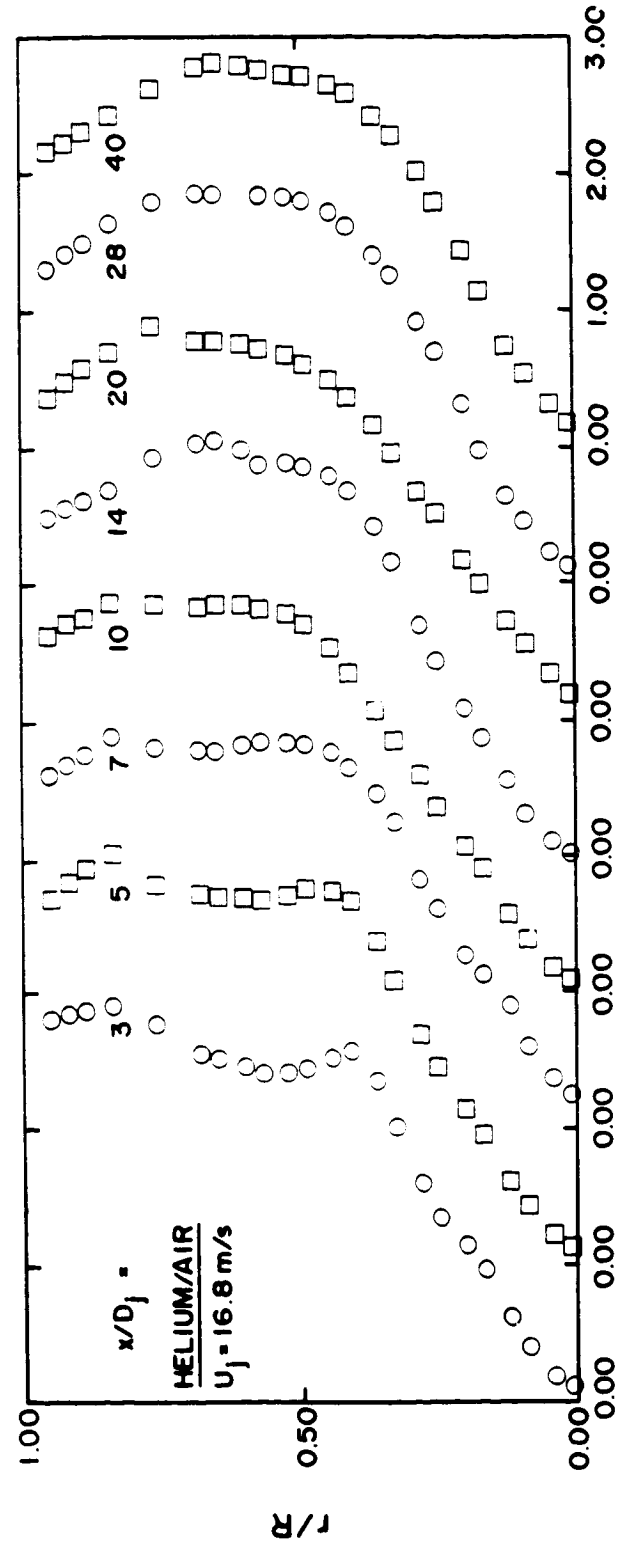

Figure 52. Evolution of W Distribution for the U_j = 16.8 m/s Helium/Air Jet Case.

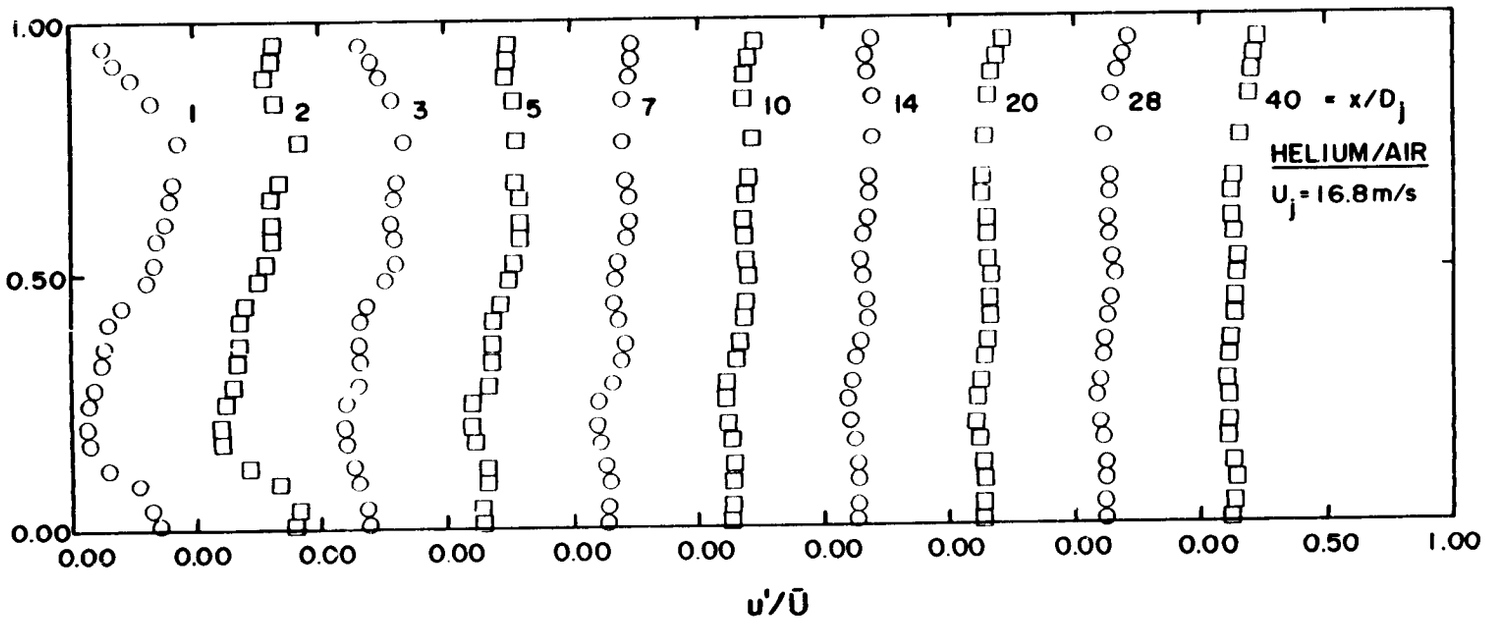

Figure 53. Evolution of u' Distribution for the U_j = 16.8 m/s Helium/Air Jet Case.

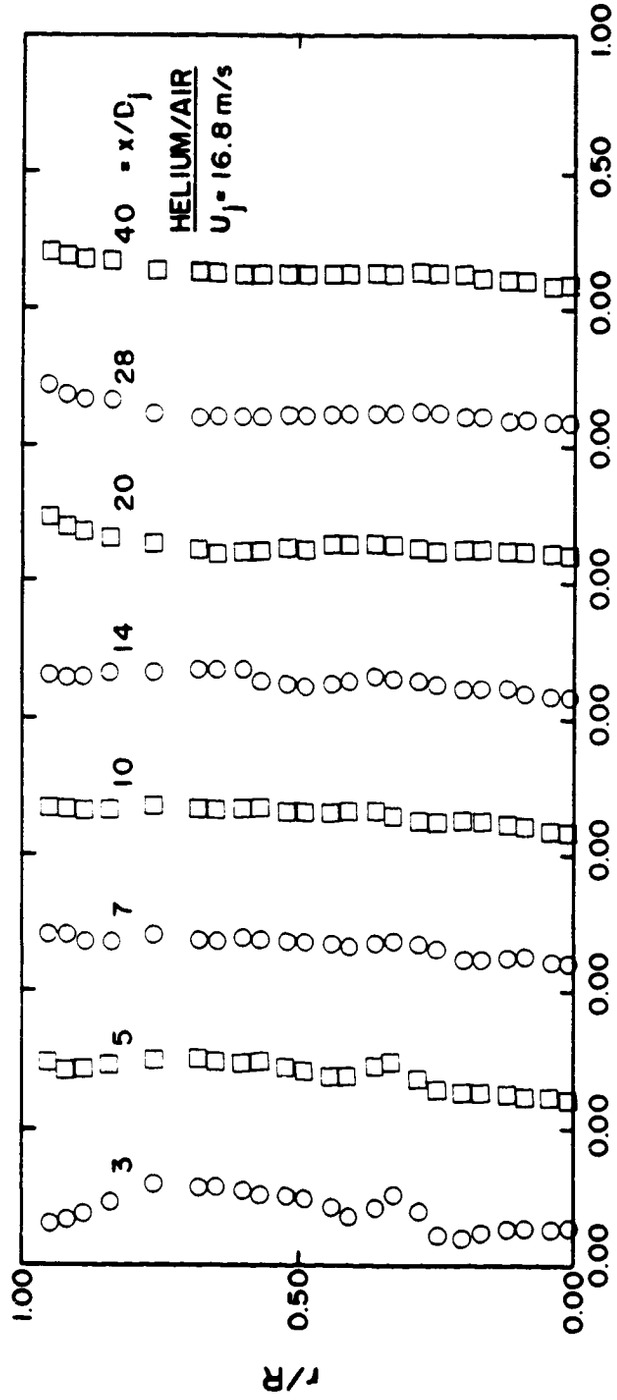

Figure 54. Evolution of w' Distribution for the U_j = 16.8 m/s Helium/Air Jet Case.

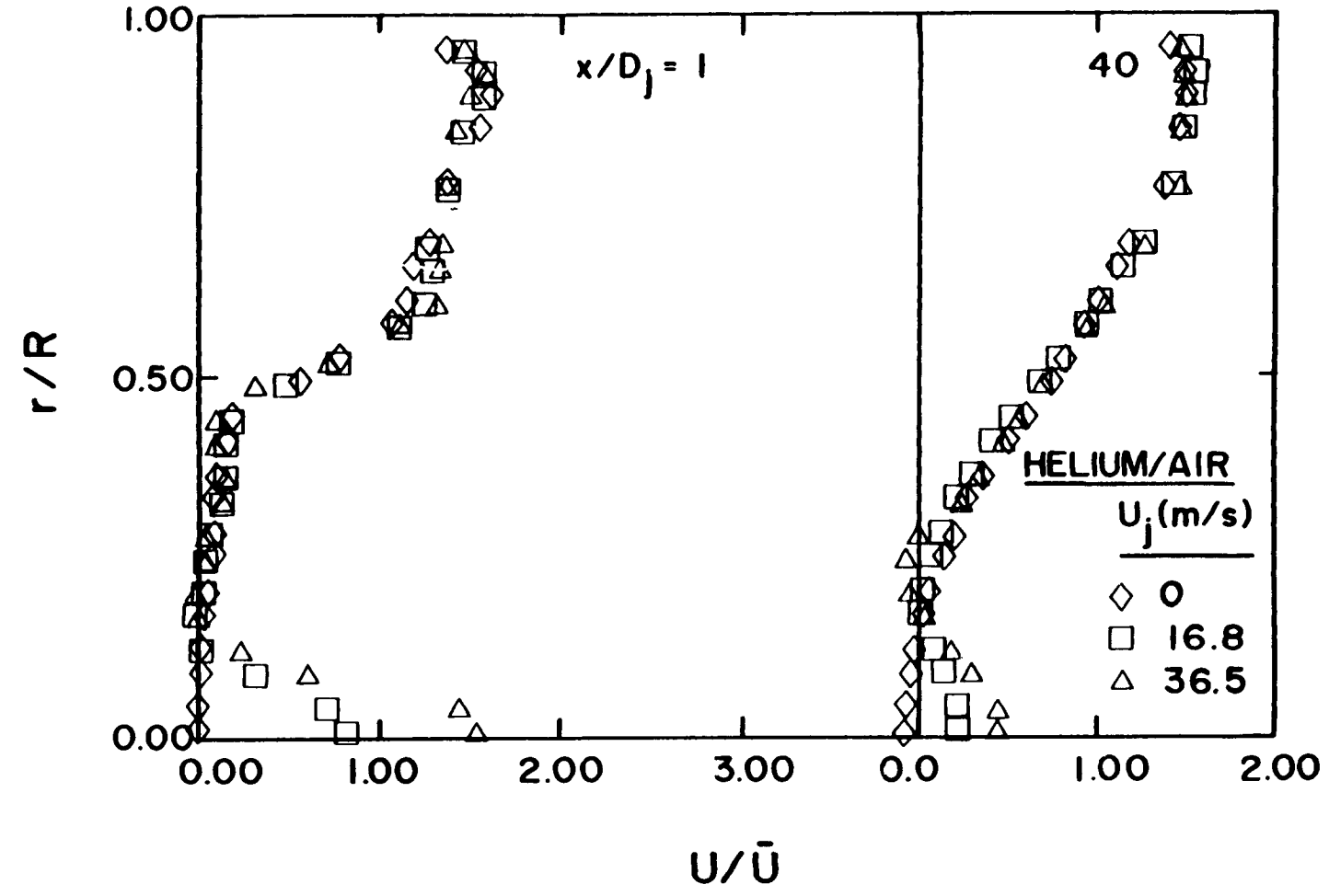

Figure 55. Comparison of U Distributions at x/D_j = 1 and 40 for the Helium/Air Jet Experiments.

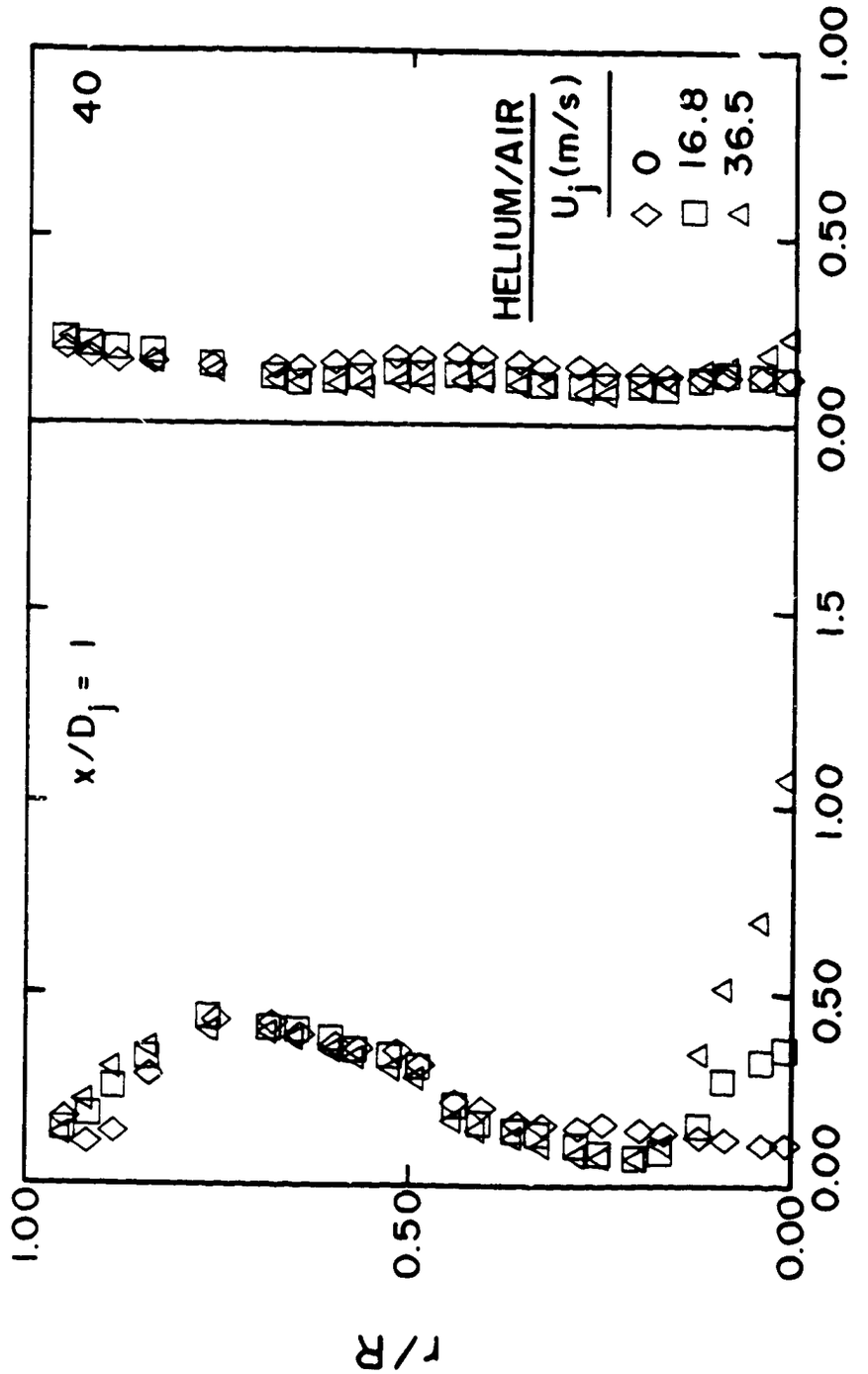

Figure 56. Comparison of u' Distributions at x/D_j = 1 and 40 for the Helium/Air Jet Experiments.

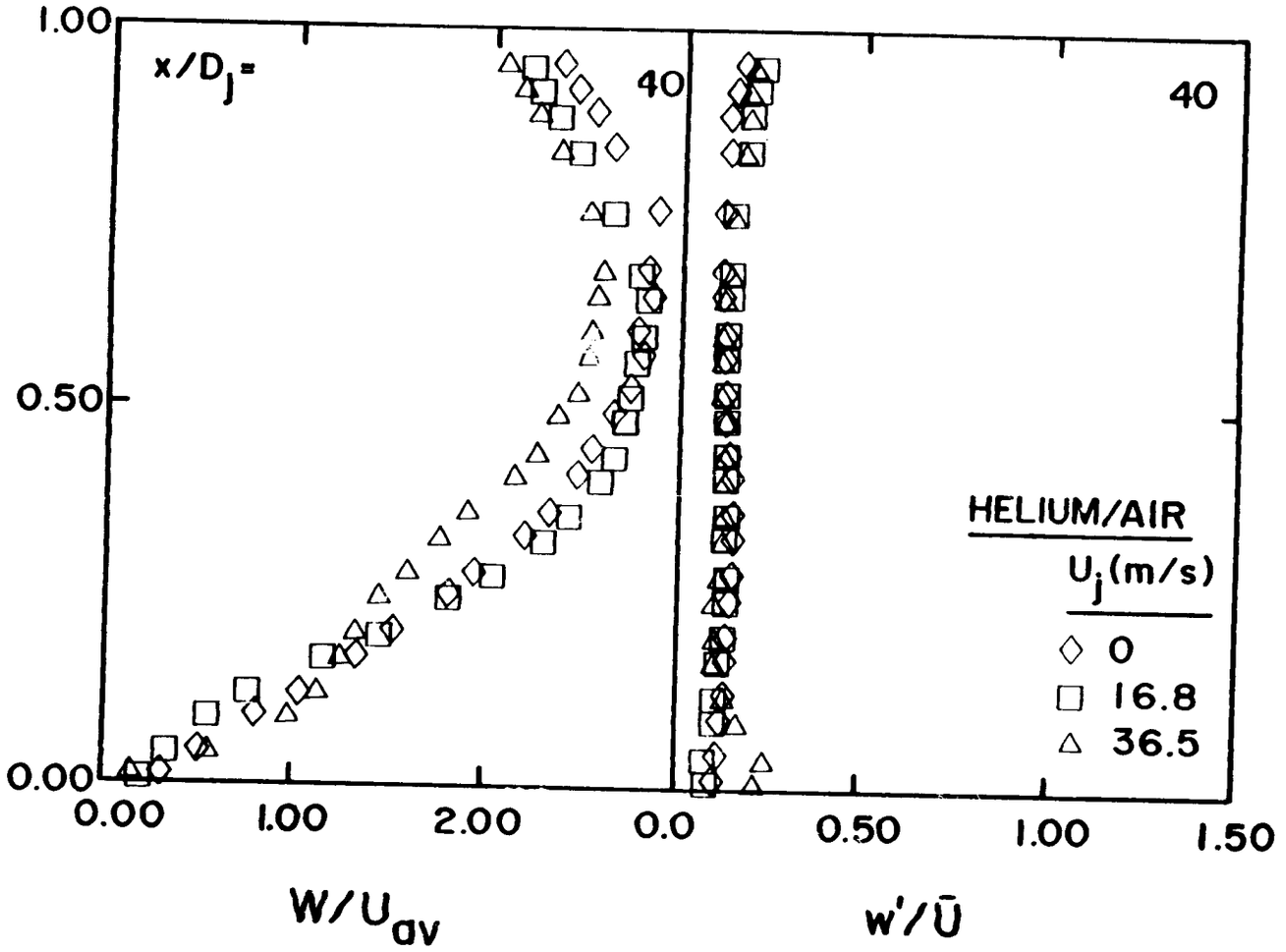

Figure 57. Comparison of W and w' Distributions at x/D_j = 1 and 40 for the Helium/Air Jet Experiments.

TABLE OF RESULTS

TABLE 1. Wall Pressure Drop Measurements for Air and Helium/Air Jets in Confined Swirling Flow.

	$\frac{p_u - p_w}{\frac{1}{2}\rho_a U_e^2}$				
U_j (m/s)	0.0	25.4	16.8	66.8	36.5
x/D_j		Air	Helium/Air	Air	Helium/Air
4	8.64	8.14	8.33	7.75	7.90
8	8.74	8.12	8.38	7.91	8.01
12	8.95	8.33	8.48	8.27	8.38
16	8.85	8.22	8.27	8.17	8.33
20	8.85	8.12	8.22	8.17	8.27
24	9.06	8.48	8.59	8.43	8.48
28	9.01	8.48	8.54	8.43	8.33
32	9.16	8.64	8.75	8.54	8.54
40	9.43	8.80	8.85	8.80	8.85
48	9.48	8.85	8.96	8.85	8.91
56	9.85	9.27	9.38	9.12	9.12
64	10.01	9.59	9.70	9.54	9.59
80	10.48	9.91	10.12	9.91	9.91
96	10.59	10.07	10.22	10.24	10.07
112	11.22	10.86	10.96	10.75	10.80

TABLE 2. Centerline Measurements of Confined Swirling Flow.

x/D_j	$U_j = 0.0$		
	U_o(m/s)	u_o'(m/s)	w_o'(m/s)
1	-.140	.953	.913
1.5	-.190	.960	.919
2	.014	1.000	.833
2.5	.051	.812	.851
3	.049	.917	.681
4	.129	.895	.743
5	.352	.878	.734
6	.200	.870	.749
7	.114	.891	.788
8	.129	.822	.773
9	.156	.919	.750
10	.069	.878	.790
12	-.012	.860	.823
14	-.056	.881	.966
16	-.103	.883	.763
18	-.190	.882	.727
20	-.191	.896	.820
24	-.340	.916	.882
28	-.645	.990	.789
32	-.568	.959	.953
36	-.610	.981	1.003
40	-.632	.945	.899

TABLE 3a. Velocity Measurements of Confined Swirling Flow.

r (mm) \ x/D_j	1	2	3	5	7	10	14	20	28	40
	U (m/s)									
0	-.140	.014	.049	.352	.114	.069	-.056	-.191	-.645	-.632
0.5	-.190	-.210	.049	.351	.114	.069	-.056	-.191	-.645	-.632
2.5	-.170	-.230	.022	.245	.198	.037	-.170	-.168	-.630	-.446
5.5	-.090	-.186	.098	.230	.172	.112	-.230	-.143	-.526	-.226
7.5	-.025	-.115	.022	.218	.125	.158	-.189	-.124	-.515	-.097
10.5	.121	.021	.146	.261	.259	.231	-.064	-.075	-.345	.176
12.5	.276	.137	.184	.299	.319	.281	.071	.131	.181	.481
15.5	.570	.440	.528	.747	.554	.619	.493	.453	.446	1.18
17.5	.730	.534	.858	1.11	.962	.871	.936	.824	.788	1.55
20.5	.755	.954	1.42	2.11	1.77	1.48	1.57	1.47	1.51	2.10
22.5	.600	1.08	1.85	2.90	2.68	2.13	2.26	2.10	1.98	2.80
25.5	.756	.999	2.20	3.67	3.68	3.23	3.19	2.94	2.90	3.84
27.5	2.74	1.24	2.24	4.01	4.51	4.07	4.08	3.60	3.65	4.53
30.5	4.00	2.19	2.70	4.40	5.35	5.22	5.36	4.81	4.66	5.65
32.5	6.60	3.22	3.76	4.69	5.84	5.94	6.31	5.30	5.44	6.30
35.5	7.72	5.39	5.74	5.94	6.76	7.14	7.67	6.40	6.43	7.07
37.5	8.00	7.00	7.50	6.92	7.10	7.66	8.41	7.04	7.20	7.71
40.5	8.28	8.59	10.30	8.67	7.80	8.36	9.32	7.63	8.10	8.50
42.5	8.12	9.13	11.36	9.50	8.22	8.65	10.06	8.04	8.75	9.04
47.5	8.63	8.50	11.67	10.70	9.34	9.12	10.83	9.56	10.30	10.5
52.5	10.40	9.53	10.50	10.50	11.00	10.00	10.60	10.90	11.01	11.21
55.5	10.20	9.20	10.30	10.40	10.97	10.78	9.85	11.20	11.40	11.50
57.5	9.71	8.91	10.90	10.78	10.90	10.85	9.34	11.70	11.40	11.30
59.5	8.82	9.80	10.70	10.70	11.00	11.06	10.98	11.90	11.10	10.74
62.5	0	0	0	0	0	0	0	0	0	0

TABLE 3b. Velocity Measurements of Confined Swirling Flow.

r (mm) \ x/D_j	1	2	3	5	7	10	14	20	28	40
	W (m/s)									
0	0	0	0	0	0	0	0	0	0	0
0.5	1.81	1.30	.903	1.43	2.02	1.86	2.56	1.26	1.59	2.19
2.5	2.80	2.46	1.88	2.70	3.00	3.10	3.74	2.22	3.03	3.60
5.5	5.00	4.18	3.59	4.46	4.80	4.66	5.43	4.05	4.89	5.71
7.5	6.30	5.40	4.80	5.73	5.97	5.97	6.83	5.54	6.43	7.40
10.5	8.37	7.20	6.83	8.04	8.00	8.20	9.40	7.66	8.59	9.57
12.5	9.97	8.78	8.30	9.56	9.50	9.95	11.00	8.98	9.85	11.03
15.5	12.56	11.50	11.08	12.14	11.68	12.10	13.20	11.30	11.75	13.00
17.5	14.27	13.60	12.91	13.82	13.30	13.45	14.90	12.73	13.20	14.03
20.5	16.13	15.90	16.05	16.60	15.45	15.80	17.10	14.84	15.00	15.96
22.5	16.90	17.54	17.92	18.10	17.00	17.00	18.25	16.00	16.20	16.85
25.5	17.21	18.22	19.21	19.91	18.38	18.40	19.50	17.31	17.50	18.01
27.5	17.29	18.29	19.40	20.30	19.20	19.15	20.00	18.08	18.34	18.60
30.5	19.40	18.42	18.95	20.60	20.10	20.11	20.50	18.94	19.27	19.50
32.5	19.80	18.28	18.80	20.63	20.70	20.50	20.50	19.48	19.61	20.00
35.5	19.20	18.31	18.90	20.50	20.90	20.90	20.50	20.01	20.10	20.40
37.5	19.55	18.69	18.70	20.30	20.70	21.07	20.30	20.38	20.30	20.30
40.5	20.45	19.00	19.30	20.10	20.80	21.05	20.30	20.70	20.43	20.77
42.5	20.80	19.53	19.70	20.13	20.70	21.90	20.20	20.83	20.50	20.70
47.5	22.38	19.60	20.30	19.86	20.75	20.60	19.97	21.61	20.50	20.90
52.5	23.30	20.84	21.63	20.70	21.66	19.60	19.75	20.20	19.20	19.30
55.5	22.40	21.20	21.70	20.90	21.40	19.30	19.92	19.60	18.39	18.55
57.5	21.37	20.50	21.07	21.10	21.00	19.50	19.96	19.06	17.82	17.80
59.5	20.40	19.80	20.43	21.20	20.40	19.33	19.90	18.40	17.31	17.20
62.5	0	0	0	0	0	0	0	0	0	0

TABLE 3c. Velocity Measurements of Confined Swirling Flow.

x/D_j / r (mm)	1	2	3	5	7	10	14	20	28	40
	u' (m/s)									
0	.953	1.00	.917	.878	.891	.878	.881	.896	.990	.945
0.5	.970	.990	.917	.878	.891	.878	.881	.896	.990	.945
2.5	.950	.986	.884	.853	.860	.925	.891	.894	.968	.976
5.5	.920	.968	.866	.858	.892	.949	.901	.941	.966	.958
7.5	.980	.984	.934	.901	.886	.929	.894	.968	1.00	.962
10.5	.996	1.09	1.00	.937	.947	1.01	.911	1.04	1.02	1.00
12.5	1.13	1.19	1.08	1.03	.971	1.03	.904	1.05	1.06	1.05
15.5	1.20	1.25	1.12	1.17	1.11	1.16	.970	1.12	1.08	1.08
17.5	.956	.872	1.29	1.29	1.13	1.17	1.08	1.22	1.13	1.18
20.5	1.09	.973	1.24	1.39	1.31	1.32	1.21	1.25	1.20	1.21
22.5	1.10	1.04	1.24	1.42	1.48	1.39	1.33	1.34	1.22	1.24
25.5	1.22	1.14	1.25	.35	1.57	1.51	1.40	1.36	1.31	1.35
27.5	1.51	1.24	1.37	1.42	1.52	1.55	1.47	1.40	1.31	1.43
30.5	2.54	1.49	1.68	1.59	1.59	1.60	1.58	1.39	1.37	1.35
32.5	2.48	1.65	2.02	1.82	1.57	1.57	1.50	1.36	1.35	1.38
35.5	2.49	1.81	2.45	2.13	1.74	1.49	1.48	1.27	1.28	1.29
37.5	2.62	1.94	2.69	2.26	1.79	1.42	1.35	1.23	1.20	1.27
40.5	2.65	2.14	2.56	2.25	1.85	1.42	1.26	1.06	1.11	1.18
42.5	2.86	2.34	2.38	2.14	1.80	1.55	1.19	.966	1.16	1.17
47.5	3.20	2.67	2.47	1.97	1.67	1.56	1.32	1.09	1.15	1.22
52.5	1.61	2.20	2.27	1.92	1.56	1.43	1.31	1.17	1.27	1.28
55.5	.645	1.78	2.20	1.84	1.45	1.45	1.22	1.32	1.43	1.32
57.5	.710	2.05	2.14	1.75	1.49	1.28	1.07	1.45	1.51	1.39
59.5	.739	2.14	2.22	1.65	1.44	1.22	1.12	1.32	1.65	1.53
62.5	0	0	0	0	0	0	0	0	0	0

TABLE 3d. Velocity Measurements of Confined Swirling Flow.

x/D_j / r (mm)	1	2	3	5	7	10	14	20	28	40
	w' (m/s)									
0	.913	.833	.681	.734	.788	.790	.966	.820	.789	.899
0.5	.913	.833	.681	.734	.788	.790	.966	.820	.789	.899
2.5	1.02	.950	.760	.767	.841	.853	.953	.810	.906	.963
5.5	1.03	.950	.826	.897	.902	.912	.964	.945	.970	1.04
7.5	1.20	1.07	.920	.960	.945	1.02	1.05	1.04	1.05	1.11
10.5	1.37	1.16	1.06	1.06	1.05	1.28	1.20	1.10	1.08	1.07
12.5	1.44	1.30	1.20	1.15	1.14	1.30	1.25	1.16	1.16	1.16
15.5	1.60	1.67	1.49	1.28	1.23	1.35	1.30	1.27	1.18	1.19
17.5	1.66	1.92	1.72	1.47	1.34	1.44	1.37	1.29	1.27	1.21
20.5	1.56	1.86	1.90	1.64	1.43	1.47	1.29	1.34	1.22	1.19
22.5	1.63	1.67	1.71	1.56	1.51	1.46	1.28	1.35	1.30	1.21
25.5	1.99	1.65	1.52	1.53	1.49	1.42	1.26	1.30	1.19	1.19
27.5	2.29	[illegible].87	1.58	1.49	1.38	1.42	1.16	1.20	1.21	1.19
30.5	2.[illegible]	2.13	1.69	1.51	1.38	1.33	1.15	1.14	1.17	1.11
32.5	2.85	2.19	1.79	1.59	1.54	1.39	1.09	1.10	1.10	1.04
35.5	3.24	2.19	2.01	1.77	1.56	1.46	1.11	1.06	1.09	1.09
37.5	3.21	2.21	2.19	1.67	1.49	1.58	1.12	.961	1.16	1.04
40.5	3.51	2.66	2.35	1.99	1.51	1.61	1.12	.934	1.06	1.01
42.5	3.54	2.74	2.38	1.92	1.48	1.62	1.12	.970	1.08	.988
47.5	3.03	3.04	2.36	2.03	1.55	1.52	1.08	1.16	.857	1.02
52.5	1.38	2.41	2.05	2.05	1.40	1.38	1.07	1.25	.976	1.07
55.5	1.38	2.09	1.74	1.84	1.37	1.31	1.07	1.12	.997	1.12
57.5	1.75	1.99	1.53	1.66	1.43	1.20	1.09	1.16	1.15	1.22
59.5	1.74	1.77	1.58	1.64	1.48	1.22	1.39	1.30	1.29	1.35
62.5	0	0	0	0	0	0	0	0	0	0

TABLE 4. Centerline Measurements of Confined Air Jet.

x/D_j	U_j = 66.8 m/s	
	U (m/s)	u' (m/s)
1.25	22.20	6.94
1.5	20.80	7.50
2	19.00	7.35
2.5	18.11	7.16
3	18.16	6.24
4	17.10	5.50
5	13.81	4.60
6	12.80	4.10
7	9.93	3.64
8	6.54	3.70
9	5.74	3.11
10	5.01	3.19
12	2.96	2.60
14	1.42	1.97
16	1.00	1.71

TABLE 5a. Velocity Measurements of Confined Air Jet.

$\frac{x}{D_j}$ =	1.25		3.0			5.0	
r(mm)	U(m/s)	u'(m/s)	r(mm)	U(m/s)	u'(m/s)	r(mm)	U(m/s)	u'(m/s)
0	22.20	6.94	0	18.16	6.24	0	13.81	4.60
1	20.22	6.88	1	16.71	5.79	1	13.27	4.55
2	18.03	6.69	2	14.75	5.44	2	12.10	4.30
3	15.75	5.93	3	12.84	4.98	4	9.88	3.91
4	13.95	5.54	4	10.40	4.93	5	9.30	3.94
5	9.87	4.83	6	5.62	3.52	7	5.97	3.29
6	6.47	3.96	7	4.50	3.11	10	2.98	2.12
7	4.40	2.93	9	2.16	1.96	12	2.14	1.68
9	1.80	1.23	12	1.15	.845	15	1.26	1.17
10	1.08	.920	14	.889	.635	17	.899	.866
12	.914	.575	17	.651	.614	20	.413	.814
15	.617	.486	19	.483	.516	22	.215	.851
17	.578	.414	22	.366	.466	25	.224	.591
20	.360	.377	24	.209	.519	27	-.106	.678
22	.227	.358	27	.143	.490	30	-.249	.568
25	.300	.380	29	.053	.537	32	-.207	.576
27	.290	.346	32	-.051	.443	35	-.261	.595
30	.278	.345	34	-.033	.442	37	-.317	.593
32	.283	.288	37	-.046	.408	42	-.222	.544
35	.268	.269	39	-.095	.385	47	-.322	.618
37	.253	.265	44	-.115	.369			
40	.220	.275	49	-.155	.366			
42	.181	.296						
47	.323	.323						
52	.256	.329						

TABLE 5b. Velocity Measurements of Confined Air Jet.

x/D_j =	7			10			14	
r(mm)	U(m/s)	u'(m/s)	r(mm)	U(m/s)	u'(m/s)	r(mm)	U(m/s)	u'(m/s)
0	9.93	3.64	0	5.01	3.19	0	1.42	1.97
2	9.56	3.41	2	4.94	3.12	2	1.21	2.04
3	8.34	3.34	4	3.81	3.05	4	1.16	1.88
5	7.54	3.13	6	4.03	2.76	6	1.11	1.93
8	5.38	2.77	8	3.56	2.53	8	.990	1.82
10	4.31	2.37	10	3.27	2.70	10	1.21	1.91
13	2.82	2.19	12	2.77	2.31	12	.960	1.87
15	2.22	1.91	14	1.90	2.00	14	.720	1.76
18	.938	1.46	16	1.56	1.85	16	.760	1.59
20	.798	1.33	18	1.30	1.73	18	.450	1.49
23	.239	1.06	20	1.46	1.59	20	.720	1.49
25	.211	.956	22	1.13	1.53	22	.610	1.52
28	-.170	.818	24	.740	1.31	24	.820	1.72
30	-.301	.807	26	.790	1.30	26	.440	1.56
33	-.301	.737	28	.690	1.59	28	.570	1.64
35	-.382	.726	30	.390	1.26	30	.420	1.57
40	-.511	.615	32	.340	1.13	32	.370	1.24
45	-.593	.614	34	.370	1.11	34	.310	1.34
						36	.280	1.29
						38	.130	1.15
						40	.200	1.12

TABLE 6. Centerline Measurements of Confined Helium/Air Jets.

	U_j = 16.8 (m/s)		U_j = 36.5 (m/s)	
x/D_j	U_o(m/s)	u'_o(m/s)	U_o(m/s)	u'_o(m/s)
3	5.71	1.89		
4	3.67	1.65		
5	3.25	1.37	6.64	2.16
6	1.76	.996	5.03	1.82
7	1.55	.912	3.42	1.60
8	1.31	.707	3.62	1.68
9	1.04	.623	2.52	1.44
10	.993	.635	2.28	1.29
12	.834	.613	1.45	1.02
14	.398	.450	1.30	.871
16	.043	.390	.862	.781
18			.245	.738
20			.086	.690
24			.040	.463

TABLE 7a. Velocity Measurements of Confined Helium/Air Jet; U_j = 16.8 m/s.

x/D_j / r(mm)	3	5	7	10
	U (m/s)			
0	5.71	3.25	1.55	.993
0.5	5.57	3.25	1.55	.993
1.5	5.71	3.65	1.53	.993
2.5	4.18	3.65	1.34	.551
3.5	3.90	2.78	1.37	.674
4.5	3.16	3.26	1.33	.788
5.5	2.80	2.31	1.09	.631
6.5	2.23	1.60	1.04	.663
7.5	1.90	1.30	1.03	.431
9.5	1.62	.790	.902	.427
10.5	-.435	.852	.943	.407
12.5	-.215	.416	.628	.356
15.5	-.122	.061	.485	.334
17.5	-.078	-.200	.110	.061
20.5	-.100			
22.5	-.111			
25.5	-.090			
27.5	-.120			
30.5	-.200			
32.5	-.045			
42.5	-.121			
52.5	-.070			
57.5	-.047			
59.5	-.018			
62.5	0			

TABLE 7b. Velocity Measurements of Confined Helium/Air Jet; U_j = 16.8 m/s.

x/D_j / r(mm)	3	5	7	10
	u' (m/s)			
0	1.89	1.37	.912	.635
0.5	1.86	1.37	.912	.581
1.5	1.89	1.40	.958	.635
2.5	1.75	1.41	.906	.570
3.5	1.62	1.39	.931	.573
4.5	1.49	1.44	.932	.606
5.5	1.43	1.27	.923	.623
6.5	1.29	.983	.887	.603
7.5	1.30	.946	.825	.570
9.5	1.12	.790	.801	.570
10.5	.845	.971	.767	.630
12.5	.583	.780	.729	.511
15.5	.055	.544	.600	.513
17.5	.068	.360	.470	.433
20.5	.082			
22.5	.129			
25.5	.150			
27.5	.150			
30.5	.136			
32.5	.096			
42.5	.083			
52.5	.032			
57.5	.032			
59.5	.031			
62.5	0			

TABLE 8. Flow Conditions of Jets in Confined Swirling Air Flow; Re x 10^{-3} = 54.90. The Temperature of Jet Gas is Set Equal to Room Temperature.

Parameter	Air Jet			Helium/Air Jet	
ρ_j/ρ_a	1	1	1	.310	.228
U_j (m/s)	25.4	66.8	152.8	16.8	36.5
Re_j x 10^{-3}	14.38	37.82	86.51	1.50	2.97
$\dot{M}_j/\dot{M}$	.068	.475	2.48	.009	.032

TABLE 9a. Centerline Measurements of Air Jets in Confined Swirling Flow.

x/D_j	U_j = 25.4 (m/s)			U_j = 66.8 (m/s)		
	U_o(m/s)	u_o'(m/s)	w_o'(m/s)	U_o(m/s)	u_o'(m/s)	w_o'(m/s)
1	7.89	3.88	1.91	22.65	8.45	4.44
1.5	7.40	3.40	1.85	19.10	8.75	4.67
2	6.50	3.10	1.85	16.03	8.25	4.31
2.5	5.70	2.80	1.69	14.30	7.60	3.96
3	4.15	2.72	1.32	10.21	7.02	3.22
4	3.11	2.16	1.27	7.97	5.40	2.86
5	2.88	1.56	1.25	6.11	4.28	2.74
6	2.64	1.39	1.11	5.39	3.34	2.33
7	2.35	1.30	1.03	4.20	2.82	2.09
8	2.30	1.20	.96	3.57	2.28	1.74
9	2.17	1.25	.98	3.24	2.04	1.65
10	1.99	1.11	1.02	3.00	2.03	1.49
12	1.76	1.15	1.11	2.77	1.61	1.32
14	1.45	1.09	.98	2.72	1.44	1.30
16	1.36	1.09	.94	2.32	1.39	1.20
18	1.21	1.11	1.05	2.07	1.25	1.21
20	1.14	1.10	1.01	2.06	1.13	1.02
24	1.07	1.04	1.01	1.76	1.12	1.03
28	.715	1.03	.914	1.72	1.05	1.07
32	.529	1.08	.850	1.60	1.10	1.01
36	.531	.988	.911	1.44	1.14	1.10
40	.351	1.01	.852	1.21	.952	.947

TABLE 9b. Centerline Measurements of Air Jets in Confined Swirling Flow.

x/D_j	U_j = 152.8 (m/s)	
	U(m/s)	u'(m/s)
2.9	25.50	13.70
3.5	20.25	13.80
4.5	16.10	12.00
5.4	13.50	10.50
6.3	10.97	8.52
7.2	8.49	6.67
9.0	7.96	5.01
10.9	5.79	4.13
12.7	4.90	3.30
14.5	3.92	2.74
16.4	3.49	2.54
20	2.92	2.14
23.7	2.40	1.90
27.4	1.62	1.63
31	1.39	1.54
34.7	1.31	1.42
38.4	1.23	1.38
42	1.15	1.35

TABLE 10a. Velocity Measurements of Air Jet in Confined Swirling Flow; U_j = 25.4 m/s.

x/D_j / r (mm)	1	2	3	5	7	10	14	20	28	40
	U (m/s)									
0	7.89	6.50	4.15	2.88	2.35	1.99	1.45	1.135	.715	.351
0.5	7.85	6.40	4.15	2.88	2.35	1.99	1.45	1.135	.715	.351
2.5	6.30	5.80	3.11	2.26	1.81	1.77	1.46	1.100	.790	.356
5.5	2.92	4.00	1.24	1.16	1.36	1.32	1.14	.913	.513	.372
7.5	1.40	2.27	.255	.322	.902	.989	.869	.815	.525	.218
10.5	.628	1.00	.225	-.034	.401	.565	.364	.539	.385	.362
12.5	.586	.468	.298	.029	.310	.615	.348	.487	.300	.880
15.5	.747	.324	.840	.652	.720	.792	.494	.687	.383	1.16
17.5	.810	.485	1.15	1.31	1.24	1.03	.711	.735	.658	1.52
20.5	.811	.974	1.67	2.68	2.38	1.72	1.43	1.17	1.02	2.15
22.5	.805	1.19	1.91	3.25	2.96	2.16	2.27	1.62	1.53	2.73
25.5	.927	1.15	2.15	4.14	4.32	3.10	3.30	2.42	2.27	3.58
27.5	2.79	1.21	2.45	4.30	4.99	3.90	4.20	3.05	2.84	4.28
30.5	4.02	1.88	3.33	4.80	5.72	5.22	5.60	4.14	4.03	5.26
32.5	5.90	3.12	4.48	5.16	6.14	5.94	6.33	4.75	4.74	6.00
35.5	7.20	5.56	7.11	7.22	6.52	6.91	7.66	5.72	5.62	6.82
37.5	7.66	6.95	8.33	8.35	6.62	7.38	8.31	6.35	6.58	7.45
40.5	7.98	8.57	10.50	9.70	8.50	8.20	9.36	7.23	7.44	8.44
42.5	7.90	8.70	11.32	9.80	8.72	8.55	9.90	7.69	8.06	8.92
47.5	8.85	8.84	11.54	10.40	9.42	9.10	10.60	8.94	9.83	10.10
52.5	10.35	9.80	10.93	10.20	10.30	10.10	10.02	10.40	10.60	10.96
55.5	10.12	9.21	11.81	10.25	10.80	11.20	9.75	11.20	10.61	10.90
57.5	9.73	9.01	11.97	10.20	10.80	11.40	9.30	11.20	10.60	10.82
59.5	8.51	10.18	11.65	9.92	10.50	11.00	8.92	11.60	10.50	10.60
62.5	0	0	0	0	0	0	0	0	0	0

TABLE 10b. Velocity Measurements of Air Jets in Confined Swirling Flow: U_j = 25.4 m/s.

r (mm) \ x/D_j	1	2	3	5	7	10	14	20	28	40
	W (m/s)									
0	0	0	0	0	0	0	0	0	0	0
0.5	1.45	1.29	1.20	2.10	1.54	1.02	1.32	1.92	1.47	3.12
2.5	2.70	1.64	1.90	2.26	2.04	1.71	1.85	2.66	2.50	4.33
5.5	4.23	2.17	1.94	3.24	3.37	3.05	3.02	4.30	4.22	6.23
7.5	5.74	3.44	3.07	4.52	4.58	4.46	4.44	5.71	5.43	7.60
10.5	7.90	5.69	5.40	6.97	6.77	6.68	7.12	7.94	7.55	9.58
12.5	9.63	7.62	7.85	9.20	8.35	8.36	8.76	9.38	9.01	10.94
15.5	11.87	10.82	10.20	12.27	10.73	11.01	11.74	11.96	11.32	12.73
17.5	13.96	12.97	12.60	14.30	12.33	12.63	13.70	13.60	12.77	13.93
20.5	15.94	15.74	16.00	17.03	14.62	15.10	16.30	15.50	14.80	15.62
22.5	16.89	17.27	17.50	18.70	16.04	16.40	17.40	16.60	16.00	16.40
25.5	17.20	18.20	18.85	20.00	17.85	17.96	19.01	17.84	17.43	17.38
27.5	17.80	18.30	19.00	20.50	18.70	18.60	19.80	18.36	18.21	17.96
30.5	19.31	18.20	18.70	20.40	19.30	19.50	20.30	19.40	19.22	18.70
32.5	19.30	18.10	18.10	20.30	19.70	20.10	20.30	19.60	19.60	18.93
35.5	19.50	18.10	18.11	20.16	20.10	20.40	20.32	20.15	20.08	19.20
37.5	19.83	18.20	18.50	19.96	20.25	20.65	20.30	20.20	20.32	19.40
40.5	20.99	19.04	18.80	19.70	20.14	20.73	20.10	20.50	20.70	19.53
42.5	21.56	19.45	19.30	19.60	20.20	20.70	20.13	20.60	20.66	19.45
47.5	22.50	19.84	20.10	20.16	20.15	20.10	19.95	21.10	20.70	19.23
52.5	23.40	21.30	21.20	20.96	21.10	19.30	19.53	20.20	19.20	17.93
55.5	22.40	21.50	21.60	21.05	20.70	19.00	19.72	19.56	18.20	17.20
57.5	21.20	20.50	21.20	20.70	20.40	19.01	19.80	18.85	17.67	16.60
59.5	20.10	20.10	20.70	20.60	19.70	18.75	19.98	18.20	17.00	16.05
62.5	0	0	0	0	0	0	0	0	0	0

TABLE 10c. Velocity Measurements of Air Jet in Confined Swirling Flow; U_j = 25.4 m/s.

r (mm) \ x/D_j	1	2	3	5	7	10	14	20	28	40
	u' (m/s)									
0	3.88	3.10	2.72	1.56	1.30	1.11	1.09	1.10	1.03	1.01
0.5	3.88	3.10	2.72	1.56	1.29	1.11	1.09	1.10	1.04	1.01
2.5	3.66	2.95	2.75	1.66	1.31	1.20	1.16	1.02	1.06	.986
5.5	2.70	2.59	1.96	1.54	1.32	1.19	1.18	1.10	1.03	1.04
7.5	1.65	2.23	1.32	1.32	1.30	1.16	1.17	1.11	1.04	1.06
10.5	.888	1.55	1.20	1.20	1.14	1.17	1.12	1.09	1.06	1.03
12.5	.802	1.15	1.20	1.20	1.09	1.22	1.08	1.06	1.07	1.07
15.5	.967	.953	1.23	1.33	1.21	1.19	1.14	1.10	1.05	1.13
17.5	1.08	1.02	1.22	1.39	1.36	1.28	1.15	1.14	1.08	1.11
20.5	1.16	1.09	1.18	1.47	1.53	1.28	1.32	1.17	1.12	1.22
22.5	1.19	1.12	1.19	1.43	1.66	1.35	1.34	1.25	1.21	1.32
25.5	1.27	1.15	1.20	1.33	1.59	1.43	1.44	1.31	1.23	1.36
27.5	2.06	1.24	1.39	1.36	1.59	1.48	1.45	1.31	1.29	1.36
30.5	2.16	1.53	1.98	1.66	1.47	1.47	1.46	1.30	1.36	1.36
32.5	2.06	1.81	2.34	1.84	1.53	1.47	1.45	1.27	1.33	1.36
35.5	2.32	1.94	2.67	2.34	1.54	1.35	1.46	1.22	1.27	1.34
37.5	2.54	1.85	2.48	2.30	1.60	1.38	1.33	1.16	1.14	1.20
40.5	2.54	2.39	2.36	2.31	1.75	1.42	1.28	1.10	1.08	1.15
42.5	2.69	2.51	2.20	2.11	1.66	1.44	1.18	1.01	1.07	1.19
47.5	3.20	2.70	2.36	2.02	1.65	1.42	1.26	1.07	1.15	1.14
52.5	1.51	2.28	2.18	1.78	1.36	1.42	1.16	1.15	1.36	1.16
55.5	.747	1.97	1.89	1.66	1.33	1.36	1.07	1.25	1.38	1.19
57.5	.766	2.17	1.68	1.64	1.31	1.29	1.01	1.29	1.51	1.29
59.5	.788	2.25	1.44	1.50	1.38	1.36	1.01	1.43	1.55	1.27
62.5	0	0	0	0	0	0	0	0	0	0

TABLE 10d. Velocity Measurements of Air Jet in Confined Swirling Flow; U_j = 25.4 m/s.

r (mm) \ x/D_j	1	2	3	5	7	10	14	20	28	40
	w' (m/s)									
0	1.91	1.85	1.32	1.25	1.03	1.02	.980	1.01	.914	.852
0.5	1.91	1.85	1.32	1.25	1.03	1.017	.982	1.01	.914	.892
2.5	1.70	1.77	1.28	1.26	1.03	.988	1.02	1.04	.961	.932
5.5	1.41	1.61	1.16	1.18	1.01	1.04	1.00	1.08	1.00	1.04
7.5	1.28	1.36	1.17	1.20	1.08	1.13	1.06	1.11	1.08	1.04
10.5	1.39	1.40	1.27	1.24	1.09	1.28	1.23	1.22	1.15	1.13
12.5	1.48	1.38	1.30	1.38	1.11	1.34	1.27	1.28	1.17	1.17
15.5	1.65	1.70	1.53	1.44	1.23	1.43	1.42	1.40	1.29	1.21
17.5	1.67	1.95	1.81	1.55	1.28	1.45	1.43	1.42	1.32	1.21
20.5	1.63	1.94	2.05	1.66	1.46	1.43	1.37	1.38	1.33	1.23
22.5	1.63	1.84	1.81	1.55	1.50	1.40	1.35	1.33	1.30	1.24
25.5	1.98	1.71	1.50	1.47	1.29	1.31	1.21	1.25	1.24	1.14
27.5	2.43	1.93	1.57	1.46	1.27	1.25	1.16	1.22	1.28	1.12
30.5	2.70	2.14	1.70	1.50	1.34	1.27	1.12	1.14	1.14	1.11
32.5	2.86	2.20	2.16	1.60	1.42	1.29	1.15	1.10	1.12	1.05
35.5	3.09	2.17	2.30	1.75	1.46	1.41	1.06	1.01	1.04	1.03
37.5	3.17	2.05	2.28	1.86	1.45	1.45	1.04	1.00	1.04	.920
40.5	3.52	2.41	2.33	1.80	1.47	1.53	1.04	.924	1.10	.972
42.5	3.47	3.14	2.19	1.93	1.41	1.57	1.04	.921	1.11	.983
47.5	2.88	2.98	2.37	1.97	1.50	1.47	1.11	1.05	.907	.976
52.5	1.55	2.53	1.92	1.81	1.40	1.37	1.08	1.16	1.07	1.06
55.5	1.45	1.97	1.46	1.59	1.30	1.27	1.13	1.26	1.21	1.12
57.5	1.83	1.94	1.29	1.57	1.39	1.29	1.05	1.29	1.19	1.23
59.5	1.76	1.78	1.16	1.45	1.46	1.24	1.13	1.46	1.49	1.50
62.5	0	0	0	0	0	0	0	0	0	0

TABLE 11a. Velocity Measurements of Air Jet in Confined Swirling Flow; U_j = 66.8 m/s.

x/D_j r (mm)	1	2	3	5	7	10	14	20	28	40
	U (m/s)									
0	22.65	16.03	10.21	6.11	4.20	3.00	2.72	2.06	1.72	1.21
0.5	22.65	16.00	10.21	6.11	4.20	3.00	2.72	2.06	1.72	1.21
1.5	19.40									
2.5	17.35	13.00	10.64	5.80	3.93	2.85	2.49	2.02	1.69	1.29
3.5	13.40									
4.5	10.90									
5.5	8.51	6.81	7.24	5.02	2.58	2.67	2.24	1.83	1.60	1.29
7.5	5.44	3.86	4.90	4.15	1.86	2.29	2.04	1.57	1.37	1.31
10.5	1.15	2.30	2.10	2.62	1.30	1.60	1.63	1.14	1.27	1.43
12.5	1.10	1.69	1.46	2.25	1.35	1.26	1.56	1.34	1.29	1.56
15.5	1.45	1.66	1.33	2.05	2.26	1.18	1.73	1.40	1.44	1.75
17.5	1.81	1.75	1.87	2.41	2.65	1.31	1.97	1.61	1.83	1.99
20.5	2.00	1.98	2 82	3.26	3.45	2.15	2.50	2.26	2.12	2.48
22.5	2.04	1.97	3.18	3.95	4.06	2.70	3.27	2.78	2.55	3.00
25.5	2.45	1.95	3.44	4.88	4.86	3.66	4.25	3.74	3.28	3.78
27.5	3.24	2.03	3.60	5.28	5.38	4.50	4.87	4.22	3.93	4.34
30.5	5.90	3.15	4.22	5.84	5.81	5.73	6.16	5.33	4.93	5.10
32.5	7.25	4.11	4.93	6.07	6.20	6.50	7.01	5.83	5.62	5.74
35.5	9.05	5.92	7.40	6.68	6.76	7.32	8.01	6.75	6.90	6.91
37.5	9.20	7.17	9.14	7.40	7.42	7.91	8.66	7.30	7.52	7.43
40.5	8.86	8.28	11.30	10.01	8.84	8.62	9.72	7.80	8.52	8.55
42.5	9.28	8.72	11.70	10.75	9.81	9.03	10.50	8.26	9.23	9.28
47.5	10.50	8.88	11.66	11.65	11.01	9.53	11.67	10.39	10.70	10.50
52.5	12.37	9.89	10.70	11.23	11.30	10.40	11.43	11.60	11.97	11.30
55.5	11.95	9.22	11.10	11.10	11.67	11.14	10.60	12.10	12.38	11.53
57.5	10.99	8.77	11.45	11.20	11.66	11.47	9.80	12.30	12.35	11.50
59.5	9.84	9.76	11.40	10.98	11.57	11.57	9.20	12.10	11.80	11.20
62.5	0	0	0	0	0	0	0	0	0	0

TABLE 11b. Velocity Measurements of Air Jet in Confined Swirling Flow; U_j = 66.8 m/s.

x/D_j / r (mm)	1	2	3	5	7	10	14	20	28	40
	W (m/s)									
0	0	0	0	0	0	0	0	0	0	0
0.5	7.09	6.87	5.63	4.19	2.98	2.02	1.72	1.47	1.67	2.82
2.5	7.68	6.36	5.42	4.06	3.20	2.23	2.27	1.88	3.11	3.77
5.5	7.93	4.76	5.92	4.22	3.53	3.23	3.02	2.92	4.60	5.73
7.5	8.25	4.42	5.65	4.51	4.31	4.20	4.18	3.90	5.68	7.16
10.5	9.34	6.48	7.07	6.23	6.34	6.15	6.43	5.50	7.98	9.36
12.5	10.50	7.82	8.65	8.37	8.48	8.06	8.07	7.20	9.50	10.55
15.5	12.50	10.76	11.76	12.07	11.02	10.60	11.14	9.49	11.97	12.66
17.5	14.22	12.90	13.93	14.46	13.33	12.50	13.23	11.36	13.40	14.00
20.5	16.20	15.65	17.60	17.53	16.16	15.20	16.15	13.90	15.76	16.00
22.5	16.92	17.45	19.11	19.34	17.62	17.04	17.94	15.43	17.03	16.92
25.5	17.43	18.37	20.00	20.76	19.47	18.80	19.86	17.20	18.85	18.33
27.5	17.75	18.43	20.00	21.10	20.20	19.70	20.50	18.42	19.60	18.99
30.5	19.23	18.40	20.06	21.16	20.83	20.80	21.20	19.53	20.40	19.63
32.5	19.30	18.14	19.88	21.20	21.02	21.40	21.20	20.10	20.88	20.30
35.5	19.00	18.16	20.20	20.80	21.12	21.80	21.30	20.90	21.50	20.52
37.5	19.08	18.42	19.76	20.58	21.10	22.04	21.40	21.20	21.52	20.60
40.5	20.20	19.00	20.20	20.55	21.40	22.30	21.30	21.60	21.90	20.83
42.5	20.80	19.00	20.40	20.55	21.30	22.10	21.30	21.93	22.12	20.85
47.5	22.40	19.60	21.46	20.80	21.40	21.40	20.83	22.50	21.50	20.19
52.5	23.10	21.00	22.70	21.45	22.02	20.20	20.77	22.10	20.13	18.98
55.5	22.20	21.40	22.40	21.60	21.91	20.20	20.75	21.10	18.93	18.07
57.5	21.20	20.75	21.94	21.60	21.30	20.30	21.00	20.32	18.22	17.50
59.5	20.40	20.35	21.00	21.70	21.10	20.50	21.20	19.60	17.80	17.10
62.5	0	0	0	0	0	0	0	0	0	0

TABLE 11c. Velocity Measurements of Air Jet in Confined Swirling Flow; U_j = 66.8 m/s.

r (mm) \ x/D_j	1	2	3	5	7	10	14	20	28	40
	u' (m/s)									
0	8.45	8.25	7.02	4.28	2.82	2.03	1.44	1.13	1.05	.952
0.5	8.45	8.25	7.02	4.28	2.82	2.03	1.44	1.13	1.05	.952
1.5	8.14									
2.5	7.54	8.00	7.04	4.30	2.73	1.97	1.53	1.19	1.11	.982
3.5	6.71									
4.5	5.90									
5.5	5.11	6.35	6.39	4.17	2.49	1.89	1.53	1.15	1.07	.981
7.5	3.61	4.48	5.36	3.81	2.10	1.78	1.54	1.21	1.06	.95
10.5	1.45	2.60	3.31	2.84	1.64	1.70	1.37	1.14	1.06	1.000
12.5	1.02	1.84	2.22	2.41	1.46	1.49	1.39	1.13	1.07	1.01
15.5	1.01	1.21	1.21	1.51	1.62	1.32	1.27	1.15	1.06	1.07
17.5	1.08	1.05	1.10	1.34	1.57	1.24	1.21	1.19	1.22	1.09
20.5	.978	.964	1.09	1.35	1.69	1.29	1.21	1.24	1.18	1.15
22.5	.947	.991	1.08	1.39	1.45	1.35	1.26	1.33	1.21	1.28
25.5	1.18	.997	1.12	1.48	1.43	1.43	1.34	1.46	1.33	1.34
27.5	1.68	1.06	1.22	1.55	1.41	1.47	1.39	1.45	1.40	1.37
30.5	2.27	1.41	1.56	1.69	1.40	1.43	1.43	1.42	1.48	1.39
32.5	2.55	1.62	1.80	1.83	1.48	1.40	1.37	1.35	1.47	1.46
35.5	2.90	1.80	2.65	2.08	1.68	1.45	1.31	1.28	1.39	1.40
37.5	2.99	1.88	2.75	2.23	1.97	1.45	1.37	1.23	1.33	1.39
40.5	2.96	1.95	2.30	2.23	2.25	1.45	1.44	1.04	1.29	1.29
42.5	3.44	2.15	2.37	2.11	2.15	1.49	1.49	1.08	1.18	1.27
47.5	3.54	2.57	2.44	2.17	1.89	1.62	1.47	1.15	1.15	1.25
52.5	1.29	2.12	2.19	1.97	1.57	1.58	1.49	1.24	1.49	1.34
55.5	.846	1.80	2.18	1.75	1.47	1.49	1.41	1.39	1.61	1.31
57.5	.927	1.96	2.07	1.62	1.43	1.45	1.26	1.47	1.63	1.36
59.5	1.33	2.19	1.93	1.58	1.62	1.48	1.15	1.66	1.89	1.48
62.5	0	0	0	0	0	0	0	0	0	0

TABLE 11d. Velocity Measurements of Air Jet in Confined Swirling Flow; U_j = 66.8 m/s.

r (mm) \ x/D_j	1	2	3	5	7	10	14	20	28	40
	w' (m/s)									
0	4.44	4.31	3.22	2.74	2.09	1.49	1.30	1.02	1.07	.947
0.5	4.44	4.31	3.22	2.74	1.97	1.49	1.30	1.02	1.07	.947
2.5	4.15	4.13	3.22	2.72	2.00	1.48	1.37	1.05	1.46	1.08
5.5	2.50	3.61	2.91	2.73	1.95	1.51	1.35	1.17	1.27	1.20
7.5	1.71	2.78	2.71	2.62	1.88	1.53	1.32	1.17	1.33	1.24
10.5	1.32	1.86	2.36	2.63	1.88	1.73	1.55	1.28	1.33	1.24
12.5	1.34	1.67	2.32	2.61	1.77	1.76	1.60	1.41	1.41	1.30
15.5	1.72	1.78	2.14	2.34	1.78	1.82	1.72	1.60	1.52	1.35
17.5	1.78	2.17	2.17	2.20	1.76	1.87	1.79	1.70	1.56	1.38
20.5	1.62	2.05	2.09	1.89	1.72	1.88	1.81	1.75	1.56	1.40
22.5	1.54	1.88	1.84	1.62	1.64	1.75	1.74	1.72	1.47	1.38
25.5	1.84	1.74	1.61	1.46	1.42	1.58	1.48	1.60	1.35	1.23
27.5	2.58	1.92	1.62	1.45	1.36	1.49	1.34	1.52	1.30	1.33
30.5	2.95	2.04	1.76	1.53	1.36	1.44	1.28	1.34	1.26	1.22
32.5	2.88	2.10	1.76	1.62	1.43	1.43	1.22	1.28	1.28	1.16
35.5	3.00	2.13	2.18	1.71	1.45	1.40	1.21	1.22	1.19	1.08
37.5	3.34	2.17	2.35	1.79	1.49	1.56	1.17	1.16	1.18	1.10
40.5	3.30	2.35	2.35	1.82	1.56	1.62	1.09	1.06	1.17	1.10
42.5	3.41	3.05	2.41	1.87	1.52	1.68	1.10	1.00	1.12	1.03
47.5	2.97	2.92	2.39	2.03	1.49	1.54	1.17	1.11	1.01	1.01
52.5	1.28	2.42	2.08	1.91	1.46	1.47	1.20	1.06	1.23	1.12
55.5	1.14	1.85	1.77	1.74	1.34	1.36	1.14	1.18	1.41	1.15
57.5	1.43	1.77	1.64	1.62	1.35	1.28	1.13	1.24	1.43	1.31
59.5	1.48	1.62	1.76	1.54	1.38	1.29	1.14	1.40	1.74	1.56
62.5	0	0	0	0	0	0	0	0	0	0

TABLE 12. Velocity Measurements of Air Jet in Confined Swirling Flow; U_j = 152.8 m/s.

x/D_j	2.9	27.4	2.9	27.4
r (mm)	U (m/s)		u' (m/s)	
0	25.50	1.62	13.7	1.63
0.5	25.80	1.62	12.05	1.63
2.5	24.70	1.61	11.60	1.66
5.5	22.10	1.68	11.40	1.67
7.5	19.10	1.72	11.20	1.70
10.5	12.00	1.995	8.150	1.71
12.5	9.60	2.20	6.85	1.68
15.5	5.63	2.53	4.43	1.56
17.5	4.50	2.65	3.40	1.58
20.5	3.42	3.10	2.33	1.52
22.5	3.41	3.46	1.78	1.52
25.5	3.63	4.02	1.48	1.64
27.5	3.67	4.65	1.27	1.68
30.5	4.94	5.63	1.91	1.68
32.5	5.53	6.21	2.15	1.69
35.5	7.50	7.20	2.57	1.64
37.5	9.23	7.70	2.59	1.54
40.5	10.90	8.80	2.45	1.43
42.5	11.70	9.21	2.49	1.37
47.5	12.04	10.56	2.50	1.19
52.5	11.06	11.20	2.30	1.25
55.5	10.80	11.44	1.96	1.37
57.5	10.90	11.50	2.04	1.50
62.5	0	0	0	0

TABLE 13. Centerline Measurements of Helium/Air Jets in Confined Swirling Flow.

	U_j = 16.8 (m/s)			U_j = 36.5 (m/s)		
x/D_j	U_0(m/s)	u_0'(m/s)	w_0'(m/s)	U_0(m/s)	u_0'(m/s)	w_0'(m/s)
1	6.40	2.72		11.60	5.48	
2	4.55	2.63		8.06	4.12	
3	3.43	1.42	1.02	6.56	3.23	1.51
4	3.26	1.13	.855	5.93	2.40	1.61
5	3.07	1.01	.756	4.80	1.89	1.58
6	2.64	1.05	.749	4.42	1.71	1.38
7	2.32	1.03	.763	3.89	1.54	1.34
8	2.32	.956	.737	3.63	1.46	1.48
9	2.30	1.03	.689	3.46	1.53	1.46
10	2.25	.926	.650	3.70	1.59	1.26
12	2.17	.915	.636	3.50	1.44	1.49
14	1.84	1.01	.603	3.00	1.58	1.40
16	1.75	.906	.638	3.12	1.42	1.51
18	1.87	.932	.619	2.93	1.50	1.34
20	2.05	.87	.637	2.93	1.49	1.46
24	1.83	.932	.630	2.99	1.42	1.59
28	1.68	.883	.604	2.83	1.39	1.70
32	1.50	.820	.600	2.95	1.50	1.46
36	1.40	.879	.606	2.68	1.43	1.52
40	1.45	.906	.673	2.98	1.70	1.43

TABLE 14a. Velocity Measurements of Helium/Air Jet in Confined Swirling Flow; U_j = 16.8 m/s.

r (mm) \ x/D_j	1	2	3	5	7	10	14	20	28	40
	U (m/s)									
0	6.40	4.55	3.43	3.07	2.32	2.25	1.84	2.05	1.68	1.45
0.5	6.40	4.55	3.43	3.07	2.32	2.25	1.84	2.05	1.68	1.45
2.5	5.61	4.20	2.40	2.75	2.01	2.20	1.79	1.65	1.56	1.39
5.5	2.55	2.15	.887	1.64	1.37	1.60	1.33	1.10	1.14	.95
7.5	.190	.880	.181	.629	.838	1.21	.855	.601	.877	.535
10.5	-.077	.269	-.377	-.467	.483	.368	.272	-.096	.027	-.143
12.5	.247	.247	-.413	-.634	.324	.127	-.140	-.410	-.164	.053
15.5	.280	.370	-.374	-.61	.482	.266	-.159	-.110	.141	.413
17.5	.500	.500	.522	.192	.965	.735	.310	.735	.746	.811
20.5	1.01	.781	1.43	1.67	2.31	1.96	1.44	1.57	1.56	1.49
22.5	1.15	.987	1.77	2.69	3.55	2.56	2.25	2.20	2.18	2.08
25.5	1.13	1.18	2.00	3.55	5.19	3.52	3.80	3.03	3.24	2.86
27.5	1.45	1.71	2.18	4.13	5.90	4.18	4.94	3.76	3.87	3.68
30.5	3.77	2.70	3.29	4.79	6.11	5.47	6.31	4.94	5.39	4.89
32.5	5.99	3.87	4.62	5.23	6.37	6.64	7.08	5.58	6.19	5.61
35.5	8.59	6.19	6.67	6.20	6.79	7.40	7.73	6.45	7.33	6.77
37.5	9.74	7.23	8.65	7.04	8.57	7.80	8.48	7.05	7.95	7.34
40.5	10.04	8.43	9.67	9.67	9.34	7.97	9.72	8.08	9.01	8.27
42.5	9.81	8.73	10.30	10.00	9.53	8.15	10.05	8.30	9.46	9.10
47.5	10.70	10.10	10.40	10.57	9.97	10.31	10.31	9.57	10.63	10.30
52.5	11.20	10.52	11.23	10.48	10.42	11.10	10.75	9.92	10.75	10.80
55.5	12.20	10.10	11.87	10.32	10.20	11.25	11.00	10.20	11.01	11.15
57.5	12.20	10.40	12.05	10.00	10.22	11.04	11.21	10.40	11.10	11.30
59.5	11.30	11.15	11.74	9.75	10.26	10.98	11.10	10.50	10.91	11.10
62.5	0	0	0	0	0	0	0	0	0	0

TABLE 14b. Velocity Measurements of Helium/Air Jet in Confined Swirling Flow; U_j = 16.8 m/s.

r (mm) \ x/D_j	1	2	3	5	7	10	14	20	28	40
			W (m/s)							
0			0	0	0	0	0	0	0	0
0.5			.892	1.05	1.83	.650	.141	1.46	.910	1.31
2.5			1.38	1.64	2.69	1.28	.765	2.40	1.71	2.33
5.5			2.97	3.15	4.40	2.78	2.21	4.02	.335	3.97
7.5			4.51	4.48	6.52	4.19	4.05	5.20	4.66	5.42
10.5			7.08	6.97	8.22	6.59	6.24	7.18	7.11	8.30
12.5			8.36	8.28	9.29	7.77	7.82	8.49	9.55	10.40
15.5			9.83	10.53	11.75	9.85	10.35	10.93	12.36	13.00
17.5			11.66	12.25	13.27	11.50	12.22	12.15	13.91	14.70
20.5			14.67	15.15	16.31	13.42	15.70	14.25	16.42	16.60
22.5			17.07	17.22	17.85	15.00	17.53	15.62	17.50	17.61
25.5			18.66	19.40	19.19	16.99	19.37	17.20	19.03	18.80
27.5			18.32	19.85	20.04	18.30	20.26	18.06	19.70	19.20
30.5			17.77	20.10	20.49	19.63	20.77	18.90	20.36	19.73
32.5			17.56	19.71	20.58	20.14	20.92	19.36	20.50	19.80
35.5			17.50	19.52	20.60	20.41	20.80	19.72	20.67	20.00
37.5			17.86	19.58	20.47	20.60	21.67	19.99	20.68	20.26
40.5			18.33	19.62	20.17	20.60	22.08	20.15	20.72	20.40
42.5			18.54	19.75	20.15	20.52	21.95	20.14	20.75	20.20
47.5			20.10	20.28	20.34	20.63	21.20	20.94	20.30	19.01
52.5			21.10	21.94	20.88	20.73	19.48	19.56	19.10	17.50
55.5			20.83	21.12	19.97	19.91	18.89	18.70	18.08	16.70
57.5			20.65	20.40	19.40	19.63	18.57	18.02	17.50	16.20
59.5			20.40	19.49	18.85	18.95	18.06	17.12	16.70	15.70
62.5			0	0	0	0	0	0	0	0

TABLE 14c. Velocity Measurements of Helium/Air Jet in Confined Swirling Flow; U_j = 16.8 m/s.

x/D_j / r (mm)	1	2	3	5	7	10	14	20	28	40
	u' (m/s)									
0	2.72	2.63	1.42	1.01	1.03	.926	1.01	.870	.883	.906
0.5	2.72	2.63	1.42	1.01	1.03	.926	1.01	.870	.883	.906
2.5	2.52	2.75	1.35	.97	1.06	.977	.974	.904	.886	.944
5.5	2.10	2.22	1.12	1.11	1.06	.980	1.01	.931	.881	1.04
7.5	1.15	1.43	9.44	1.12	1.00	1.00	1.01	.879	.914	.962
10.5	.613	.654	.759	.803	.805	.952	.890	.785	.841	.790
12.5	.550	.683	.677	.646	.728	.817	.758	.679	.719	.796
15.5	.560	.801	.747	.675	.760	.721	.667	.754	.658	.844
17.5	.743	.986	1.07	1.14	1.16	.812	.803	.825	.752	.735
20.5	.989	1.11	1.16	1.27	1.46	1.10	.961	.963	.840	.830
22.5	1.06	1.15	1.13	1.27	1.53	1.20	1.09	1.02	.904	.882
25.5	1.18	1.18	1.16	1.26	1.34	1.34	1.30	1.08	1.00	1.00
27.5	1.60	1.34	1.35	1.47	1.21	1.38	1.30	1.08	1.07	1.02
30.5	2.38	1.72	1.90	1.71	1.26	1.46	1.21	1.13	1.19	1.06
32.5	2.59	1.92	2.20	1.85	1.35	1.39	1.14	1.03	1.11	1.08
35.5	2.67	2.07	2.20	2.04	1.60	1.35	1.19	1.02	1.02	.953
37.5	2.89	2.06	2.07	2.09	1.72	1.32	1.31	.993	.977	.917
40.5	3.09	2.06	2.13	2.05	1.69	1.38	1.38	.868	1.04	.884
42.5	3.18	2.26	2.25	1.91	1.60	1.49	1.37	.898	1.04	.986
47.5	3.35	2.79	2.47	1.96	1.47	1.57	1.49	.980	.883	1.16
52.5	2.50	2.15	2.13	1.86	1.50	1.33	1.50	1.04	1.09	1.42
55.5	1.92	1.87	1.70	1.65	1.68	1.34	1.35	1.13	1.25	1.49
57.5	1.36	2.08	1.50	1.68	1.74	1.47	1.28	1.28	1.46	1.58
59.5	1.10	2.10	1.16	1.72	1.77	1.68	1.46	1.42	1.60	1.71
62.5	0	0	0	0	0	0	0	0	0	

TABLE 14d. Velocity Measurements of Helium/Air Jet in Confined Swirling Flow; U_j = 16.8 m/s.

x/D_j / r (mm)	1	2	3	5	7	10	14	20	28	40
	w' (m/s)									
0			1.02	.758	.763	.650	.603	.637	.604	.673
0.5			1.02	.758	.763	.650	.603	.637	.604	.672
2.5			1.02	.804	.841	.688	.628	.698	.640	.648
5.5			1.06	.858	.960	.803	.721	.778	.700	.764
7.5			1.05	.917	.951	.880	.857	.764	.681	.782
10.5			.927	.952	.901	.951	.871	.818	.837	.829
12.5			.777	.939	.900	.965	.885	.839	.841	.935
15.5			.825	1.02	1.18	.901	.963	.814	.916	.956
17.5			1.49	1.28	1.31	.929	1.07	.855	.946	.980
20.5			1.93	1.74	1.41	1.10	1.11	.976	.908	.917
22.5			1.64	1.64	1.32	1.24	1.18	.976	.860	.914
25.5			1.34	1.38	1.25	1.24	1.03	.954	.899	.926
27.5			1.64	1.37	1.33	1.19	.993	.968	.882	.930
30.5			1.84	1.53	1.34	1.18	.936	.839	.844	.905
32.5			1.91	1.61	1.40	1.20	.944	.880	.821	.904
35.5			1.97	1.74	1.43	1.30	1.05	.827	.799	.887
37.5			2.05	1.72	1.49	1.28	1.44	.793	.803	.900
40.5			2.17	1.80	1.41	1.25	1.43	.748	.820	.949
42.5			2.17	1.82	1.45	1.27	1.39	.854	.800	.971
47.5			2.25	1.81	1.56	1.37	1.30	1.01	.912	1.04
52.5			1.78	1.69	1.38	1.23	1.27	1.13	1.26	1.28
55.5			1.42	1.57	1.42	1.26	1.19	1.27	1.26	1.34
57.5			1.29	1.54	1.59	1.30	1.19	1.41	1.42	1.42
59.5			1.17	1.76	1.58	1.28	1.25	1.66	1.67	1.55
62.5			0	0	0	0	0	0	0	0

TABLE 15a. Velocity Measurements of Helium/Air Jet in Confined Swirling Flow; U_j = 36.5 m/s.

r (mm) \ x/D_j	1	2	3	5	7	10	14	20	28	40
	U (m/s)									
0	11.60	8.06	6.56	4.80	3.89	3.70	3.00	2.93	2.85	2.98
0.5	11.60	8.06	6.56	4.80	3.89	3.70	3.00	2.93	2.81	2.98
2.5	10.90	5.81	5.22	4.77	3.42	3.40	3.00	2.69	2.68	3.01
5.5	4.60	5.33	2.78	3.54	2.87	2.98	2.49	2.38	2.44	2.01
7.5	1.78	2.89	1.80	2.51	1.62	2.32	1.79	1.57	1.81	1.27
10.5	-0.03	.786	.765	.550	.608	1.06	.607	.056	.403	.116
12.5	-.081	.560	.386	-.338	.126	.336	-.502	-.764	-.506	-.370
15.5	.280	.628	.161	-.131	-.308	-.212	-1.22	-1.07	-.732	-.516
17.5	.320	.752	.084	-.140	-.304	.022	-1.03	-.752	-.362	-.113
20.5	.980	1.21	1.53	.400	.835	1.24	.220	.954	1.55	1.61
22.5	1.10	1.46	2.11	2.82	2.28	2.56	1.58	1.82	2.42	2.23
25.5	.790	1.94	2.54	4.02	4.30	3.52	3.07	2.95	3.63	3.31
27.5	.800	2.39	3.04	4.44	5.75	4.29	4.25	3.70	4.36	3.81
30.5	2.46	3.81	4.00	5.01	6.56	5.40	5.78	4.80	5.56	4.77
32.5	5.50	5.14	4.75	5.24	6.86	6.50	6.50	5.57	6.49	5.58
35.5	8.42	6.64	6.34	5.96	7.36	7.41	7.39	6.60	7.51	6.50
37.5	9.98	7.80	7.91	6.72	7.79	7.61	7.92	7.24	8.09	7.20
40.5	10.12	8.53	9.45	7.73	8.34	7.63	8.95	7.92	8.94	8.10
42.5	10.19	9.43	10.80	10.37	8.67	8.74	9.30	8.10	9.58	8.77
47.5	10.27	9.55	11.23	10.86	10.35	9.50	9.52	9.34	10.04	10.14
52.5	10.88	10.00	11.60	10.60	10.20	10.36	9.84	9.32	10.07	10.22
55.5	11.44	9.39	12.70	10.43	10.40	10.99	10.33	9.67	10.52	10.38
57.5	11.93	9.16	12.70	10.37	10.41	10.85	10.50	10.00	10.66	10.29
59.5	11.20	10.36	11.31	9.98	10.01	10.89	10.60	10.00	10.66	10.20
62.5	0	0	0	0	0	0	0	0	0	0

TABLE 15b. Velocity Measurements of Helium/Air Jet in Confined Swirling Flow; U_j = 36.5 m/s.

x/D_j / r (mm)	1	2	3	5	7	10	14	20	28	40
			W (m/s)							
0			0	0	0	0	0	0	0	0
0.5			1.82	1.34	1.70	1.39	1.72	2.34	2.52	1.06
2.5			3.94	2.88	3.42	2.47	4.48	4.81	5.68	4.00
5.5			7.54	7.20	6.54	5.18	7.07	6.96	8.26	7.07
7.5			9.06	9.10	8.34	7.13	8.03	8.01	9.01	8.13
10.5			9.20	9.55	9.08	8.36	8.63	8.21	9.26	9.04
12.5			8.94	9.65	9.37	8.73	9.04	8.43	10.08	9.50
15.5			9.19	10.20	10.02	9.14	10.10	9.43	11.11	10.40
17.5			10.34	10.70	11.07	9.60	11.70	10.48	11.89	11.37
20.5			13.02	13.00	13.50	10.89	14.13	12.12	13.72	12.68
22.5			15.04	15.40	15.10	12.24	16.10	13.34	15.16	13.73
25.5			16.87	17.61	17.80	14.64	18.20	15.42	17.05	15.53
27.5			17.53	18.56	18.64	16.60	19.21	16.48	17.58	16.33
30.5			17.04	18.56	19.57	18.10	19.92	17.50	18.54	17.13
32.5			16.65	18.44	19.66	18.80	20.20	17.91	18.75	17.91
35.5			16.93	18.01	19.33	19.48	20.76	18.54	19.00	18.32
37.5			17.00	18.11	19.27	19.73	21.00	18.62	19.14	18.40
40.5			17.30	18.00	19.12	19.77	21.20	18.94	19.41	18.63
42.5			17.50	18.14	19.00	19.54	21.50	18.90	19.51	18.85
47.5			18.96	18.50	19.43	19.50	20.15	19.20	18.97	18.32
52.5			20.10	19.21	20.24	19.80	18.75	18.20	18.10	17.02
55.5			19.98	19.61	19.52	19.30	18.05	17.31	17.03	16.17
57.5			19.52	19.10	18.63	18.65	17.78	16.71	16.45	15.55
59.5			19.53	18.32	17.80	18.10	17.35	16.21	15.70	14.86
62.5			0	0	0	0	0	0	0	0

TABLE 15c. Velocity Measurements of Helium/Air Jet in Confined Swirling Flow; U_j = 36.5 m/s.

x/D_j / r (mm)	1	2	3	5	7	10	14	20	28	40
	u' (m/s)									
0	5.48	4.12	3.23	1.89	1.54	1.59	1.58	1.49	1.39	1.70
0.5	5.48	4.12	3.23	1.89	1.54	1.59	1.58	1.49	1.39	1.70
2.5	5.30	3.92	3.08	1.89	1.47	1.46	1.47	1.38	1.35	1.45
5.5	3.94	3.55	2.02	1.80	1.38	1.40	1.41	1.26	1.21	1.19
7.5	2.59	2.30	1.61	1.79	1.26	1.31	1.34	1.20	1.09	1.15
10.5	.790	.517	.936	1.47	1.00	1.10	1.23	1.06	.942	.964
12.5	.540	.504	.565	1.22	.801	.958	.915	.733	.734	.756
15.5	.510	.568	.497	.764	.676	.693	.558	.500	.487	.596
17.5	.581	.650	.522	.681	.691	.711	.534	.557	.569	.641
20.5	.747	.784	.873	.924	1.18	1.04	.791	.837	.884	.789
22.5	.890	.889	.968	1.07	1.43	1.19	1.04	.945	.948	.815
25.5	1.08	.972	.954	1.10	1.36	1.28	1.18	.981	.985	.890
27.5	1.30	1.10	1.14	1.12	1.33	1.36	1.25	.971	1.04	.870
30.5	2.10	1.40	1.59	1.41	1.41	1.37	1.17	1.00	1.04	.866
32.5	2.28	1.78	1.80	1.56	1.49	1.27	1.09	.968	.976	.876
35.5	2.52	1.95	1.99	1.72	1.59	1.29	1.03	.912	.864	.846
37.5	2.63	1.98	2.09	1.85	1.68	1.29	1.08	.874	.848	.818
40.5	2.86	2.08	2.03	2.04	1.70	1.36	1.13	.835	.895	.907
42.5	3.01	2.50	2.23	2.05	1.59	1.61	1.16	.828	.820	.909
47.5	3.07	2.69	2.32	1.98	1.52	1.50	1.34	1.15	.873	1.11
52.5	2.67	2.26	2.09	1.92	1.50	1.25	1.40	1.27	1.05	1.24
55.5	2.26	1.92	1.64	1.69	1.37	1.35	1.21	1.30	1.28	1.38
57.5	1.62	2.27	1.40	1.57	1.42	1.42	1.21	1.44	1.37	1.55
59.5	.960	2.27	1.61	1.57	1.53	1.65	1.28	1.53	1.63	1.75
62.5	0	0	0	0	0	0	0	0	0	0

TABLE 15d. Velocity Measurements of Helium/Air Jet in Confined Swirling Flow; U_j = 36.5 m/s.

r (mm) \ x/D_j	1	2	3	5	7	10	14	20	28	40
						w' (m/s)				
0			1.51	1.58	1.34	1.26	1.40	1.46	1.70	1.43
0.5			1.51	1.58	1.34	1.26	1.40	1.46	1.70	1.43
2.5			2.17	1.82	1.44	1.35	1.36	1.40	1.59	1.59
5.5			1.84	1.93	1.52	1.38	1.19	1.03	.951	1.14
7.5			1.45	1.34	1.10	1.24	.903	.744	.745	.853
10.5			.908	.734	.676	.720	.699	.697	.708	.717
12.5			.862	.741	.780	.648	.645	.636	.723	.699
15.5			.883	.917	.790	.690	.719	.662	.727	.683
17.5			1.14	1.07	1.01	.770	.892	.758	.834	.751
20.5			1.75	1.60	1.40	.870	1.11	.903	.905	.812
22.5			1.71	1.65	1.40	1.04	1.10	.947	.918	.853
25.5			1.43	1.29	1.24	1.23	1.03	.958	.860	.836
27.5			1.35	1.34	1.26	1.21	.930	.890	.855	.833
30.5			1.62	1.45	1.28	1.09	.920	.852	.781	.836
32.5			1.80	1.52	1.24	1.13	.920	.825	.775	.766
35.5			1.89	1.57	1.33	1.28	1.14	.788	.729	.763
37.5			1.92	1.59	1.32	1.31	1.33	.758	.745	.750
40.5			1.88	1.63	1.40	1.21	1.36	.757	.798	.787
42.5			1.95	1.72	1.40	1.17	1.33	.821	.750	.866
47.5			2.14	1.75	1.36	1.17	1.27	.998	.774	.912
52.5			1.71	1.63	1.31	1.20	1.21	.967	1.05	1.11
55.5			1.42	1.60	1.39	1.16	1.16	1.03	1.15	1.17
57.5			1.34	1.65	1.48	1.19	1.20	1.03	1.20	1.16
59.5			1.25	1.84	1.66	1.27	1.32	1.24	1.36	1.29
62.5			0	0	0	0	0	0	0	0

END

DATE

FILMED

NOV 22 1984